TECHNICAL REPORT STANDARD PAGE

1. Report No. **FHWA/LA.08/439**	2. Government Accession No.	3. Recipient's Catalog No.
4. Title and Subtitle **Update of Correlations between Cone Penetration and Boring Log Data**	5. Report Date **March 2008**	
	6. Performing Organization Code	
7. Author(s) **Khalid Alshibli, Ph.D., P.E.** **Ayman M. Okeil, Ph.D., P.E.** **Bashar Alramahi, Ph.D.**	8. Performing Organization Report No.	
9. Performing Organization Name and Address **Department of Civil and Environmental Engineering** **Louisiana State University** **Baton Rouge, LA 70803**	10. Work Unit No.	
	11. Contract or Grant No. **LTRC Project Number: 06-6GT** **State Project Number: 736-99-1406**	
12. Sponsoring Agency Name and Address **Louisiana Department of Transportation and Development** **P.O. Box 94245** **Baton Rouge, LA 70804-9245**	13. Type of Report and Period Covered **Final Report** **February 2007 – March 2008**	
	14. Sponsoring Agency Code	

15. Supplementary Notes
Conducted in Cooperation with the U.S. Department of Transportation, Federal Highway Administration

16. Abstract

The cone penetration test (CPT) has been widely used in Louisiana in the last two decades as an in situ tool to characterize engineering properties of soils. In addition, conventional drilling and sample retrieval using Shelby tube followed by laboratory testing is still the acceptable practice in identifying soils engineering properties. The main objective of this project is to update the correlations that are currently used by Louisiana Department of Transportation and Development (LADOTD) to interpret CPT data for engineering design purposes and to assess the reliability of using CPT data to predict soil shear strength in both the magnitude and spatial variations in the field with respect to the Load and Resistance Factor Design (LRFD) methodology. The results of laboratory soil testing were retrieved from borehole logs and were used as reference measurements in this study.

The research team collected project data files in paper printout format from LADOTD and soil testing engineers. Most project files did not have spatial coordinates; therefore, aerial images were used to identify latitude and longitude coordinates of CPT and borehole locations. The borehole data was not available for all the located CPT soundings. Efforts were made to obtain any available data from LADOTD electronic archive as well as paper project documents. A total of 752 CPT tests were documented in which 503 were matched with adjacent boreholes and 249 did not have adjacent borehole data available. The CPT data was used to predict soil undrained shear strength, bulk density and classification according to Robertson and Zhang and Tumay methods [*1*], [*2*].

The CPT data was then used to develop a database of undrained shear strength estimates with corresponding results from boreholes. The results in the database were preprocessed to apply some constraints on data points included in the calibration study, such as setting a maximum threshold on the distance between CPT and borehole locations; a minimum and maximum threshold on undrained shear strength values were used to represent realistic soil properties. The resulting database included results from 251 CPT soundings with borehole results in their vicinity that meet the aforementioned constraints. From these CPT soundings, 862 unique undrained shear strength data points were obtained at various depths. The dataset was analyzed for general as well as specific trends in order to identify appropriate parameters to be included in the study. Soil classification was clearly the most plausible parameter based on which the CPT undrained shear strength estimates should be calibrated.

The calibration of the CPT expression for undrained shear strength was conducted using two approaches. The first approach is a direct correlation based of the transformation model currently used by LADOTD for estimating the shear strength. The First Order Reliability Method (FORM) forms the basis for the second approach, which is more detailed and accounts for all sources of uncertainty. Optimum CPT coefficient values were computed for various target reliability values. The results were summarized and implementation procedures were recommended for future research.

17. Key Words **cone penetrometer; soil testing; reliability; geographical information system**	18. Distribution Statement **Unrestricted.**

19. Security Classification (of this report) **N/A**	20. Security Classification (of this page) **N/A**	21. No. of Pages **172**	22. Price **N/A**

Project Review Committee

Each research project will have an advisory committee appointed by the LTRC Director. The Project Review Committee is responsible for assisting the LTRC Administrator or Manager in the development of acceptable research problem statements, requests for proposals, review of research proposals, oversight of approved research projects, and implementation of findings.

LTRC appreciates the dedication of the following Project Review Committee Members in guiding this research study to fruition.

LTRC Administrator/ Manager

Zhongjie "Doc" Zhang, Ph.D., P.E.
Pavement Geotechnical Research Administrator

Members

Dr. Ching Tsai, Geotechnical Section
Ben Fernandez, Geotechnical Section
Dr. Murad Abufarsakh, LTRC
Dr. Recep Yilmaz, Fugro Geosciences
Bert Wintz, Materials Laboratory
Kim Carlington, Geotechnical Section
Philip Arena, FHWA
Gavin Gautreau, LTRC

Directorate Implementation Sponsor

William B. Temple
DOTD Chief Engineer

Update of Correlations between Cone Penetration and Boring Log Data

by

Khalid Alshibli, Ph.D., P.E.
Associate Professor

Ayman Okeil, Ph.D., P.E.
Assistant Professor

Bashar Alramahi, Ph.D.
Research Associate

Department of Civil and Environmental Engineering
3505 Patrick F. Taylor Hall
Louisiana State University
Baton Rouge, LA 70803

LTRC Project No. 06-6GT
State Project No. 736-99-1406

conducted for

Louisiana Department of Transportation and Development
Louisiana Transportation Research Center

March 2008

ABSTRACT

The cone penetration test (CPT) has been widely used in Louisiana in the last two decades as an in situ tool to characterize engineering properties of soils. In addition, conventional drilling and sample retrieval using Shelby tube followed by laboratory testing is still the acceptable practice in identifying soils engineering properties. The main objective of this project is to update the correlations that are currently used by Louisiana Department of Transportation and Development (LADOTD) to interpret CPT data for engineering design purposes and to assess the reliability of using CPT data to predict soil shear strength in both the magnitude and spatial variations in the field with respect to the Load and Resistance Factor Design (LRFD) methodology. The results of laboratory soil testing were retrieved from borehole logs and were used as reference measurements in this study.

The research team collected project data files in paper printout format from LADOTD and soil testing engineers. Most project files did not have spatial coordinates; therefore, aerial images were used to identify latitude and longitude coordinates of CPT and borehole locations. The borehole data was not available for all the located CPT soundings. Efforts were made to obtain any available data from LADOTD electronic archive as well as paper project documents. A total of 752 CPT soundings were documented in which 503 were matched with adjacent boreholes and 249 did not have adjacent borehole data available. The CPT data was used to predict soil undrained shear strength, bulk density and classification according to Robertson and Zhang and Tumay methods [*1*], [*2*].

The CPT measurements were then used to develop a database of undrained shear strength estimates with corresponding results from boreholes. The results in the database were preprocessed to apply some constraints on data points included in the calibration study, such as setting a maximum threshold on the distance between CPT and borehole locations; a minimum and maximum threshold on undrained shear strength values were used to represent realistic soil properties. The resulting database included results from 251 CPT soundings with borehole results in their vicinity that meet the aforementioned constraints. From these CPT soundings, 862 unique undrained shear strength data points were obtained at various depths. The dataset was analyzed for general as well as specific trends in order to identify appropriate parameters to be included in the study. Soil classification was clearly the most plausible parameter based on which the CPT undrained shear strength estimates should be calibrated.

The calibration of the CPT expression for undrained shear strength was conducted using two approaches. The first approach is a direct correlation based of the transformation model currently used by LADOTD for estimating the shear strength. The First Order Reliability Method (FORM) forms the basis for the second approach, which is more detailed and accounts for all sources of uncertainty. Optimum CPT coefficient values were computed for various target reliability values. The results were summarized and implementation procedures were recommended for future research.

ACKNOWLEDGMENTS

The authors gratefully acknowledged the financial support provided by the Louisiana Transportation Research Center (LTRC) and Louisiana Department of Transportation and Development (LADOTD).

The authors also acknowledge the assistance of the graduate students Chaytanya Mamidala and Ashwin Bommathanahalli who helped in data archiving and analysis. The authors would also like to thank Benjamin Fernandez from LADOTD geotechnical section and Jesse Rauser from Ardaman & Associates, Inc. for providing the CPT and borehole data.

The constructive criticism and suggestions of Dr. Zhongjie "Doc" Zhang, pavement geotechnical research administrator, and Mark Morvant, associate director of research at LTRC, are highly valued and appreciated.

IMPLEMENTATION STATEMENT

The results of this study demonstrated the benefit of performing in depth statistical analyses of soil property estimation methods. The cone penetration test has been in service for years, and it is prudent to update its coefficients and identify limits on its application so safe design can be achieved. In this study, a database of CPT soundings has been compiled with corresponding borehole results where available. The developed database should be updated as more borehole and CPT data become available for future projects. The database is useful and has been integrated into a Geographic Information Systems (GIS) system so LADOTD engineers may have easy access to its components. Comparison of the undrained shear strengths obtained from the CPT soundings and unconfined compression test on borehole samples revealed that it is possible to identify unique trends. These trends were used in updating the correlation of the CPT coefficient, N_{kt}. As a side product of this study, a procedure for identifying site variability is proposed that does not involve any subjective interpretation of the results. The procedure may be used when implementing new Load and Resistance Factor Design (LRFD) design codes where some design coefficients are varied based on the site variability.

Based on the results of this study, it is recommended that the findings of this research be implemented for a pilot testing period where LADOTD engineers gradually start using the newly correlated CPT coefficient, N_{kt}, for estimating the undrained shear strength in conjunction with the traditional borehole assessments. During this period, it is important to assess the validity of the proposed changes from this study and document its outcome for future reference. As the findings get updated, it is anticipated that LADOTD engineers can gradually move toward replacing the conventional reliance on boreholes for undrained shear estimates with CPT soundings. This will translate, in the long run, as a cost benefit to LADOTD.

TABLE OF CONTENTS

ABSTRACT III
ACKNOWLEDGMENTS V
IMPLEMENTATION STATEMENT VII
TABLE OF CONTENTS IX
LIST OF TABLES XIII
LIST OF FIGURES XV
Part I: Cone Penetration Test (CPT) 1
Historic Background 1
Apparatus Description and Correction Factors 3
Soil Classification using CPT 6
Strength Characteristics 10
Effective Stress Strength Parameters 14
Stress History 16
Relative Density from CPT Data 18
Correlations with Standard Penetration Test (SPT) 21
Part II: Load and Resistance Factor Design (LRFD) 23
LRFD in Geotechnical Applications 24
OBJECTIVE 27
SCOPE 29
METHODOLOGY 31
CPT Database 31
Locating CPT Sites using GIS 31
Borehole Data 33
CPT and Borehole Data Analysis and Archiving 35
Reliability Analysis of CPT 42
Direct Correlation of CPT and Boring Results–1st Approach 42
Detailed Reliability Analysis for Correlation of CPT and Boring Results–2nd Approach 43
Preprocessing CPT Data 45
Matching CPT and Borehole Data 45

Averaging CPT Readings 47
Filtering Data Results 49
Calibration of CPT Coefficient 51
Limit State Function 51
Chi-Square Statistical Test "Goodness of Fit" 55
Reliability-based Calibration 56
DISCUSSION OF RESULTS 57
Repeatability Tests 57
Statistical Characteristics of Repeatability Data 59
Utilizing CPT for Assessment of Site Variability 67
Initial Data Analysis 69
General Trends 69
Specific Parameter Trends 73
CPT Reading Values ($q_c - \sigma_{vo}$) 77
Chi-Square Results 89
Calibration of CPT Coefficient for Undrained Shear Strength 95
Calibration–1st Approach 95
Calibration–2nd Approach 99
Correlation Between Unit Weight, γ_T, from CPT and Boring Data 109
SUMMARY AND CONCLUSIONS 111
Summary 111
Conclusions 111
RECOMMENDATIONS 115
ACRONYMS, ABBREVIATIONS, AND SYMBOLS 117
REFERENCES 121
APPENDIX A 133
List of Projects Included in Database 133
APPENDIX B 139
First Order Reliability Method (FORM) 139
APPENDIX C 143
Chi-Square Statistical Test: Goodness-of-fit Test 143
APPENDIX D 145

Normal and Lognormal Distribution Types 145
Normal or Gaussian Distribution 145
Lognormal Distribution The random variable *X* is a lognormal random 146
APPENDIX E 149
Example Excel Template to Analyze CPT Data 149

LIST OF TABLES

Table 1 Nc values theoretically derived by different researchers (*11*) 12
Table 2 Constants for determination of D_r [*65*] 19
Table 3 Suggested Q_c values [*67*] 20
Table 4 Typical I_c ranges for different soil types [*73*] 22
Table 5 Random variables used in reliability calibration 54
Table 6 Statistical characteristics of transformation model (Robertson classification) 54
Table 7 Statistical characteristics of transformation model (Zhang and Tumay classification) 55
Table 8 Range of parameters covered in reliability study 56
Table 9 Discrete tip resistance, q_c, readings at 5 ft. intervals. 60
Table 10 Discrete unit weight, γ_T, results at 5 ft. intervals. 60
Table 11 Discrete overburden pressure readings at 5 ft. intervals. 61
Table 12 Effect of soil depth on uncertainty of CPT results 75
Table 13 Effect of net difference between CPT readings, $q_c - \sigma_{vo}$, on uncertainty of CPT results 78
Table 14 Effect of soil classification on uncertainty of CPT results 81
Table 15 Effect of soil classification on uncertainty of CPT results 83
Table 16 Effect of soil classification on uncertainty of CPT results (Robertson) 85
Table 17 Effect of Plasticity Index on uncertainty of CPT results 87
Table 18 Summary of chi-square test results for transformation model 89
Table 19 Calibrated N_{kt} values for different probability of exceedance, P_e, values 96
Table 20 Reliability results (β_T = 0.0, σ_{vo}/q_c = 0.10, Robertson classification) 100
Table 21 Reliability results (β_T = 0.1257, σ_{vo}/q_c = 0.10, Robertson classification) 101
Table 22 Reliability results (β_T = 0.4308, σ_{vo}/q_c = 0.10, Robertson classification) 102
Table 23 Optimum N_{kt} values (β_T = 0.0, Robertson classification) 104
Table 24 Optimum N_{kt} values (β_T = 0.1257, Robertson classification) 104
Table 25 Optimum N_{kt} values (β_T = 0.4308, Robertson classification) 105
Table 26 Reliability results (β_T = 0.0, σ_{vo}/q_c = 0.10, Zhang and Tumay classification) 106
Table 27 Reliability results (β_T = 0.1257, σ_{vo}/q_c = 0.10, Zhang and Tumay classification) 107
Table 28 Reliability results (β_T = 0.4308, σ_{vo}/q_c = 0.10, Zhang and Tumay classification) 108
Table 29 Optimum N_{kt} values (β_T = 0.0, Zhang and Tumay classification) 108

Table 30 Optimum N_{kt} values (β_T = 0.1257, Zhang and Tumay classification)..... 109
Table 31 Optimum N_{kt} values (β_T = 0.4308, Zhang and Tumay classification)..... 109
Table 32 Recommended N_{kt} values using 2nd approach (Robertson classification)..... 113
Table 33 Recommended N_{kt} values using 2nd approach (Zhang and Tumay classification) 113
Table 34 Projects with CPT and borehole data..... 133
Table 35 Projects with CPT data without borehole data..... 136
Table 36 CDF of the chi-square distribution (Nowak and Collins 2000)..... 144

LIST OF FIGURES

Figure 1 Early cone penetrometers (a) Dutch cone with conical mantle, (b) Begemann cone with friction sleeve [*11*] 2
Figure 2 Typical Schematic of Piezocone [*12*] 4
Figure 3 Typical results of CPT 5
Figure 4 Douglas and Olsen classification chart [*18*] 8
Figure 5 Classification charts presented by Robertson et al. [*19*] 9
Figure 6 Eslami and Fellenius classification chart [*26*] 9
Figure 7 Charts to obtain Su from excess pore water pressure measurements [*51*] 14
Figure 8 Interpretation diagrams for $\beta = 0$ and $\beta = -15^{o}$ [*57*] 15
Figure 9 Empirical correlations of OCR vs. normalized PCPT parameters [*58*] 16
Figure 10 Comparison between the measured and predicted $\sigma`_{p}$ values [*62*] 17
Figure 11 Variation of q_c/N with d_{50} [*19*] 22
Figure 12 Uncertainty in soil property estimates [*93*] 25
Figure 13 CPT data points from LADOTD and STE 33
Figure 14 CPT data points with and without borehole data from LADOTD and STE 34
Figure 15 Example CPT point information displayed by selecting a CPT location 37
Figure 16 Example CPT classification file displayed by selecting the PDF link 38
Figure 17 Zoomed view of the northern part of Louisiana where a higher number of CPT points were available 39
Figure 18 Zoomed view of the southwestern part of Louisiana where a smaller number of CPT points were available 40
Figure 19 Histogram of depths for CPT points included in database 41
Figure 20 Depth histograms for different soil classifications [*4*], [*5*], [*19*] 41
Figure 21 Array of CPT repeatability tests 44
Figure 22 Distance threshold between CPT and borehole locations showing number of data points included in analyses 46
Figure 23 Averaging raw CPT readings 48
Figure 24 Histogram of S_u frequency in compiled database 49
Figure 25 Effect of S_u thresholds on uncertainty of transformation model 50
Figure 26 Illustration of the limit state function (LSF) used in this study (general case) 52
Figure 27 Illustration of the limit state function (LSF) used in this study (special case) 52
Figure 28 Cone data from all repeatability tests 58
Figure 29 Analysis of repeatability data for cone tip resistance 62

Figure 30 Study of unit weight data scatter from repeatability tests 63
Figure 31 Study of overburden pressure data scatter from repeatability tests 64
Figure 32 Tip resistance, q_c, readings from all CPT repeatability tests 65
Figure 33 Study of tip resistance data scatter, COV(q_c), vs. soil classification. 66
Figure 34 Study of unit weight data scatter, COV(γ_T), vs. soil classification 66
Figure 35 Study of overburden pressure data scatter, COV(σ_{vo}), vs. soil classification 67
Figure 36 Comparison of undrained shear strength, S_u, from CPT and UC tests 70
Figure 37 Analyzing data trends of different CPT readings versus S_u^{UC} 72
Figure 38 Comparison of undrained shear strength, S_u, from CPT and UC tests 76
Figure 39 Comparison of undrained shear strength, S_u, from CPT and UC tests at different CPT readings net difference, $q_c - \sigma_{vo}$, values 79
Figure 40 Comparison of undrained shear strength, S_u, from CPT and UC tests for different soil classifications (Zhang and Tumay – clay only) 82
Figure 41 Comparison of undrained shear strength, S_u, from CPT and UC tests for different soil classifications (Zhang and Tumay – clay and silt) 84
Figure 42 Comparison of undrained shear strength, S_u, from CPT and UC tests for different soil classifications (Robertson) 86
Figure 43 Comparison of undrained shear strength, S_u, from CPT and UC tests for different Plasticity Index values 88
Figure 44 Chi square test results for transformation model (all data points) 90
Figure 45 Chi square test results for transformation model (Soil Classification 2) 91
Figure 46 Chi square test results for transformation model (Soil Classification 3) 92
Figure 47 Chi square test results for transformation model (Soil Classification 4) 93
Figure 48 Chi square test results for device uncertainty 94
Figure 49 Histogram of N_{kt} –values obtained from equation (42) –all data points 95
Figure 50 Cumulative distribution function (CDF) for N_{kt} –values [all data points] 96
Figure 51 Histogram of N_{kt} –values obtained from equation (42) (by Robertson soil classification) 97
Figure 52 Histogram of N_{kt} –values obtained from equation (42) (by Zhang and Tumay's soil classification) 98
Figure 53 Determining optimum N_{kt} values (β_T = 0.1257, σ_{vo}/q_c = 0.05) 103

Figure 54 Unit weight correlation γ_T (CPT vs. boring results) 110
Figure 55 Histogram of unit weight ratio $\gamma_{T,\mathrm{CPT}} / \gamma_{T,\mathrm{BoreHole}}$ 110
Figure 56 Reliability index evaluated at design point (Nowak and Collins 2000)..... 139
Figure 57 Graphical representation of normal distribution..... 146
Figure 58 Graphical representation of lognormal distribution 147

INTRODUCTION

Part I: Cone Penetration Test (CPT)

In recent years, the Cone Penetration Test (CPT) has gained popularity as a fast, inexpensive, and fairly accurate method for in-situ characterization of sub-surface soil layers. This is attributed to its ability to obtain nearly continuous measurements providing a much higher data resolution than standard soil sampling procedures. The data obtained from a CPT sounding can be used to determine the soil shear strength (e.g., [*3*], [*4*], and [*5*]), soil classification, in-situ stresses, compressibility, permeability, and other soil properties. The CPT is a simple, quick, and economical test that provides reliable and continuous in-situ soundings of subsurface soil.

In a CPT, a series of metal rods with a cone-shaped tip are pushed into the ground at a constant penetration rate. During this process, load sensors measure the amount of force required to penetrate different soil layers. Mainly, two force components are measured during a CPT: the force acting on the cone (Q_c) and the total combined force acting on the cone and cylindrical friction sleeve located behind the tip (Q_t). The cone resistance (q_c) is calculated as the force (Q_c) divided by the projected area of the cone (A_c), while the sleeve friction (f_s) is calculated as the net force acting on the friction sleeve (Q_t - Q_c) divided by the surface of the sleeve (A_s).

To further improve the interpretation ability of the CPT, pore water pressure transducers were added to the cone; it is referred to as Piezo-Cone Penetration Test (PCPT). Pressure measurements are usually obtained at three locations: the tip of the cone (u_1), behind the cone (u_2), and behind the friction sleeve (u_3). The following sections present a historic background, a detailed description of the CPT/PCPT, and a brief overview of the measured and calculated parameters used to interpret CPT/PCPT data.

Historic Background

The cone penetration test, in its current form, was invented in the Netherlands in 1932 by P. Barentsen. It was referred to as the Dutch cone penetrometer. It consisted of a steel rod with a cone tip sliding inside a metal gas pipe. While the rod was manually pushed in the ground, load measurements were performed at different depths. The apparatus was mainly used by Dutch engineers to determine the ultimate capacity of driven piles in sand [*6*].

The Dutch cone was later improved by Vermeiden and Plantema by adding a conical mantle just above the cone to prevent soil from entering the gap between the rod and the pipe

(Figure 1a) [*7*], [*8*]. A major improvement was introduced by Begemann by adding a friction sleeve behind the cone which enabled the measurement of friction as well as the cone resistance (Figure 1b) [*9*].

Several methods were used over time to advance the cone into the ground. The development of a cone penetrometer that consisted of a conical point connected to the piston of a small hydraulic jack at the base of the rod was reported by Sanglerat [*10*]. He also reported the development of a hydraulic penetrometer by the Centre Expérimental du Bâtiment et des Travaux Publics (CEBTP) in France in 1966. These types of mechanical cones are still in use because of their low cost and simplicity of use [*11*].

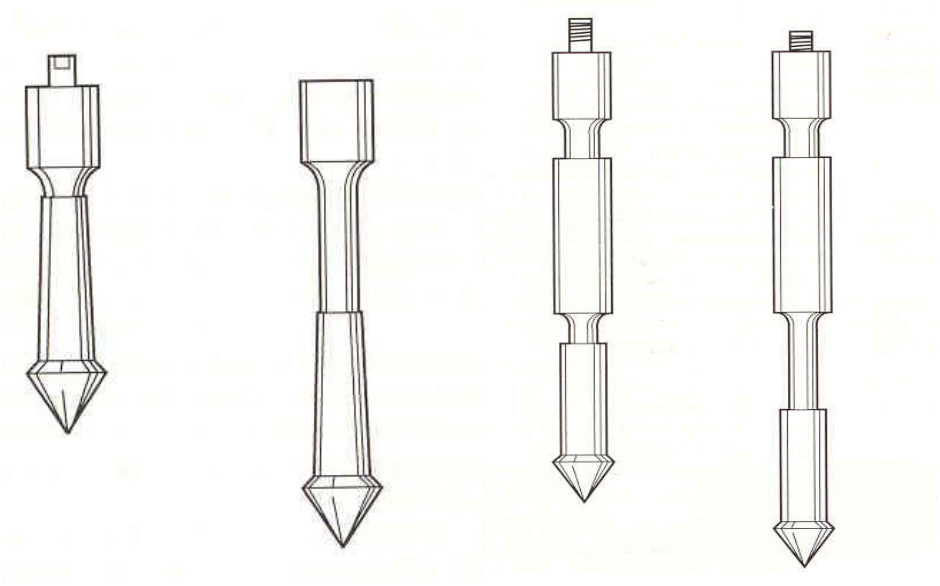

(a) **(b)**

Figure 1
Early cone penetrometers (a) Dutch cone with conical mantle, (b) Begemann cone with friction sleeve [*11*]

Apparatus Description and Correction Factors

A typical CPT apparatus consists of a 60° conical tip with a 10 or 15 cm^2 base and a 150 cm^2 friction sleeve located behind it. Figure 2 illustrates a typical PCPT apparatus showing the geometry of the cone and the friction sleeve in addition to the pore water pressure transducers.

As mentioned earlier, the main parameters measured during a PCPT are the cone resistance (q_c) and the sleeve friction (f_s) in addition to three pore water pressure measurements performed at different locations: u_1 measured on the cone tip, u_2 measured behind the cone, and u_3 measured behind the sleeve. Many methods are employed to obtain the cone resistance and sleeve friction. Most popularly, two load cells are used: one is located behind the cone while the other is located behind the sleeve. The cone resistance is directly obtained from the reading of the first load cell while the sleeve friction is calculated from the difference between the first and second load cell readings. This type is called a "subtraction cone" and is preferred due to the overall robustness of the penetrometer [*13*].

Depending on the cone geometry, sensors' locations, and temperature effects among other factors, several correction factors are suggested in order to ensure the quality of the obtained CPT data and to account for the different types of penetrometers that might be used.

Due to the "unequal area effect," where the pore water pressure acts on the shoulders behind the cone and the sleeve, a cone area ratio (a) is used to correct the obtained cone resistance. It is approximately equal to the ratio of the area of the load cell or shaft to the projected area of the cone. The corrected cone resistance is defined as:

$$q_t = q_c + u_2(1-a) \tag{1}$$

The sleeve friction is also influenced by the unequal area effect; therefore, it is also corrected to account for the difference in the pore water pressure between the front (u_2) and the shoulder (u_3) of the sleeve. The corrected sleeve friction is calculated as:

$$f_t = f_s - \frac{(u_2 \cdot A_{sb} - u_3 \cdot A_{st})}{A_s} \tag{2}$$

where, A_{sb} is the cross sectional area at the bottom of the friction sleeve, A_{st} is the cross sectional area at the top of the friction sleeve, and A_s is friction sleeve surface area. Lunne et al. noted that this correction is rarely carried out because u_3 is seldom measured [*11*]. On the other hand, the pore water pressure at the front of the cone can be estimated from pore water pressure readings at the tip of the cone using the following equation (14):

$$u_2 = u_o + k(u_1 - u_o) \tag{3}$$

where,

u_o = hydrostatic or initial in-situ pore pressure, and

k = adjustment factor (function of soil type and properties)

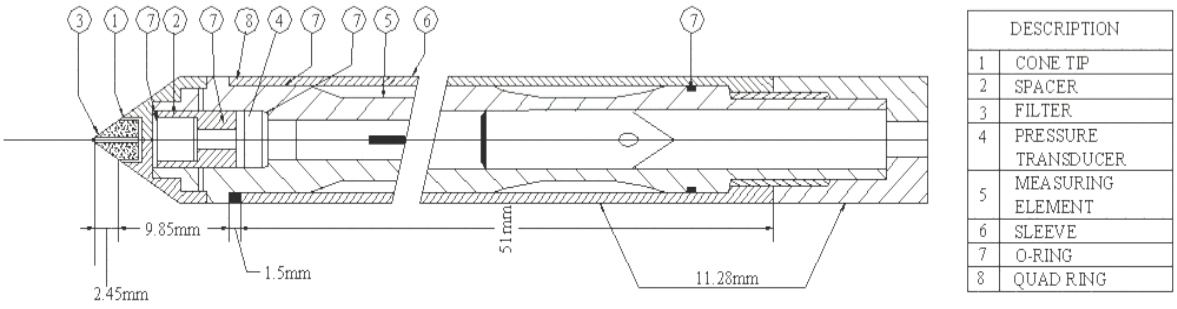

Figure 2
Typical Schematic of Piezocone [*12*]

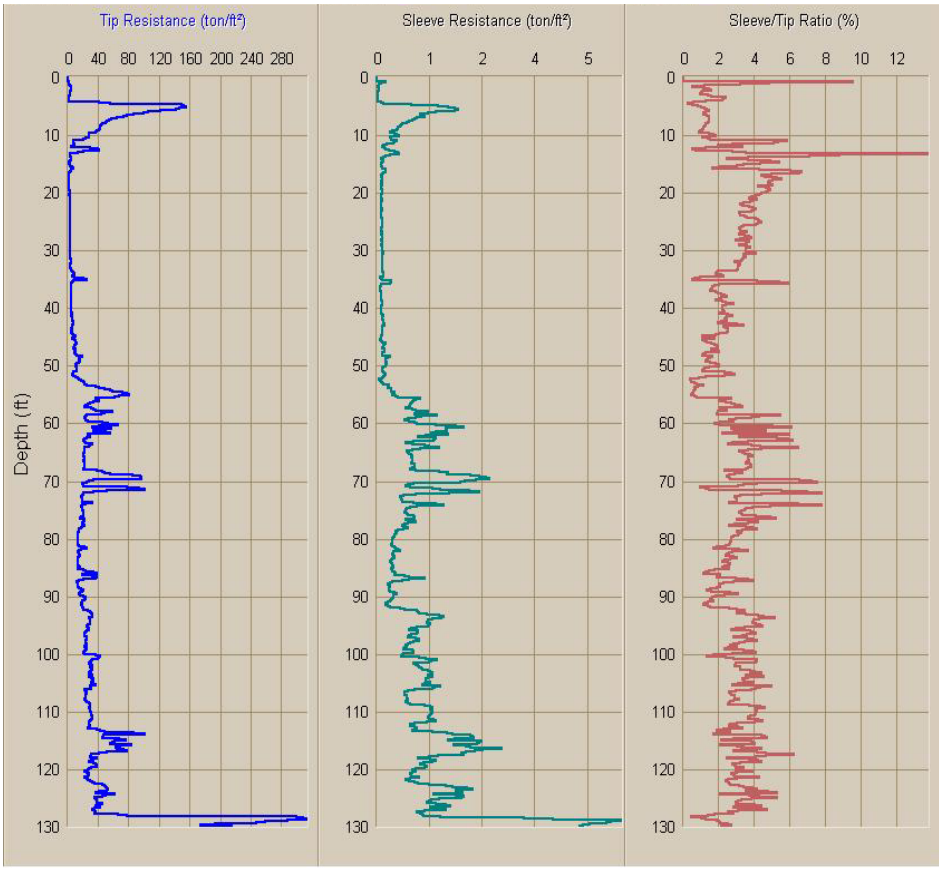

Figure 3
Typical results of CPT

Another parameter commonly calculated from CPT data is the ratio of the sleeve friction to the tip resistance, known as the friction ratio illustrated in equation (4). This parameter is particularly useful in soil classification because different soil types exhibit different relative amounts of tip resistance and sleeve friction. Therefore, this ratio provides a useful tool to determine different soil types. This parameter is usually plotted alongside the tip resistance and sleeve friction when reporting CPT results. An example presentation of CPT data is illustrated in Figure 3.

$$R_f = \frac{f_t}{q_t} \tag{4}$$

Soil Classification using CPT

Data obtained from a CPT can be used to classify the different types of soils along the path of the cone. It was observed that different types of soils exhibit distinctive responses during cone penetration making it possible to classify the soils based on their response. For example, while sandy soils are characterized by high cone resistance and low friction ratio, soft clays produce low cone resistance and high friction ratio [*11*]. Begemann noted that soil type is not a strict function of the tip resistance or sleeve friction but rather a combination of these values [*15*].

Several efforts were made to present a dependable classification chart using cone penetrometer data [*16*], [*17*]. Using an extensive database of CPT results in different soil types, Douglas and Olsen presented a chart that can be used to classify different types of soils using the cone resistance and the friction ratio (Figure 4) [18]. They noted that this classification provides a guide to the soil types based on their behavior and cannot be expected to provide accurate prediction about the soils grain size distribution.

In the following years, different classification charts were suggested using broader soil database; most of them still used the cone resistance and the friction ratio as a basis for classification [*19*], [*20*]. However, it was noticed that even with careful procedures and corrections for pore pressure effects, sleeve friction measurements are often less accurate and less reliable than the cone resistance [*21*], [*22*]. Therefore, classification charts have been proposed based on the tip resistance and pore water pressure [*23*], [*24*], [*25*]. A pore water pressure index B_q was used in the classification; it is defined as [*11*]:

$$B_q = \frac{u_2 - u_o}{q_t - \sigma_{vo}} \tag{5}$$

where,

u_2 = Pore pressure measured between the cone and the friction sleeve,

u_o = equilibrium pore pressure,

σ_{vo} = total overburden stress, and

q_t = cone resistance corrected for unequal end area effects.

In order to perform a more accurate classification scheme, Robertson et al. as suggested classification charts based on all three pieces of data (q_t, f_s, and B_q), shown in Figure 5 [*19*]. These charts classify the soils based on their response to 12 distinct soil types and provide information about the relative density and over-consolidation ratio (OCR) of the soils.

Eslami and Fellenius presented a classification chart based on data obtained from 20 sites in 5 countries [*26*]. They used an "effective" tip resistance parameter ($q_E = q_t - u_2$) to provide a more consistent delineation of envelopes than a plot of only the cone resistance. This parameter along with the sleeve friction were used to classify soils into five main categories as shown in Figure 6.

After comparing several soil classification methods using CPT data, Fellenius and Eslami concluded that the classification methods that do not correct for the pore pressure on the cone shoulder may not be relevant outside the areas where they were developed, and the error due to omitting the pore water pressure is highest in fine grained soils [*27*].

Since soil classification based on CPT data depends on the mechanical properties of the soils, such as strength and compressibility; Zhang and Tumay argued that due to complicated environmental conditions, the correlation between soil and mechanical properties will never be a simple one-to-one correspondence [*2*]. They also indicated that the CPT classification charts do not present an accurate prediction of soil types based on compositional properties but rather a guide to soil behavior type. They suggested an alternative classification method using statistical and fuzzy subset approaches to calculate a soil classification index (U) from CPT data that is used to determine probable Unified Soil Classification System (USCS) (compositional) soil types.

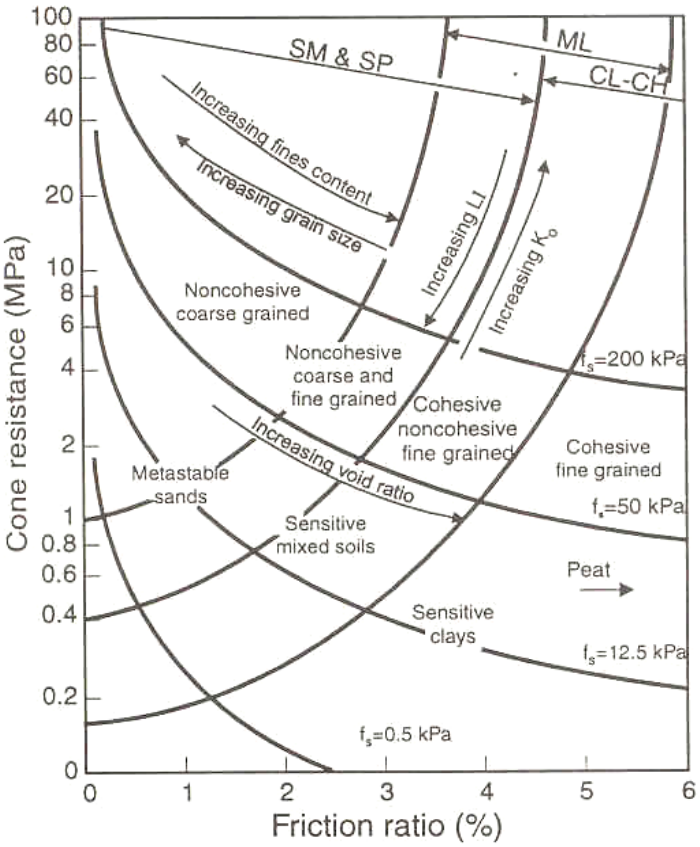

Figure 4
Douglas and Olsen classification chart [*18*]

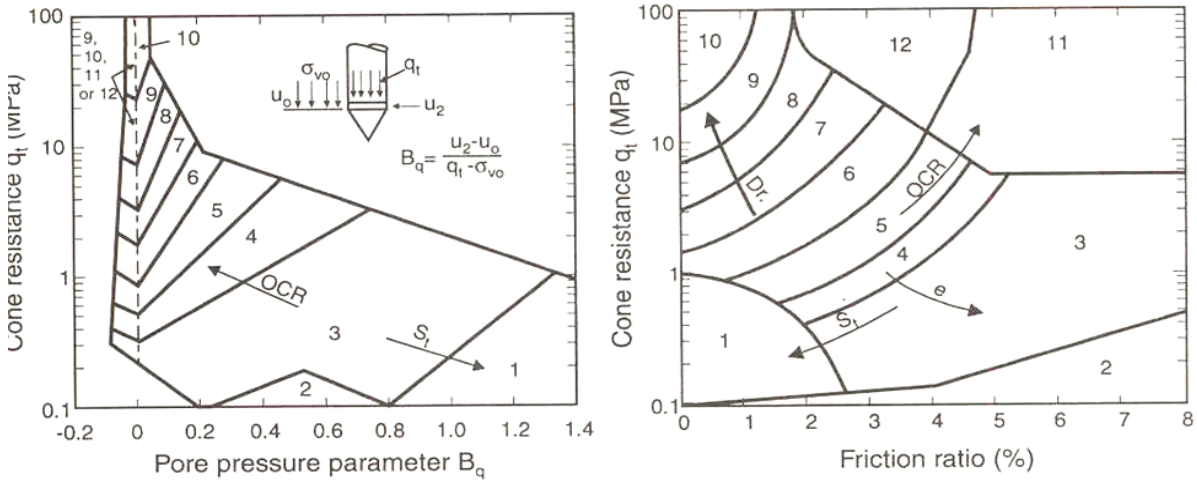

Figure 5

Classification charts presented by Robertson et al. [*19*]

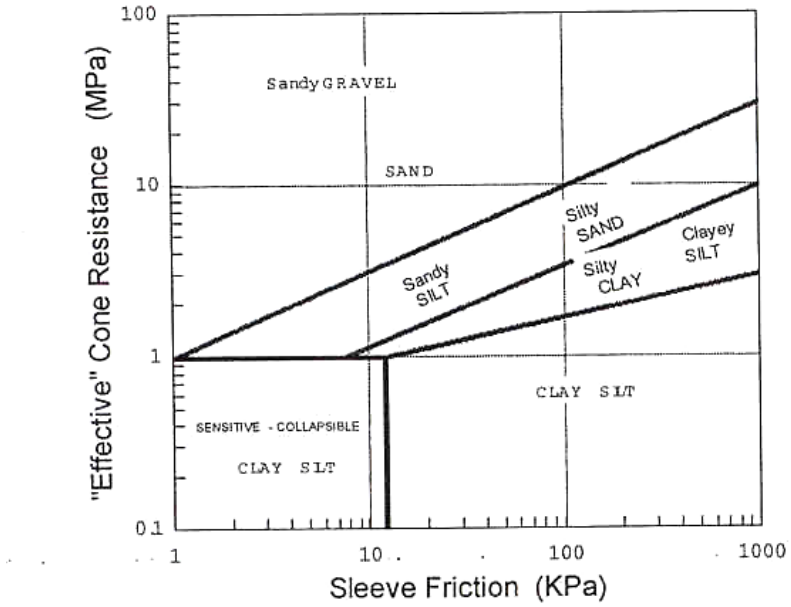

Figure 6

Eslami and Fellenius classification chart [*26*]

This alternative classification method utilizes the fuzzy subset approach which aims to release the constraint of soil composition and put emphasis on the soil behavior instead [*28*], [*29*]. Three empirically defined density functions that correspond to three soil groups are presented: highly probable clay (HPC), highly probable mixed (HPM), and highly probable sand (HPS). The three functions as a whole will reflect the overall perspective of soil properties. This results in a classification that does not yield sharp boundaries between layers but rather a smooth transition from one soil type to another. This statistical approach has been adopted by LADOTD as a standard procedure for the interpretation on CPT data.

Strength Characteristics

Undrained Shear Strength. Many researchers attempted to develop a dependable correlation between the parameters obtained from cone penetration tests and the undrained shear strength of cohesive soils. Some of the presented correlations were based on theoretical solutions like the bearing capacity theory, cavity expansion method strain path method and numerical methods using linear and non-linear soil models [*30*], [*31*], [*32*], [*33*], [*34*]. Other correlations, however, were empirically developed by comparing CPT results with laboratory shear strength experiments.

In theoretical solutions, the undrained shear strength is expressed as a function of the cone tip resistance using the following equation:

$$S_u = \frac{q_c - \sigma}{N_c} \tag{6}$$

where, N_c is a theoretical cone factor, and σ is the in-situ total pressure. Depending on the theory used to calculate N_c, σ can be the total vertical (σ_{vo}), horizontal (σ_{ho}), or mean (σ_{mean}) stress. Table 1 presents a summary of N_c values theoretically derived by different researchers.

Since cone penetration is a complex phenomenon, all theoretical solutions make several simplifying assumptions regarding soil behavior, failure mechanism, and boundary conditions. The theoretical solutions need to be verified from actual field and/or laboratory test data. Theoretical solutions have limitations in modeling the real soil behavior under conditions of varying stress history, anisotropy, sensitivity, aging and micro fabric. Hence,

empirical correlations are generally preferred although the theoretical solutions have provided a useful framework of understanding. Lunne and Kleven presented an equation to predict the undrained shear strength using the total cone resistance [*44*]:

$$S_u = \frac{q_c - \sigma_{vo}}{N_k} \tag{7}$$

where, q_c is the measured cone resistance, σ_{vo} is the in situ vertical stress, and N_k denotes the cone factor that includes the influence of the cone shape and depth factor; its value typically ranges from 11 to 19 for normally consolidated clays [*11*]. Kjekstad et al. reported a N_k value of 17 for over-consolidated clays [*45*]. Equation (7) was later modified where the corrected cone resistance (q_t) was used:

$$S_u = \frac{q_t - \sigma_{vo}}{N_{kt}} \tag{8}$$

Many experiments were performed to estimate the value (or range of values) for N_{kt} [*46*], [*47*], [*48*]. A wide range of values were reported depending on the type of cone, field conditions, penetration rate and laboratory testing method. However, most of the reported values of N_{kt} ranged between 10 and 30.

Table 1
Nc values theoretically derived by different researchers [*11*]

$N_c(\phi = 0)$	σ_i	Remarks	Reference
7.41	σ_{vo}		[*35*]
7.0	σ_{vo}		[*36*]
9.34	σ_{vo}	Smooth Base	[*37*]
9.74	σ_{vo}	Rough Base	
9.94	σ_{vo}		[*38*]
$\frac{4}{3}\left[1+\ln\frac{E_t}{3s_u}\right]+1$	σ_{vo}	Spherical cavity expansion, E_t: initial tangent modulus	[*37*]
$\frac{4}{3}\left[1+\ln\frac{E_s}{s_u}\right]+1$	σ_{vo}	Spherical cavity expansion, E_s: secant modulus at 50% failure	[*39*]
$\frac{4}{3}\left[1+\ln\frac{E_s}{3s_u}\right]+\cot\theta$	σ_{vo}	Spherical cavity expansion	[*40*]
$\frac{4}{3}\left[1+\ln\frac{E_s}{s_u}\right]+\cot\theta$	σ_{vo}	Spherical cavity expansion, finite strain theory	[*40*]
$\frac{4}{3}\left[1+\ln I_R\right]$	σ_{vo}	Spherical cavity expansion	[*31*]
$\frac{4}{3}\left[1+\ln I_R\right]+2.57$	σ_{mean}	Spherical cavity expansion	[*31*]
$\left[1+\ln I_R\right]+11$	σ_{ho}	Cylindrical cavity expansion	[*41*]
$\frac{s_a}{s_u}+\frac{4}{3}\frac{s_r}{s_u}\left[1+\ln\frac{E_r}{3s_{ur}}\right]+\frac{4}{3}$	σ_{vo}	Trilinear stress-strain relationship	[*42*]
$\left[\frac{E_u/s_u - E_r/s_{ur}\cdot s_{ur}/s_u}{E_u/S_u - E_r/s_{ur}}\right]\ln\frac{E_u}{s_u}\frac{s_{ur}}{E_r}$ $+0.19+2.64\ln(I_r)-\frac{\sigma`_{vo}}{s_u}(1-K_o)+2\alpha$	σ_{vo}	Elastic perfectly plastic- strain path approach	[*43*]

θ: semi apex angle; IR: rigidity index.

Another equation was suggested by Senneset et al. using the effective in lieu of the total cone resistance [*49*]:

$$S_u = \frac{q_E}{N_c`} = \frac{q_t - u_2}{N_c`} \tag{9}$$

They reported an average value of 15 for $N_c`$ with a likely variation of ±3. They also noted that $S_u$ values are particularly questionable for small excess pore pressures corresponding to $B_q < 0.4$ that is for materials coarser than clayey silt. Using the same equation, Lunne et al. reported $N_c`$ values of 1 to 13 [*50*]. Campanella and Robertson noted that although this method might work well for some deposits, it is not recommended to use the effective cone resistance to estimate S_u [*51*]. They explained that in soft normally consolidated clays, the total pore pressure behind the cone is approximately 90 percent or more of the measured cone resistance. This results in a very small value of q_c that is very sensitive to small errors in q_u or u_2 measurement.

Several other researchers attempted to use the excess pore water pressure ($\Delta u = u_2 - u_o$) to estimate the undrained shear strength [*31*], [*52*], [*53*], [*54*], [*55*]. They used:

$$S_u = \frac{\Delta u}{N_{\Delta u}} \tag{10}$$

The obtained values of $N_{\Delta u}$ were between 2 and 20. One advantage of these methods over the effective cone resistance method is that Δu can be very large, especially in soft clays, making the effect of measurement errors less significant and resulting in a better accuracy for this method.

Based on cavity expansion theory, Massarch and Broms presented a semi-empirical solution that included the effects of overconsolidation and sensitivity of soils by using Skempton's pore pressure parameter at failure (A_f) [*55*]. They presented a set of charts to obtain S_u based on excess pore pressure measurements (Figure 7).

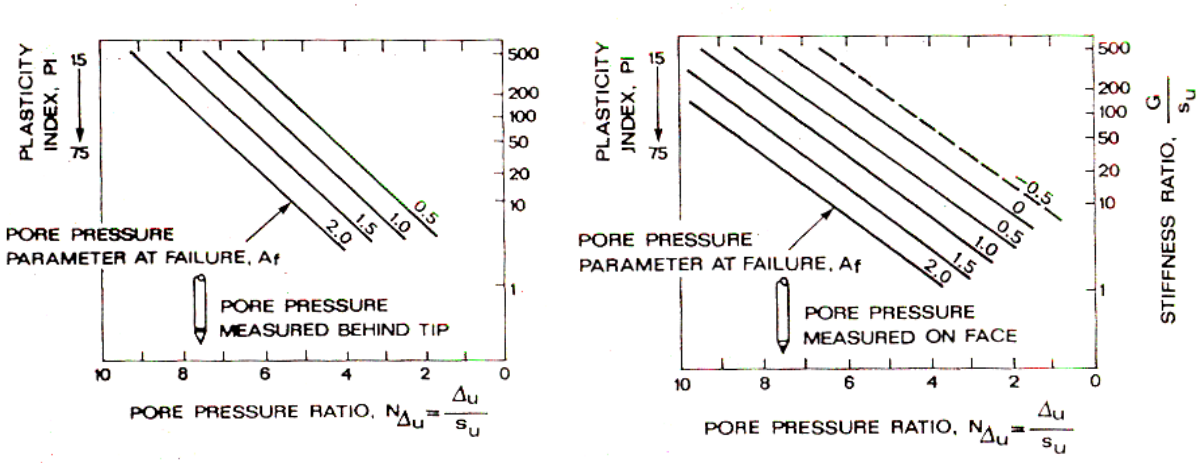

Figure 7

Charts to obtain S_u from excess pore water pressure measurements [*51*]

Effective Stress Strength Parameters

Many correlations were suggested to calculate the effective stress parameters: friction angle φ` and attraction a ($= \frac{c}{\tan \varphi`}$) from CPT data. Using the bearing capacity approach based on the theory of plasticity, Senneset et al. presented a theoretical approach for using PCPT data to determine the effective stress parameters [*49*]. However, Campanella and Robertson argued that since this method is based on the bearing capacity theory and as with any method for determining drained parameters from undrained cone penetration, it can be subject to serious problems [*51*]. One of which is the location of the porous element, where different locations give different measures of the total pore pressures.

Keaveny and Mitchell suggested another method that uses empirical correlations to estimate the overconsolidation ratio (OCR), Skempton's pore pressure parameter (A_f), lateral earth pressure parameter (K_o), and Vesic's cavity expansion method to estimate the undrained shear strength (S_u) [*56*]. These parameters are used to estimate the effective stress at failure, which combined with S_u to provide an estimate of the effective stress strength parameters. They reported good results for silts and overconsolidated clays; however, results for normally consolidated clays were poor. Although this method accounts for different pore pressure

measurement locations, it relies on simplified empirical correlations to estimate OCR, A_f, and K_o, which could cause poor interpretations [*51*].

Senneset et al. presented another solution based on the bearing capacity theory [*57*]. They suggested two parameters that can be calculated from measured PCPT data:

The cone resistance number: $$N_m = \frac{q_t - \sigma_{vo}}{\sigma`_{vo} + a} \quad (11)$$

The pore pressure ratio: $$B_q = \frac{u_1 - u_o}{\sigma`_{vo} + a} \quad (12)$$

where, $\sigma`_{vo}$ is the effective overburden pressure. The friction angle is then found from an interpretation chart based of the two parameters in addition to the angle of plastification (β) which expresses an idealized geometry of the generalized failure zones around the advancing cone. Figure 8 presents example interpretation charts.

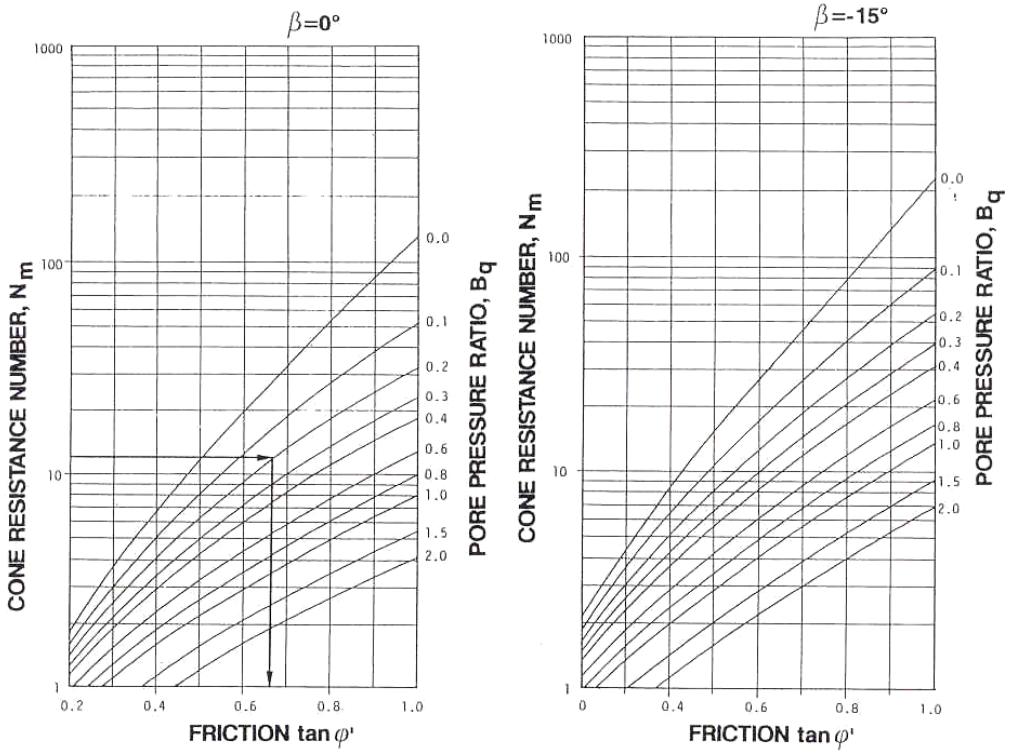

Figure 8
Interpretation diagrams for β = 0 and β = -15^o [*57*]

Stress History

Stress history can be expressed by either defining the maximum past effective stress $\sigma`_p$ or the over-consolidation ratio OCR ($=\sigma`_p/\sigma`_v$). Many approaches were suggested to correlate CPT data to stress history parameters. Based on data collected from high quality undisturbed specimens; Lunne et al. presented a set of charts to predict OCR from CPT measurements (Figure 9) [*58*]. They noted that these figures are based on local correlations and should be updated as local experience is obtained.

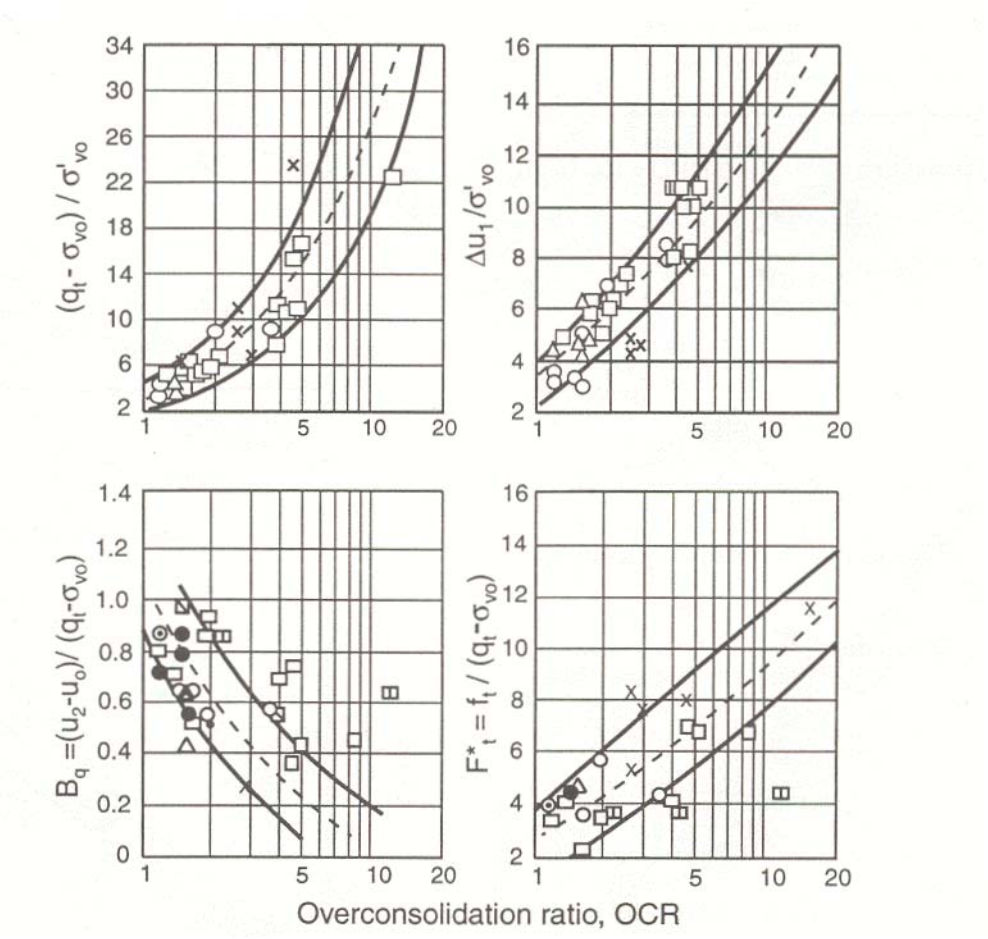

Figure 9
Empirical correlations of OCR vs. normalized PCPT parameters [*58*]

On the other hand, Sully et al. presented an expression for OCR based solely on pore pressure measurements, which is shown in equation (13) [*59*]. This correlation, however, cannot be extended to clays with very high OCR values.

$$OCR = 0.66 + 1.43\left(\frac{u_1 - u_2}{u_o}\right) \tag{13}$$

After reviewing the methods used to obtain OCR from CPT measurements, Mayne suggested an expression based on critical state soil mechanics and cavity expansion theory [*60*]:

$$OCR = 2\left[\frac{1}{1.95M + 1}\left(\frac{q_t - u_2}{\sigma`_{vo}}\right)\right]^{1.33} \tag{14}$$

As a first order estimate, Mayne suggested an expression to predict $\sigma`_p$ using the corrected tip resistance $q_t$, i.e., equation (15) [*61*]. While this expression yielded good estimates of $\sigma`_p$ for a wide variety of clays, it underestimated the values for fissured clays. Figure 10 presents a comparison between the values of $\sigma`_p$ obtained from one-dimensional oedometer test and the values predicted by equation (15).

$$\sigma`_p = 0.33(q_t - \sigma`_v) \tag{15}$$

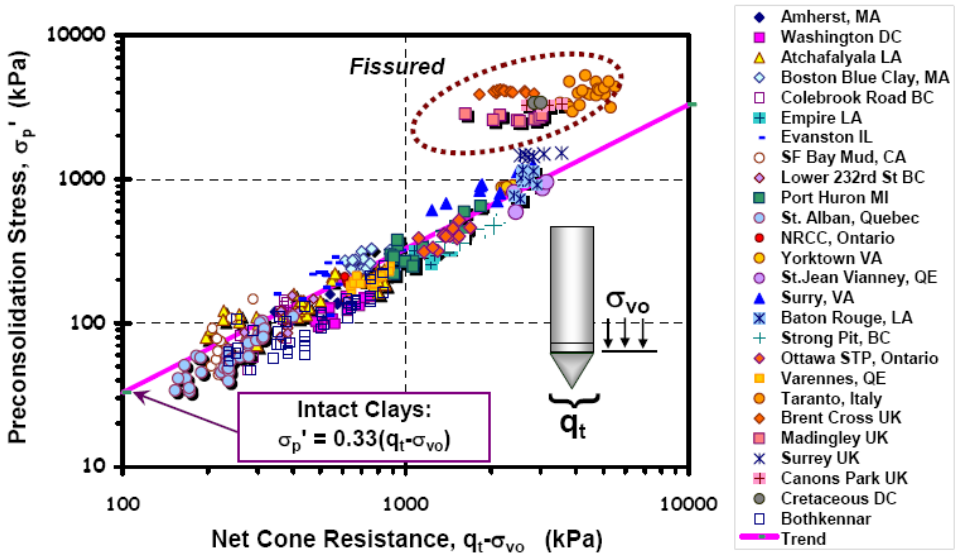

Figure 10

Comparison between the measured and predicted $\sigma`_p$ values [*62*]

Chen and Mayne presented a set of expressions to estimate $\sigma_p^{'}$ incorporating pore water pressure measurements, i.e., equations (16) through (19) [*63*]. They argued that the redundancy of expressions give an opportunity to confirm the value of the calculated parameter in case they agree and gives a reason to further investigate the results if a discrepancy exists [*62*].

$$\sigma`_p = 0.41(u_1 - u_o) \tag{16}$$

$$\sigma`_p = 0.53(u_2 - u_o) \tag{17}$$

$$\sigma`_p = 0.75(q_t - u_2) \tag{18}$$

$$\sigma`_p = 0.60(q_t - u_2) \tag{19}$$

Not as many correlations were presented for determining OCR for sandy soils. This is because it is more challenging to determine the stress history for sandy soils. Mayne noted that this challenge is caused by two main reasons: (1) one dimensional oedometric experiments for sandy soils yield a fairly flat e-log(σ`) curve making it difficult to detect the pre-consolidation pressure, and (2) it is difficult to obtain undisturbed specimens of sandy soil deposits [*62*]. Therefore, a relationship to obtain OCR for clean sands was empirically derived based on data from 24 calibration chamber experiments [*11*], [*64*]:

$$OCR = \left[\frac{0.192 \cdot (q_t / p_a)^{0.22}}{(1 - \sin\phi`) \cdot (\sigma`_{vo} / p_a)^{0.31}} \right]^{\left(\frac{1}{\sin\phi` - 0.27}\right)} \tag{20}$$

Relative Density from CPT Data

The relative density (D_r) of sands is an important engineering index property that gives an indication about the level of compaction (or density) that can be used to estimate other properties like the angle of internal friction. It is traditionally calculated as:

$$D_r = \frac{e_{\max} - e}{e_{\max} - e_{\min}} \tag{21}$$

where, e is the void ratio, and e_{max} and e_{min} are the maximum and minimum void ratios. It is well known that it is difficult to obtain reliable values for e_{max} and e_{min} because of variations

in sample preparation procedures (e.g., compaction effort) and their dependency on the operator. Therefore, CPT can provide a useful alternative for determining the in-situ relative density of sands.

D_r is commonly related to the cone tip resistance (q_c) with consideration to the overburden pressure ($\sigma`_v$) and soil compressibility [*65*]. Baldi et al. performed calibration testing on clean Ticino silica sand that has a moderate compressibility and proposed the following equation [*66*]:

$$D_r = c_1 \cdot \ln\left(\frac{q_c}{c_2 \cdot \sigma`_v^{c_3}}\right) \tag{22}$$

where, c_1, c_2, and c_3 are constants dependent on the compressibility; their values for high, moderate, and low compressibility sands are presented in Table 2.

Table 2
Constants for determination of D_r [*65*]

Compressibility	c_1	c_2	c_3
High	0.35	68.1	0.35
Moderate	0.41	157	0.55
Low	0.42	53.6	0.81

Based on experiments performed on clean fine to medium silica sands, Kulhawy and Mayne suggested the following formula [*67*]:

$$D_r^{\,2} = \frac{1}{305 \cdot Q_c \cdot OCR^{0.15} \cdot Q_A} \cdot \frac{q_c}{p_a} \cdot \left(\frac{p_a}{\sigma`_v}\right)^{0.5} \tag{23}$$

where,

p_a = atmospheric pressure;

OCR= over-consolidation ratio;

Q_c= compressibility factor, suggested values for this factor are summarized in Table 3; and

Q_A= Aging factor, defined as:

$$Q_A = 1.2 + 0.05 \log\left(\frac{t}{100}\right) \tag{24}$$

where, t is time. The previous correlations used calibration chamber testing without considering the boundary effects. Jamiolkowski et al. re-examined a large set of calibration chamber tests and presented another expression for D_r that incorporates the boundary effects, [*68*].

Table 3
Suggested Q_c values [*67*]

Compressibility	Description	Q_c
Low	Predominantly quartz sands, rounded grains with little or no fines	0.91
Medium	Quartz sands with some feldspar and/or several percent fines	1.00
High	High fines content, mica or other compressible materials	1.09

$$D_R = 100 \cdot \left[0.262 \cdot \ln\left(\frac{q_t / p_a}{\sqrt{\sigma`_{vo} / p_a}} \right) - 0.675 \right] \tag{25}$$

Kulhawy and Mayne used a database of 24 sands to establish a simpler correlation that uses an empirical constant of the least-square regression Q_F, [*67*].

$$D_r^{\,2} = \frac{1}{Q_F} \cdot \left(\frac{q_c / p_a}{\left(\sigma`_v / p_a\right)^{0.5}} \right) \tag{26}$$

Juang et al. argued that although the previous methods are based on the compressibility of soils, compressibility itself is not well defined [*69*]. It is influenced by mineral type, particle angularity, particle gradation, particle size, particle surface roughness, and stress history. They also noted that sands with the same mineral type could be under different categories of compressibility (low, medium, or high) depending on D_r and stress history.

Based on these observations, they presented an approach using fuzzy sets to determine D_r from CPT data. In this method, the friction ratio R_f is used to calculate three weight factors (W_L, W_M, and W_H) that correspond to the three compressibility categories (low, medium, and high, respectively). These factors reflect how close the actual compressibility is to each of the three predefined categories. They also calculated three values of D_r corresponding to each of the three categories (Dr_L, Dr_M, and Dr_H) using the Kulhawi and Mayne model, i.e., equation (*26*). A weighted D_r value is then calculated as:

$$D_r = Dr_L \cdot W_L + Dr_M \cdot W_M + Dr_H \cdot W_H \tag{27}$$

Correlations with Standard Penetration Test (SPT)

The standard penetration test is the most widely used method for in-situ characterization of subsurface soils. While CPT is gaining popularity as a simple, fast and reliable in-situ testing tool, many researchers attempted to develop correlations between CPT measurements and SPT *N* value [*70*], [*71*], [*17*], [*72*]. The relation between CPT and SPT is usually expressed as the ratio of the tip resistance to the *N* value (q_c/N). Robertson et al. compiled the results for a number of studies correlating q_c/N to the mean grain size and soil type (Figure 11) and demonstrated that q_c/N_{60} ratio increases with increasing grain size [*19*]. They also noted that the scatter in results also increases with increasing grain size. Equations (28) and (29) show that q_c and N were also correlated with the mean particle size (d_{50}) and the fines content (FC – passing sieve #200). Lunne et al. noted that if no grain size distribution is available for the in-situ soils, classification charts can be used to estimate d_{50} or FC [*11*].

$$\left(\frac{q_c}{p_a}\right) \cdot N = 5.44 \cdot D_{50} \tag{28}$$

$$\frac{(q_c/p_a)}{N} = 4.25 - \frac{FC}{41.3} \tag{29}$$

Jefferies and Davies developed an algorithm for estimating SPT N_{60} value from PCPT data without soil sampling [*73*]. They presented an equation that uses a soil classification index I_c to calculate q_c/N_{60} ratio, i.e., equation (30). Typical I_c ranges for different soil types are presented in Table 4.

$$\frac{q_c(MPa)}{N_{60}(Blows/300mm)} = 0.85\left(1 - I_c/4.75\right) \tag{30}$$

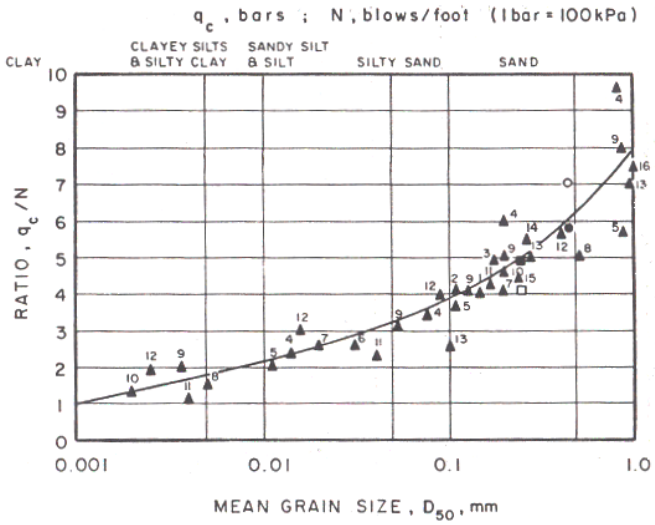

Figure 11
Variation of q_c/N with d_{50} [*19*]

Table 4
Typical I_c ranges for different soil types [*73*]

I_c	Soil Classification
$I_c < 1.25$	Gravelly sand
$1.25 < I_c < 1.90$	Sands – clean sand to silty sand
$1.90 < I_c < 2.54$	Sand mixtures – silty sand to sandy silt
$2.54 < I_c < 2.82$	Silt mixtures – clayey silt to silty sand
$2.82 < I_c < 3.22$	Clays

Part II: Load and Resistance Factor Design (LRFD)

Most civil engineering design codes have been adopting the Load and Resistance Factor Design (LRFD) philosophy and moving away from the Allowable (Working) Stress Design (ASD) approach. This shift may be attributed to the many shortcomings associated with ASD such as:

- the inability to address the different levels of uncertainty associated with calculations/estimations of both loads and resistances;
- the inability of addressing stress concentrations, stress interactions, and residual stresses;
- the assumption that materials are elastic and are not representative of the condition at failure;
- the treatment of different kinds of load (e.g., dead and live) as if they share the same variability; and
- the designed members lack a uniform probability of failure.

In the U.S., the American Concrete Institute (ACI) was the first to adopt LRFD in its 1963 Building Code Requirements for Concrete Structures (ACI 318). Today, design codes for concrete (ACI 318-05), steel (AISC 2001), and highway bridges [*74*] are all based on the LRFD design philosophy. LRFD design codes appear to be deterministic to their user; while in fact they are probabilistically calibrated to ensure that a target risk level is not exceeded. This is achieved using a number of design coefficients that help account for excessive overloading conditions (load factors) and unforeseen strength deficiencies (resistance factors). In general, the main design equation is usually given as:

$$\phi R_n \geq \sum_i \gamma_i Q_i \tag{31}$$

where, R_n is the nominal capacity of the designed member, ϕ is a resistance factor, Q_i is the demand due to applied loads (dead, live, etc.), and γ_i is the load factor. The development of LRFD codes was initially started for structural applications. The resistance of structural components has variabilities associated with it; however, more uncertainty is inherent in loads than in resistance. Geotechnical applications are unique in the sense that uncertainties

are high on the resistance side as well. Nevertheless, LRFD research ensued in the geotechnical engineering community early on to develop a rational design methodology based on available statistical information of geotechnical applications.

LRFD in Geotechnical Applications

Hansen investigated the use of independent load and resistance factors for geotechnical applications within a Limit State Design (LSD) framework [*75*]. This work was later formulated into code where the resistance factors were applied to the soil properties rather than the nominal resistance [*76*]. Over the last decade, several researchers investigated the application of LRFD in geotechnical applications. The efforts covered a wide range of applications such as offshore structures general foundation design and deep foundations [*77*], [*78*], [*79*], [*80*], [*81*]. The findings of NCHRP Project 24-04 established load and resistance factors for transportation foundations that were incorporated in the AASHTO LRFD Bridge Design Specifications [*80*], [*82*]. NCHRP Project 20-07 (Task 88) dealt with LRFD design of retaining walls which was further investigated in NCHRP Project 12-55 for earth pressure in general terms [*83*], [*84*]. In another effort through NCHRP Project 24-17, Paikowsky et al. conducted a study to develop resistance factors that focused on driven piles and drilled shaft foundations, which are recommended for inclusion in Chapter 10 of the latest version of AASHTO-LRFD [*74*], [*85*].

Despite the extensive efforts in this field, the geotechnical profession has not fully accepted the new load and resistance factors developed for AASHTO-LRFD. This is one of the most difficult hindrances of LRFD to implement in geotechnical applications. As a result, more research studies have been conducted to alleviate doubts and overcome the reluctance in the geotechnical community. For example, Allen developed geotechnical resistance factors and downdrag load factors for LRFD foundation strength limit state design based on the information used in NCHRP Projects 12-04 and 12-17 [*86*]. These efforts cover a wide range of geotechnical applications including shallow foundations, deep foundations, and retaining structures [*86*], [*87*], [*88*], [*89*], [*90*], [*91*], [*92*].

There are two main approaches for addressing uncertainties in geotechnical applications. In the first approach, uncertainties are dissected to their main sources and each source is investigated methodically in a rational way. The main sources of uncertainty for geotechnical applications include inherent soil variability, measurement errors, and expression

(transformation model) uncertainty. Figure 12 shows a schematic of these sources [*93*]. Several researchers used this approach to study geotechnical design within a reliability based framework [*94*], [*95*].

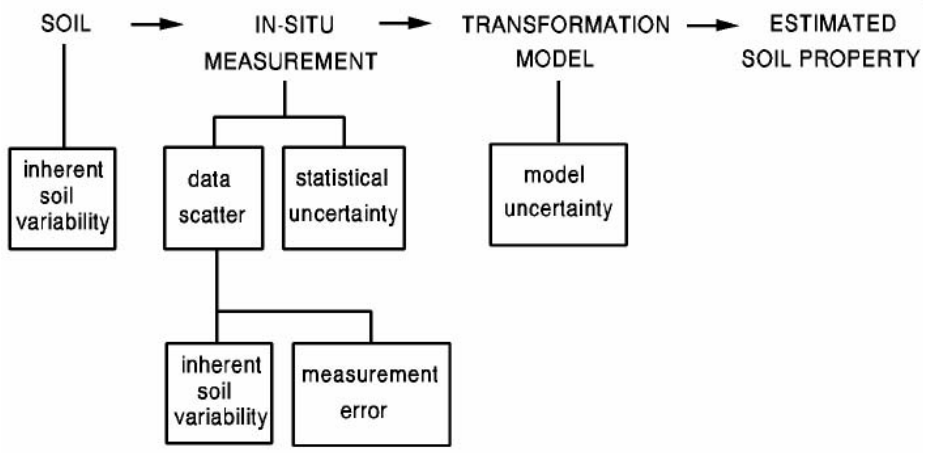

Figure 12
Uncertainty in soil property estimates [*93*]

Conversely, reliability studies for geotechnical applications are often conducted at the foundation capacity level rather than the soil property level. In this second approach, the resistance of the component is investigated by comparing analytical estimates with experimental results for which a database of available results is assembled. This approach helps in overcoming the complexity and lack of information that may exist at the soil property level. Several researchers followed this approach. Investigations of reliability methods as related to Cone Penetration Test (CPT) are relatively limited. Babu et al. studied cone tip resistance (q_c) data obtained from a static cone penetration test on a stiff clay deposit [*98*]. The data from these tests were analyzed by using random field theory, which estimated statistical parameters such as the mean, variance, and autocorrelation function. These parameters were then used in evaluating the reliability of the allowable bearing capacity of a strip footing founded on the above deposit. Abu-Farsakh and Nazzal investigated the reliability of seven interpretation methods for the piezocone penetration test (PCPT) in estimating the vertical coefficient of consolidation, c_v, of cohesive soils [*99*]. Six Louisiana sites were included in the study where piezocone penetrations were conducted and high-quality Shelby tube samples were collected to serve as reference. Estimates of c_v were

obtained using six different methods and compared to the oedometer laboratory. The authors concluded that the scatter was generally high. However, two of the six methods appeared to better predict c_v than the other methods. Roy et al. compared the reliability of the Self-boring Pressuremeter Test (SBPMT), which is often regarded to be less reliable, with the Cone Penetration Test (CPT) for seven sand silt sites in western Canada [*100*]. They concluded that observations do not support the notion of a general lack of reliability of the self-boring pressuremeter at sand-silt sites.

Several researchers studied the reliability of CPT as a feasible tool for identifying the probability of soil liquefaction for a given factor of safety. For example, Liu and Chen used data from 49 sites (71 cone penetrations) to develop statistical parameters for cone tip resistance, q_c, sleeve friction, f_s, groundwater Table, GWT, and soil unit weight, γ [*101*]. This information was then used to treat each parameter as a random variable in analyzing both demand (cyclic resistance ratio – CRR) and resistance (cyclic stress ratio – CSR). Based on this information, Monte Carlo simulations were conducted to determine soil properties in unsampled sites, which were then used to map the liquefaction potential.

Juang et al. also studied the liquefaction potential using CPT results after accounting for parameter and/or model uncertainties [*69*]. The First-order Reliability Method (FORM) was used to estimate the reliability index, β, based on a limit state function involving CRR, CSR, and the model uncertainty, c1. Each of the six input parameters (q_c, f_s, σ_v, $\sigma_v^{'}$, $a_{\max}$, and M_w) was considered to be a random variable and correlation between these parameters was accounted for. The study used a database of 96 liquefaction case histories to determine these parameters, where they considered spatial variations using Bayesian mapping functions. The authors concluded that traditional liquefaction boundaries are often biased on the conservative side, which may lead to erroneous post-earthquake investigations.

OBJECTIVE

The main objective of this research is to update the correlations that are currently used to interpret CPT and PCPT data for engineering design purposes and to assess the reliability of using CPT and PCPT data to predict soil shear strength in both the magnitude and spatial variations in the field with respect to the LRFD methodology. Specifically the following objectives will be fulfilled by this research:

1. Collect the available CPT and PCPT soundings with the corresponding boring log data from the LADOTD and other possible sources. Process/analyze the data and update the correlations of the shear strength and soil classification, which are currently used by the design section of LADOTD.
2. Evaluate the spatial variations of soil engineering properties in the field. Develop the Louisiana CPT database for corresponding engineering properties as a general guideline for design purposes with reliability consideration in preparation for use in the LRFD method.

SCOPE

This study focuses on the utilization of the CPT to estimate undrained shear strengths, S_u, which is an important soil property for structural projects in Louisiana. While methodologies used in this study are applicable to any location where CPT's can be used, the study was limited to data obtained from Louisiana projects; hence, it is a direct representation of soil conditions in the state. Initially, the objective was to perform a complete study on the effects of spatial variations on the reliability of CPT results. However, because of the limited amount of data that the research team was able to collect, it was only possible to study the soil depth, *h*, parameter on the results. A complete investigation of this parameter should also cover the geographic location, which was not possible as can be seen from the sparsely covered maps showing CPT locations included in the database. The research team compensated for this hurdle by studying other factors that are somewhat related to spatial variations albeit indirectly (e.g., soil classification).

As more CPT data is included in the database, it will be possible to extend this study and cover such parameters that were not covered in the current study.

METHODOLOGY

CPT Database

Three databases were created for this study:

- The first database is GIS-based where all information pertinent to CPT and borehole data was merged such that they could be easily retrieved by engineers via a GIS-based user interface.
- The second database is Excel-based and is a compilation of analyses conducted for each CPT sounding identified for this study. The analyses in this database are mainly based on LTRC CPT computer program and a special excel template.
- The third and final database is an extraction of data points from the second database. This database was used for the reliability-based calibration of the CPT coefficient, N_{kt}.

The following sections describe the details about these databases.

Locating CPT Sites using GIS

CPT projects data were received from LADOTD in the form of paper documents containing CPT logs, borehole logs, and project maps. The data also included electronic raw (voltage) CPT data. The first task was to create an electronic archive of all the CPT sites using the geographic information system ArcView. However, most of the projects did not include the spatial coordinates of the CPT soundings. Therefore, in order to find the CPT coordinates, a procedure was implemented utilizing readily available high resolution satellite imagery along with digital orthophoto quarter quad (DOQQ) images.

In some recent projects, aerial images and/or high resolution maps of the project location were included in the project documents making it fairly easy to identify the location of the CPT soundings; however, in most projects such maps were missing. The documents only contained a map of the project location with the CPT soundings marked on it. Therefore, to find the accurate coordinates of every CPT point, some specific (stationary) features in the paper project map were located in the GIS satellite imagery using Google Earth. Such features included street intersections, buildings, bridges, and rivers. By determining the

locations of the CPT tests relative to these features in the paper project document, the points were marked on the electronic maps and the Latitude and Longitude data for each CPT sounding were determined and recoded. Moreover, station numbers of the CPT soundings were used to confirm the recorded coordinates where the distance between the points were compared to the distance calculated from the station numbers.

In many cases, the satellite imagery provided by Google Earth did not have sufficient resolution for the features to be accurately located. This issue was encountered when the projects where in remote locations away from inhabited areas. Therefore, an alternative method was implemented to locate the CPT soundings in such location. High resolution DOQQ images were acquired from the LSU ATLAS website for these locations. These images have much higher resolution; however, they had very large sizes and small land coverage area per images. Downloading and displaying these images was time-consuming and required much more computer storage space. Therefore, this procedure was used only when locating the CPT coordinates was not possible using Google Earth. These procedures were used to attempt to locate the CPT soundings in all the projects from LADOTD as well as LA1 project data received from Soil Testing Engineers (STE) Company.

Although the mentioned procedures were successful in determining the accurate locations of many CPT soundings, it was not possible to apply this procedure on all the CPT data received from LADOTD for different reasons. For example, some paper project documents could not be located for the files received in electronic format (raw CPT data), while in other instances, the project documents were located; however, they did not include the project maps, so it was not possible to pinpoint the location of the CPT project. After locating all the CPT soundings and recording their coordinates, ArcMap was used to plot all the CPT locations on a map of Louisiana. Figure 13 displays the CPT projects located using the mentioned procedures.

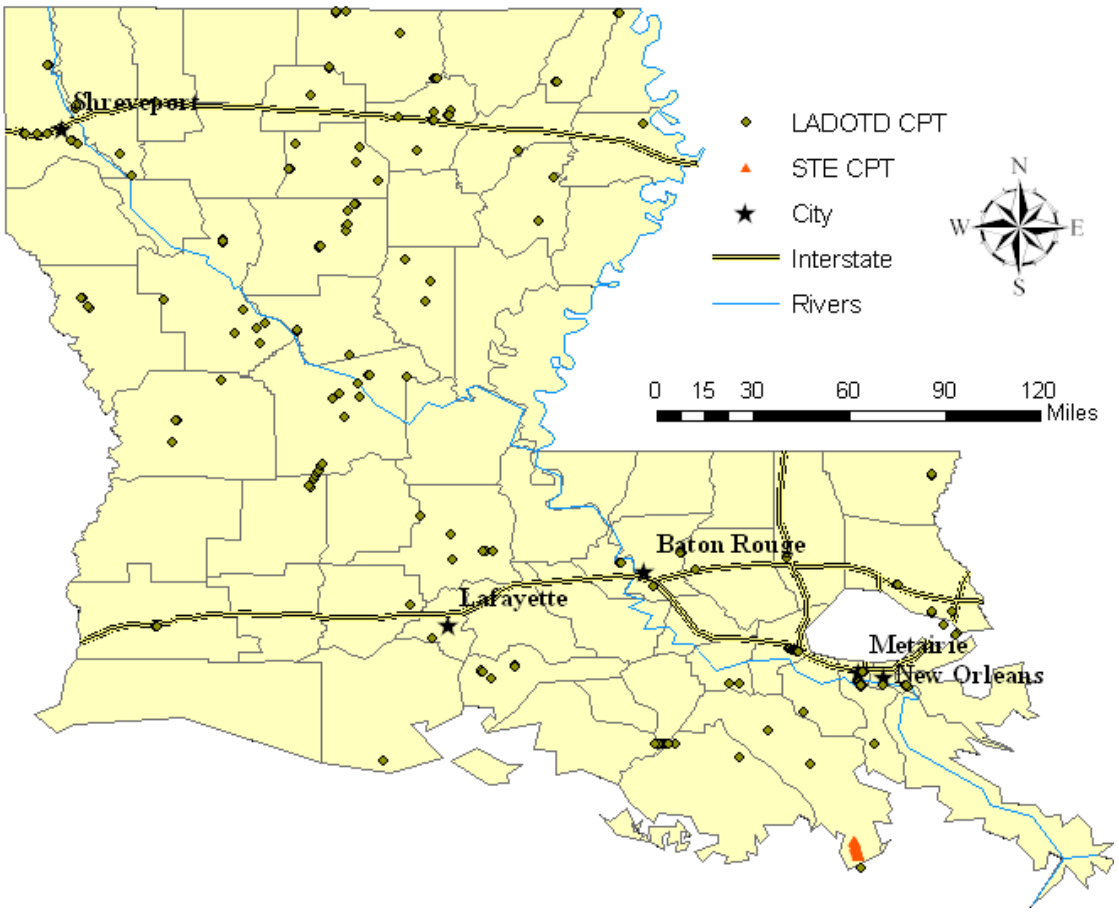

Figure 13
CPT data points from LADOTD and STE

Borehole Data

The next step was to match the CPT data with adjacent borehole data. Therefore, for every CPT sounding, one or more boreholes were identified based on the distance from the CPT to allow for the comparison of parameters obtained from boreholes and CPT. The borehole data were included in the paper project documents; therefore, all the data had to be input into the excel spreadsheet to allow for the comparison. For every borehole, the density, water content, Atterberg limits, and undrained shear strength were recorded at different depths (when available as a measurement in the borehole log) to be later used in the correlation with the CPT data. Moreover, Atterberg limits were used to obtain the USCS classification based on the plasticity chart if the soil is fine-grained.

The borehole data was not available for all the located CPT soundings. Efforts were made to obtain any available data from LADOTD electronic archives as well as paper project documents. Figure 14 illustrates the projects where the borehole data was located along with the projects where the data could not be located. In summary, a total of 752 CPT soundings were documented, of which 503 were matched with adjacent boreholes, and 249 did not have adjacent borehole data available. Appendix A lists a summary of all projects included in this study. Table 34 and Table 35 list projects where CPT soundings were paired with boreholes and projects where borehole information could not be located, respectively.

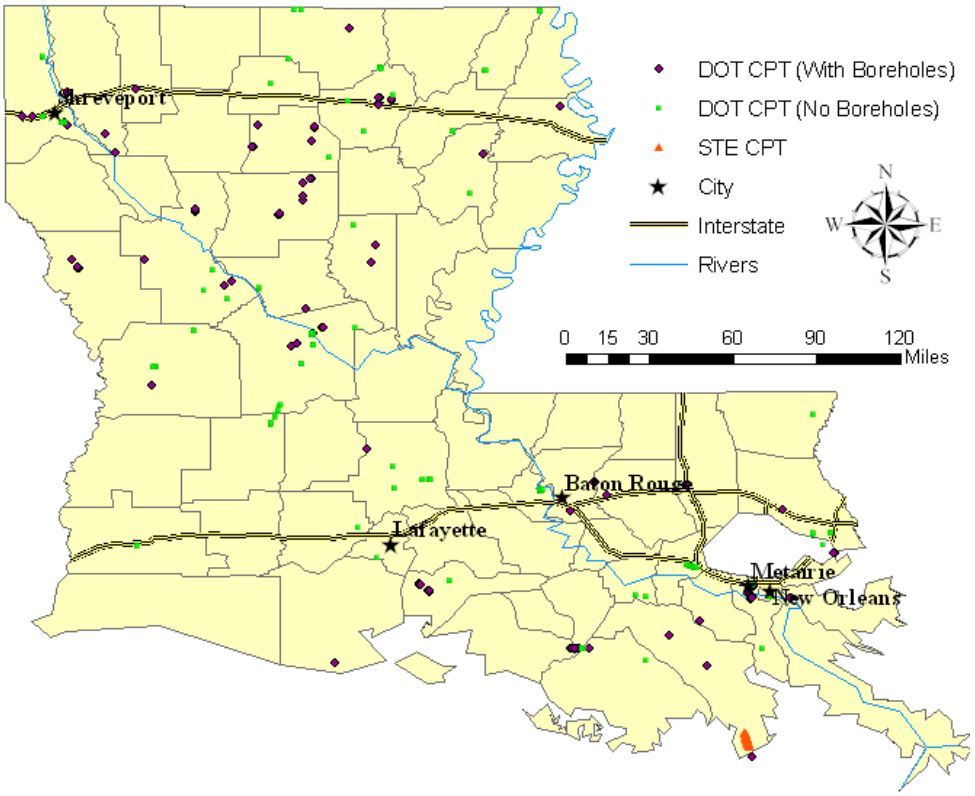

Figure 14
CPT soundings with and without borehole data from LADOTD and STE

CPT and Borehole Data Analysis and Archiving

In order to be analyzed and compared to the borehole data, every CPT raw data file was input into an Excel data template to perform various calculations and produce different plots of the CPT data. The spreadsheet starts by converting the input voltage values from the load cells located at the tip and the sleeve of the cone apparatus to tip resistance and sleeve friction (pressure) along the depth of the CPT soundings and used these values to calculate different parameters. The following paragraph presents a detailed description of the spreadsheet along with the equations used to calculate each parameter. An electronic version of all the Excel spreadsheets used in this study, plus others that did not have a matching borehole, are provided to LTRC. Appendix E shows an example excel template.

The CPT raw data are imported from the text file that contains raw data and pasted in the "Raw data" sheet of the template. The following are processed data in the analysis sheet of the template. Columns A and B include the depth values in meters and feet, respectively, while the tip resistance and sleeve friction in MPa are displayed in columns C and D. These values are converted to tons per square foot (tsf) and displayed in columns E and G. In order to reduce the random noise (spikes) in q_c and f_s, a smoothing function was used where every value was calculated by averaging five points above and below the point. The smoothed values are listed in columns F and H; these values make it easier to select a representative data values and discreet depths to be used later in the analysis. The friction ratio (FR) was calculated in column I. The estimated shear wave velocity (V_S) is calculated in column L using the correlation presented by Hegazy and Mayne [*102*]:

$$V_s(\text{m/s}) = \left[10.1 \cdot \log(q_c) - 11.4\right]^{1.67} \left[\frac{f_s * 100}{q_t}\right]^{0.3} \tag{32}$$

The calculated shear wave velocity was then used to calculate the soil unit weight (γ_T) using the equation proposed by Mayne, i.e., equation (33). The calculated unit weight values are listed in column M. These values are converted to pounds per cubic foot and displayed in column N. The calculated unit weight along with the depth (z) were then used to calculate the total overburden pressure (σ_{vo}). Columns O and P contain the calculated σ_{vo} values in kPa and tsf, respectively. The depth of the ground water table is then used to calculate the pore water pressure (column Q), which is then used with the overburden pressure to calculate the

effective pressure (columns R and S). Then the net tip resistance $q_{t\text{-}net}$ was calculated in column T as shown in equation (34).

$$\gamma_T(\text{kN/m}^3) = 8.32\log(V_s) - 1.61\log(z) \tag{33}$$

$$q_{tnet} = q_t - \sigma_{vo} \tag{34}$$

Columns V, W, and X are the normalized parameters Q, F, and B_q, respectively, used to determine the behavioral soil type; they are calculated using equations (35) through (37). Next, the soil behavioral type index presented by Robertson et al., in equation (38), is calculated in column Y. The index is then used to determine the soil "Zone Number" in column Z. Similarly, the soil behavioral type index and zone numbers are determined using the equations presented by Jefferies and Davies, i.e., equation (39), in columns AA and AB. Finally, The undrained shear strength (S_u) is calculated using equation (40) assuming a value of N_{kt} = 15 in column AC.

$$Q = \frac{q_t - \sigma_{vo}}{\sigma_{vo}`} \tag{35}$$

$$F = \frac{f_s}{q_t - \sigma_{vo}} \tag{36}$$

$$B_q = \frac{u_2 - u_o}{q_t - \sigma_{vo}} \tag{37}$$

$$I_c = \sqrt{\left[3.47 - \log(Q)\right]^2 + \left[\log(F) + 1.22\right]^2} \tag{38}$$

$$I_c ** = \sqrt{\left[3 - \log(Q \cdot (1 - B_q))\right]^2 + \left[1.3 \cdot \log(F) + 1.5\right]^2} \tag{39}$$

$$S_u = \frac{q_c - \sigma_{vo}}{N_{kt}} \tag{40}$$

Moreover, the LTRC CPT plotting and classification software were used to classify the soils using Zhang and Tumay statistical approach method [*2*]. Probability Density Functions (PDF) files were generated for each CPT sounding. The excel sheets and the PDF

classification files were used to generate an electronic archive of the CPT locations using ArcMap software. The GIS database included all the CPT soundings that were located throughout the state. Each point on the map contained the information about the CPT soundings including the job number, job location, parish, district, date, and station number. Clicking on any point on the map will display all the information of that test. Figure 15 depicts an example record where the information is displayed in a popup window when the location is selected. Such a database allows for the selection of a point or a group of points based on any of the mentioned attributes (e.g., district, job number, etc.). Moreover, when selecting a CPT sounding on the CPT map, two links are provided, one for the CPT classification PDF file generated from the LTRC CPT software and the other for the Excel data sheet where the CPT and borehole information are documented. Clicking on any of the links opens the PDF or Excel data sheet for the location selected. Figure 16 illustrates an example archive where the PDF classification file is displayed by selected the link for that file from the popup window.

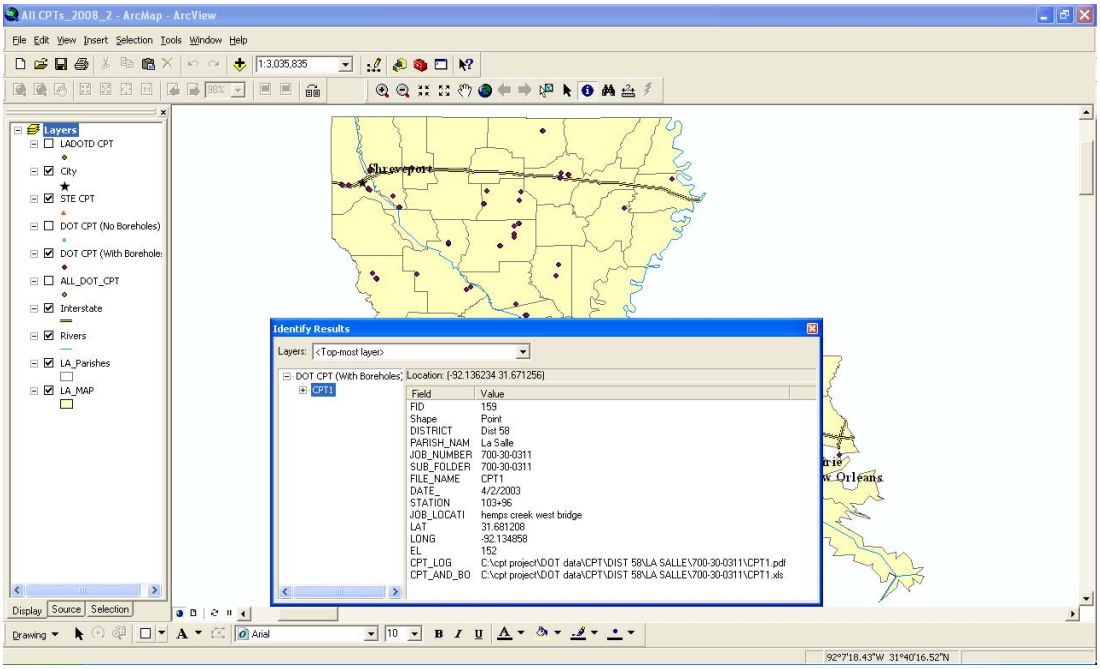

Figure 15

Example CPT data information displayed by selecting a CPT location

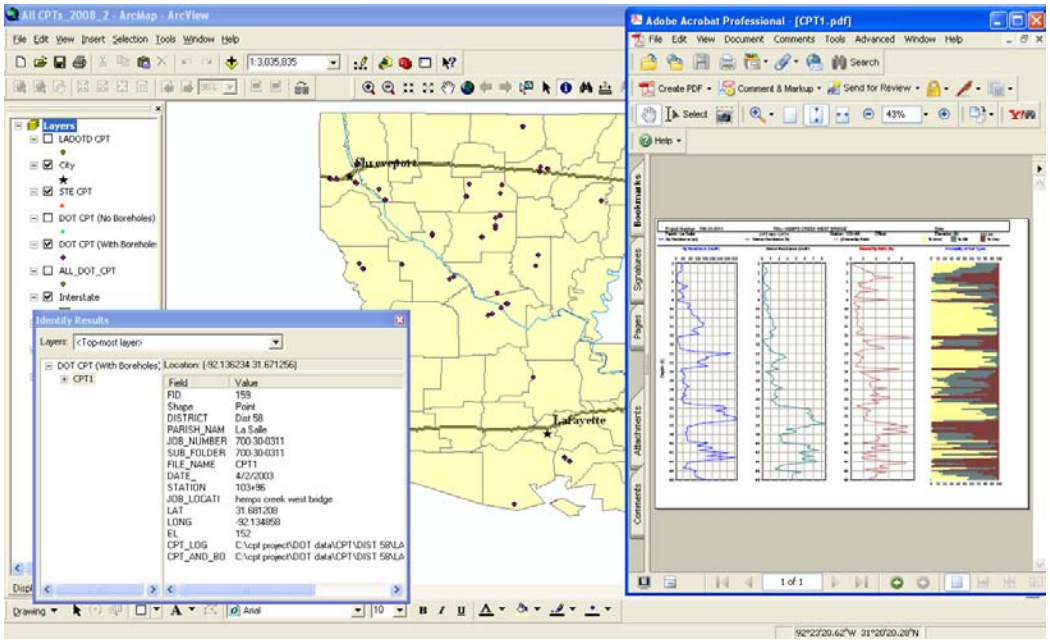

Figure 16
Example CPT classification file displayed by selecting the PDF link

It can be seen from Figure 14 that some regions of Louisiana have a large number of CPTs with boreholes while other regions contained a very small number of data. The northern and southeastern parts of the state have higher numbers of CPT soundings while the southwestern part of the state have very few CPT soundings. Figure 17 and Figure 18 depict zoomed views of northern and southwestern parts of the state where the difference in the number of CPT and borehole data points can be clearly noticed.

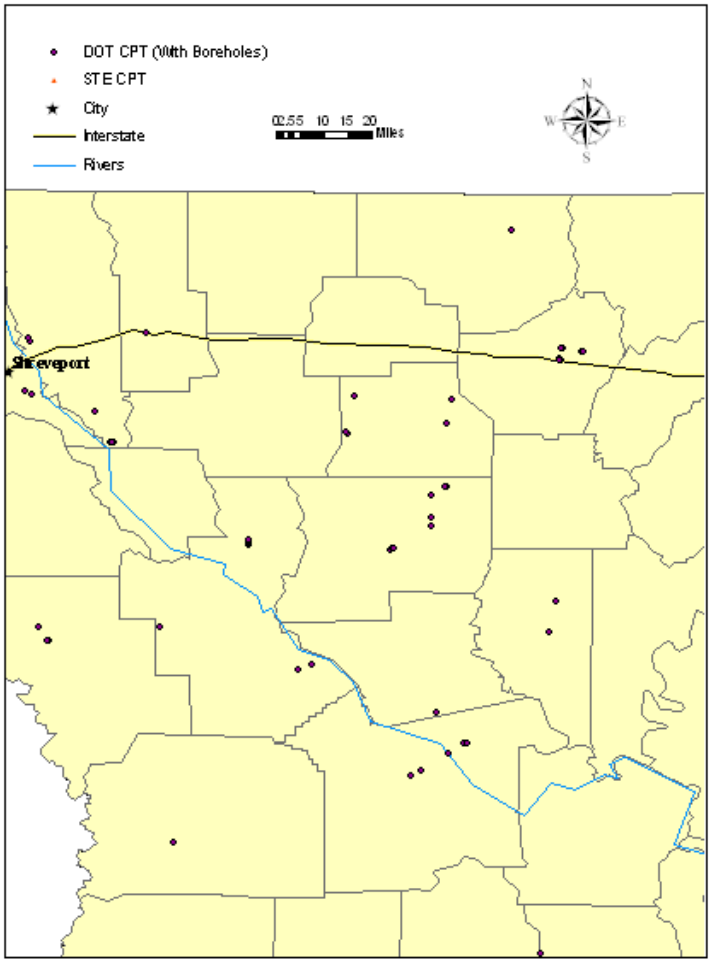

Figure 17

Zoomed view of the northern part of Louisiana where a higher number of CPT soundings were available

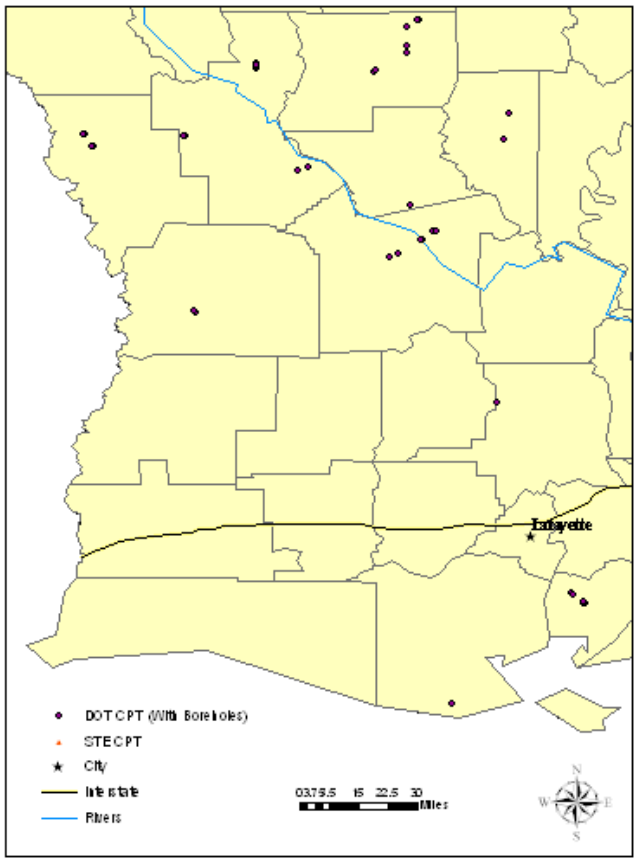

Figure 18
Zoomed view of the southwestern part of Louisiana where a smaller number of CPT soundings were available

To further illustrate the spatial variations in the assembled database of CPT results, a histogram of CPT depths of extracted soil engineering data is provided in Figure 19. It can be seen that a wide range of depths of extracted properties from CPT soundings is included in the database ranging from 2 ft. to 100 ft. However, the depths are not distributed uniformly. This means that the database is biased toward lower depths (< 25 ft.) than higher depths. It will be seen later in this report that for the database used in this study, depth variations do not significantly affect the correlation of the CPT coefficient. Hence, the results in the database are still viable for the purpose of this study. Similar depth histograms for each soil classification are also plotted in Figure 20.

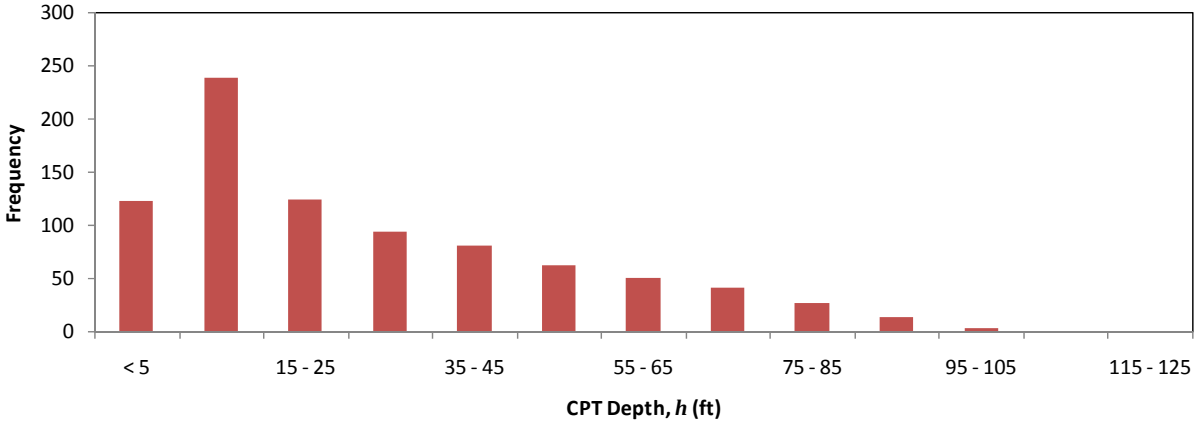

Figure 19
Histogram of depths for CPT measurements included in database

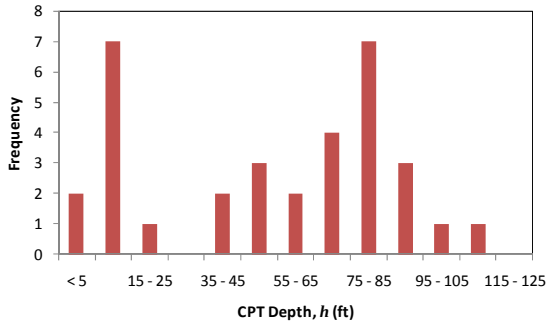

Classification 2

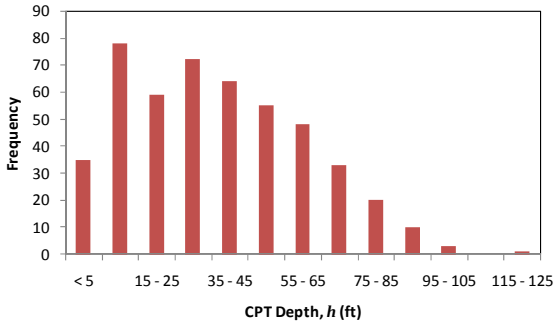

Classification 3

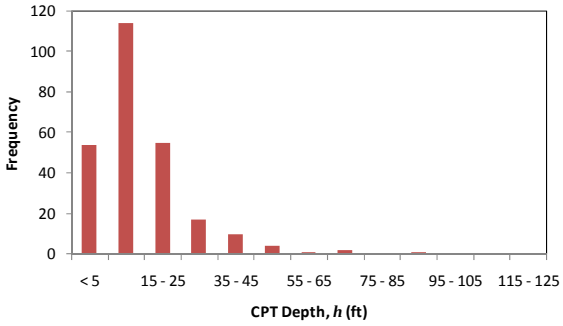

Classification 4

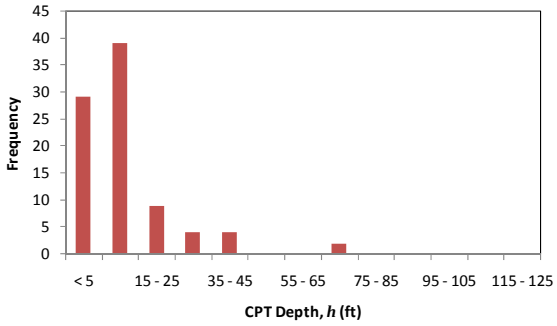

Classification 5

Figure 20
Depth histograms for different soil classifications [*4*], [*5*], [*19*]

Reliability Analysis of CPT

Two approaches were followed to correlate the undrained shear strength results obtained from CPTs and adjacent borings. Both approaches relied on the formula (transformation model) currently used by LADOTD for estimating the undrained shear strength from CPT readings, S_u^{CPT}, which is given as:

$$S_u^{CPT} = \frac{q_c - \sigma_{vo}}{N_{kt}} \tag{41}$$

The first approach was a direct correlation based on the formula in equation (41). In the second approach, a more detailed investigation in which all sources of uncertainty were accounted for utilizing the First Order Reliability Method (FORM). Both approaches are described in detail in the following sections.

Direct Correlation of CPT and Boring Results–1st Approach

In this approach, the currently used expression, transformation model given in equation (41), will be correlated by equating the undrained shear strength values from both tests (S_u^{CPT} from CPT and S_u^{UC} unconfined compression test) to achieve the goal of this study. By rearranging the expression, one can obtain N_{kt} values for each CPT result in the database as follows:

$$N_{kt} = \frac{q_c - \sigma_{vo}}{S_u^{UC}} \tag{42}$$

Due to the uncertainties detailed earlier (inherent soil variability, device measurement, and used expression – transformation model), a constant N_{kt} is not to be expected, but rather a scatter of results. The resulting N_{kt} values can be studied statistically to establish appropriate probability density functions (PDF) and cumulative distribution functions (CDF) for N_{kt} that describe the scatter of N_{kt} values. Once these relations (PDF and CDF) are established, they can be used to determine acceptable N_{kt} for various probability of exceedance levels. Here, the probability of exceedance (P_e) is defined as the probability of the borehole result

(benchmark) exceeding the CPT estimate for undrained shear strength. A higher probability of exceedance indicates a more conservative estimate of the undrained shear strength from CPT readings.

Detailed Reliability Analysis for Correlation of CPT and Boring Results–2nd Approach

The second approach that was adopted in this study for calibrating the CPT coefficient N_{kt} is more involved and accounts for all uncertainties associated with CPT testing. In addition to the uncertainty caused by the used formula or transformation model, equation (41) that was covered in the first approach, uncertainties inherent in soil properties and device measurement are also accounted for. Before this approach could be carried out, the statistical characteristics of each of these sources of uncertainty will first need to be determined. In the next few sections, the methodology adopted for quantifying these uncertainties is explained.

Statistical Analysis of CPT Repeatability

One of the identified sources of uncertainty is the inherent variations in the device and measurement equipment (see Figure 12). This uncertainty needs to be accounted for in the reliability analysis forming the basis for the correlation of the CPT coefficient. Lacking readily available repeatability test results, a test program was conducted to assess the variability inherent in CPT measurements. In planning the repeatability test program, the following factors were kept in mind:

- The CPT tests had to be closely spaced since the purpose of these tests was to identify the variations in the recorded readings under "almost identical" soil conditions.
- The CPT penetration should extend to a depth of 80 ft., which covers most of the LADOTD applications.
- A single boring is also requested to provide reference soil information with which the CPT readings can be related. The boring should be taken after the conclusion of the CPT tests to avoid disturbing the soil.

Sixteen CPT penetrations were conducted in dual polar array as shown in Figure 21. This layout was chosen because it allows a central zone where a soil boring can be taken for further analysis and comparison with CPT results. The minimum distance between adjacent CPT penetrations did not fall below 3 ft., and the farthest distance between penetrations did not exceed 12 ft. Thus, it can be said that the CPT readings are representative of "identical"

soil conditions. Figure 21b shows a photograph of the actual site where the 16 repeatability penetrations took place at LTRC's Accelerated Testing Facility (ALF) site. LTRC and LADOTD staff conducted the tests.

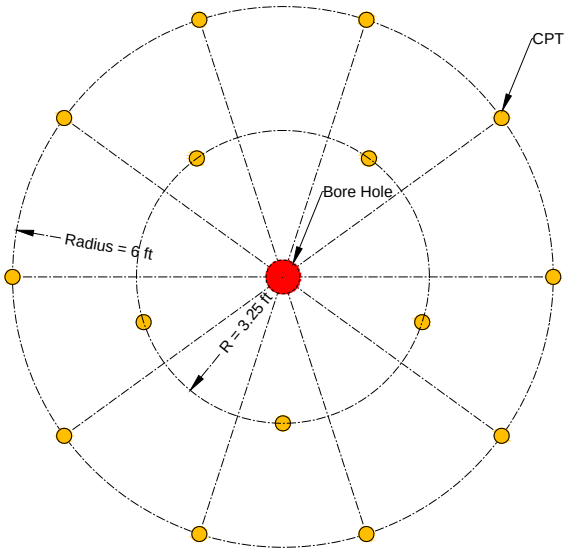

(a)

(b)

Figure 21
Array of CPT repeatability tests

Preprocessing CPT Data

The compiled database of CPT results was used to study the calibration of undrained shear strength, S_u, transformation model for Louisiana soils. The database comprised of results from over 700 CPTs. This database was obtained from projects all over Louisiana. The goal of the project is to calibrate the transformation models utilized by geotechnical engineers by comparing CPT results to corresponding results from borehole tests, specifically the more acceptable unconfined compression (UC) undrained shear strength, S_u^{UC}. It was possible to identify boreholes in the vicinity of 334 CPT soundings out of all those included in the database. The distance between the boreholes and the CPT soundings varied from site to site and limits on distance between both locations were set as is described next. Each CPT test provided several data points to the database. The soil properties were computed at the depth intervals that match the reported borehole results. In all, 2,630 data points for undrained shear strength results from boreholes were compiled. It was only possible to compute the undrained shear strength from CPT readings in 1,886 locations and depths. However, the number of data points where undrained shear strength results were available from matching CPT and borehole data was 1,814.

The following section describes the methodology by which the results were preprocessed, analyzed and presented in this study.

Matching CPT and Borehole Data

As expected, the CPT and borehole locations were not exact matches. This was due to many site factors and is now considered historic data that are not changeable at the time of conducting this research. Thus, it was imperative that acceptable criteria be set to justify the hypothesis of *equal* soil properties at both CPT and borehole locations. These criteria address the fact that the distance between the CPTs and boreholes ranged from 1 ft. to 1,844 ft. Furthermore, it was not possible to exactly identify the coordinates of some locations, which had to be excluded from the database. At the same time, more than one borehole existed in the vicinity of some CPTs in the database, and a weighing function was needed for these locations. Criteria were set in this project to address these issues:

- A maximum distance between the CPT and borehole location was set to be 150 ft. Figure 22 shows a plot showing the number of matches between CPTs and boreholes

at different distance intervals. Accordingly, the number of data points included in subsequent analyses is 1,263 from 251 CPT soundings.

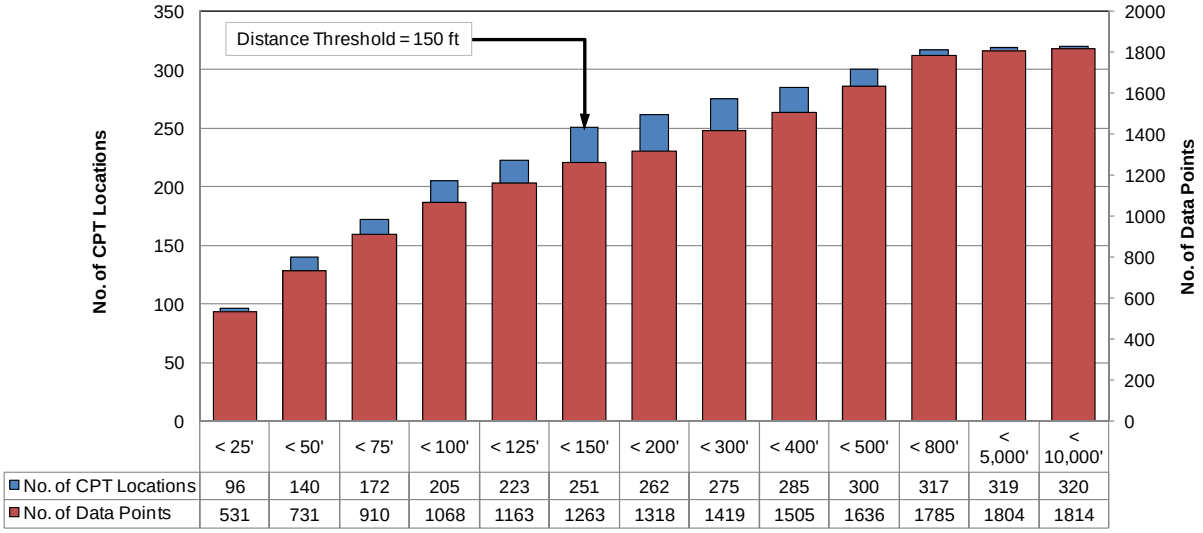

	< 25'	< 50'	< 75'	< 100'	< 125'	< 150'	< 200'	< 300'	< 400'	< 500'	< 800'	< 5,000'	< 10,000'
No. of CPT Locations	96	140	172	205	223	251	262	275	285	300	317	319	320
No. of Data Points	531	731	910	1068	1163	1263	1318	1419	1505	1636	1785	1804	1814

Figure 22
Distance threshold between CPT and borehole locations showing number of data points included in analyses

- In the case of having more than one borehole in the vicinity of a CPT sounding, a $1/D$ weight function was used to account for the proximity of borehole locations to CPT sounding. The weighted average function for any quantity, q, based on the results from n boreholes at distances $D_1, D_2, \cdots, D_i, \cdots, D_n$ can be written as:

$$q = \sum_{i=1}^{n}\left[q_i \left(\frac{\sum_{j=1}^{n} D_j - D_i}{\sum_{j=1}^{n} D_j} \right) \right] \tag{43}$$

This function yields the following weighted averages for the cases of two and three boreholes consecutively:

$$q = \left[q_1 \left(\frac{\{D_1 + D_2\} - D_1}{\{D_1 + D_2\}} \right) \right] + \left[q_2 \left(\frac{\{D_1 + D_2\} - D_2}{\{D_1 + D_2\}} \right) \right] = q_1 \left(\frac{D_2}{D_1 + D_2} \right) + q_2 \left(\frac{D_1}{D_1 + D_2} \right) \tag{44}$$

$$q = \left[q_1 \left(\frac{\{D_1 + D_2 + D_3\} - D_1}{\{D_1 + D_2 + D_3\}} \right) \right] + \left[q_2 \left(\frac{\{D_1 + D_2 + D_3\} - D_2}{\{D_1 + D_2 + D_3\}} \right) \right] + \left[q_3 \left(\frac{\{D_1 + D_2 + D_3\} - D_3}{\{D_1 + D_2 + D_3\}} \right) \right]$$
$$= q_1 \left(\frac{D_2 + D_3}{D_1 + D_2 + D_3} \right) + q_2 \left(\frac{D_1 + D_3}{D_1 + D_2 + D_3} \right) + q_3 \left(\frac{D_1 + D_2}{D_1 + D_2 + D_3} \right) \quad (45)$$

For illustration purposes, a scenario of two boreholes at distances D_1=35 ft. and D_2=110 ft. would yield the following weighted average :

$$q = 0.7586 q_1 + 0.2414 q_2 \quad (46)$$

Averaging CPT Readings

CPT readings are known to have spikes due to many factors. One of these factors is the fact that continuous readings are recorded at very small intervals which is in many cases smaller than 1.0 in. of depth. Relying on pinpoint data readings would result in unnecessary scatter, especially that soil properties obtained from borehole tests are usually based on specimens of tangible dimensions (8 in. in the case of Shelby Tube sample). As a result, it was deemed necessary to average CPT data readings over a depth similar to what is used in borehole soil property testing. In this study, 11 consecutive CPT data readings were averaged around every desired depth where borehole data was available. These readings correspond to a depth of about 7.8 in. Figure 23 illustrates the averaging of device readings for the cone tip resistance, q_c. Figure 23a is a plot of the raw data obtained from the CPT device, while Figure 23b shows the same results after averaging them over a depth of about 7.8 in. It can be seen that localized spikes are almost eliminated without losing the general trend of the readings. This is the purpose of the averaging and is done for all CPT readings in the assembled database.

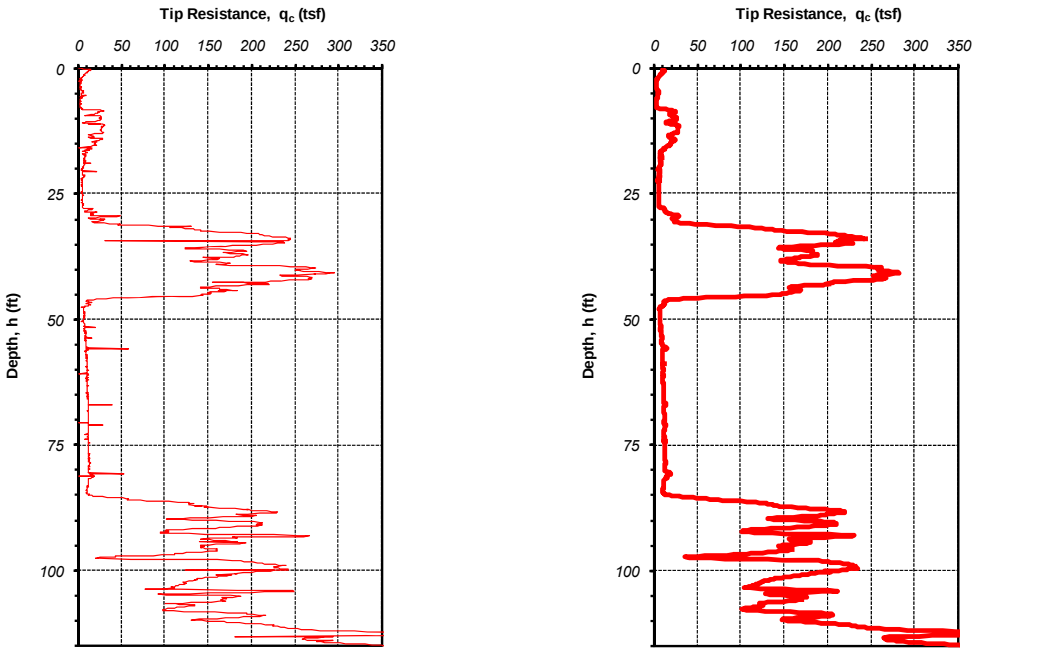

(a) raw tip resistance readings, q_c **(b) averaged tip resistance readings, q_c**

Figure 23
Averaging raw CPT readings

Filtering Data Results

As is the case with any natural and hence uncontrollable material, a wide range of readings is always expected. Soils fall under this category of materials. Nevertheless, soil properties are known to fall within a confined physical range albeit it may be a wide range. Values outside this range represent soil properties that represent soil conditions that may lead to outcast data points. For example, extremely low undrained shear strength results indicate very soft soils that are difficult to test under normal laboratory conditions, thus results within this low range are in many cases unrepresentative of actual soil conditions. At the other extreme, high undrained shear strength values are usually attributed to stiff clays, which fluctuations in the cone readings may be excessive leading to unreliable CPT estimates of the undrained shear strength. It was therefore deemed necessary to set limits on the range of undrained shear strength, S_u, collected in the database. Values that exceed a maximum threshold or fall below a minimum threshold were excluded from the database.

Figure 24 shows a histogram of the undrained shear strength complied in the database. The plot shows that the database includes points of extremely low and extremely high S_u values. Based on the literature, S_u values falling below 150 psf and above 2,500 psf were excluded from the database in subsequent analyses.

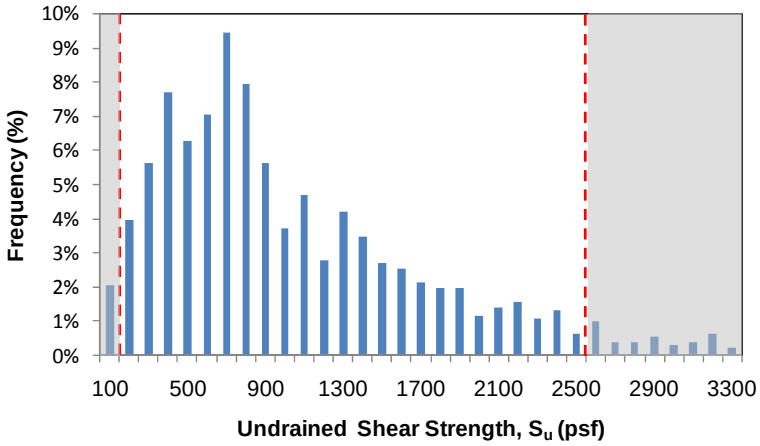

Figure 24
Histogram of S_u frequency in compiled database

Figure 25 shows the impact the chosen threshold has on the scatter of the transformation model used in this study. The scatter is measured by the coefficient of variation, COV, of the ratio S_u^{CPT}/S_u^{UC} . It can be seen that as more data points with high or low undrained shear strength values are excluded, the smaller the COV of the transformation model becomes. Filtering the data using these two threshold results in a reduction in the number of data points used in the subsequent analyses. The database included 862 data points after applying the aforementioned thresholds.

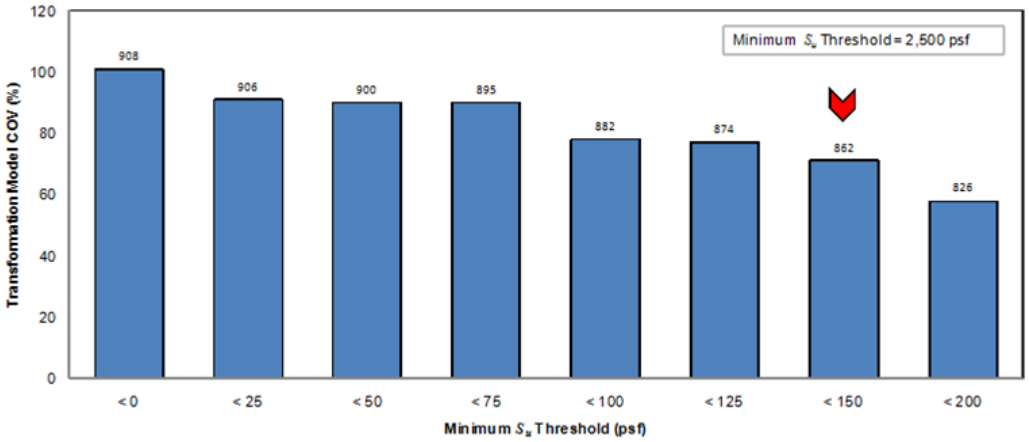

(a) minimum S_u threshold

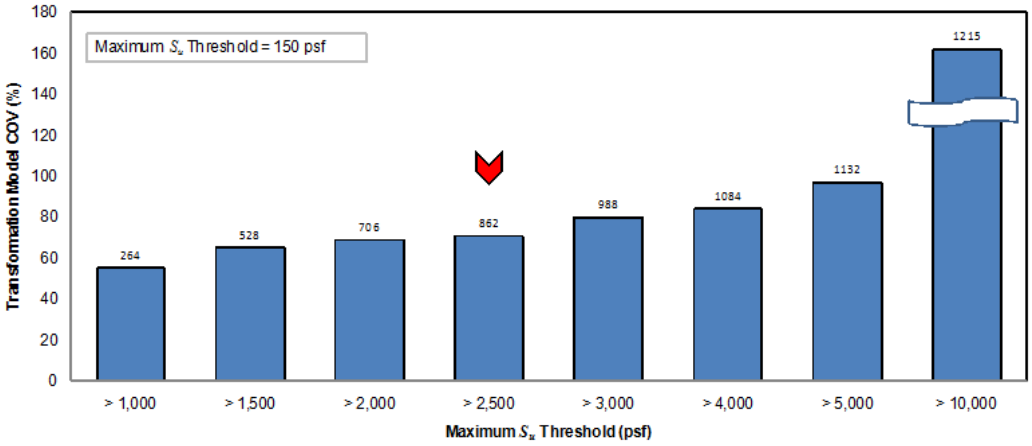

(b) maximum S_u threshold

Figure 25

Effect of S_u thresholds on uncertainty of transformation model

Calibration of CPT Coefficient

The calibration of the CPT coefficient, N_{kt}, to achieve acceptable reliability in undrained shear strength, S_u, estimates will be conducted using the methodology described next. An acceptable reliability can be defined in terms of a probability of exceedance, P_e, which is described in detail in the next section. The statistical characteristics of the data in the compiled database of CPT results are first analyzed. These characteristics are essential for the reliability-based calibration. Statistical characteristics of random variables not analyzed in this study are obtained from the literature. A limit state function is first established, which is then used to calibrate N_{kt}. The calibration is performed for different soil classifications, different target reliability levels, and σ_{vo}/q_c ratio.

Limit State Function

The limit state function is simply the boundary between acceptable and unacceptable performance. In this study, the undrained shear strength estimates from borehole data, S_u^{UC}, and CPT data, S_u^{CPT}, should be identical in ideal circumstances. In real life, the difference between both is inevitable. An acceptable performance is achieved if CPT estimates for the undrained shear strength, S_u^{CPT}, is less than the borehole result, S_u^{UC}, and an unacceptable performance is to be expected if the opposite is true. Since both terms have inherent randomness in their values, they can be illustrated graphically as can be seen in Figure 26a. If the formula used in the determining S_u^{CPT}, transformation model in equation (41) is conservative, then the mean value of CTP estimates, $\mu_{S_u^{CPT}}$, would be less than the mean value of borehole results, $\mu_{S_u^{UC}}$. Alternatively, this can be described using a limit state function (LSF) that represents the difference between both estimates ($Z = S_u^{UC} - S_u^{CPT}$), which will also be a random variable that can be plotted as can be seen in Figure 26b. The probability of estimating the undrained shear strength from borehole unconfined compression tests that will be higher than those obtain from the CPT readings is graphically represented by the shaded area. It can be seen that the larger this area, the safer the CPT estimates. An indirect measure of the area is the distance from the mean, μ_Z, to the origin, which can be represented in multiples of the standard deviation, σ_Z. This multiple is defined as the reliability index, β. The higher the reliability index, the higher the probability of

exceedance, P_e. In the special case of calibrating a formula (transformation model) that results in equal mean values, i.e., $\mu_{S_u^{CPT}} = \mu_{S_u^{UC}}$ as illustrated in Figure 27a (the probability of exceedance, P_e) would be equal to 50 percent as can be seen in Figure 27b. Hence, the corresponding reliability index would be equal to zero, which will be one of the target reliability levels in this study.

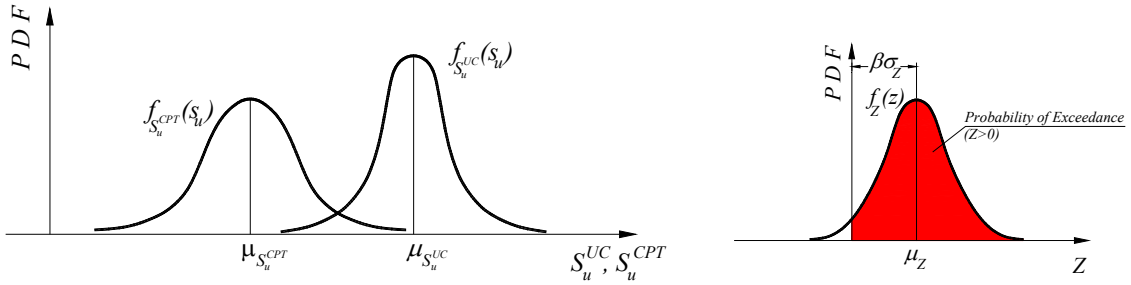

(a) **(b)**

Figure 26

Illustration of the limit state function (LSF) used in this study (general case)

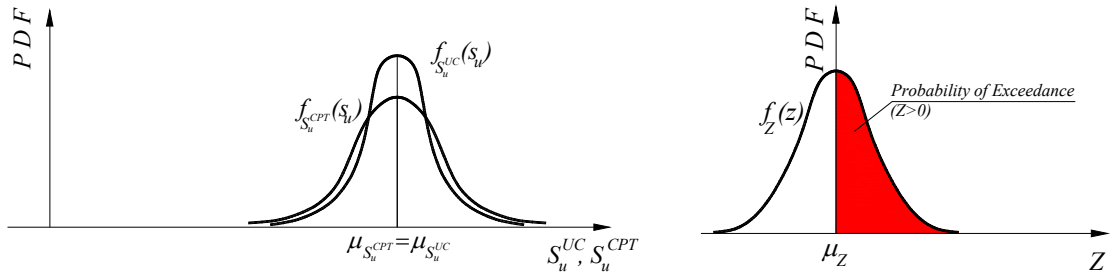

(a) **(b)**

Figure 27

Illustration of the limit state function (LSF) used in this study (special case)

The reliability calibration conducted in this study is based on the limit state function (LSF) described above. However, the CPT estimate, S_u^{CPT}, will be replaced by the transformation model used to obtain its values, equation (41). This allows for including the uncertainties inherent in the original CPT readings, namely q_c and σ_{vo}. Equation (47) shows the details

the LSF starting with the random variables $\boldsymbol{S_u^{UC}}$ and $\boldsymbol{S_u^{CPT}}$. The expanded version is shown in equation (47-b), where $\boldsymbol{S_u^{UC}}$ is replaced by $\boldsymbol{\gamma}\, S_u^{UC}$ in which $\boldsymbol{\gamma}$ is random variable that accounts for uncertainty inherent in the soil property, S_u^{UC}, which is taken as a deterministic value representing soils in location under investigation. The other two newly introduced random variables, $\boldsymbol{\xi}$ and $\boldsymbol{\eta}$, represent the uncertainties in the transformation model and tip resistance readings, respectively.

$$Z = \boldsymbol{S_u^{UC}} - \boldsymbol{S_u^{CPT}} \tag{47-a}$$

$$Z = \boldsymbol{\gamma}\, S_u^{UC} - \boldsymbol{\xi}\left[\frac{\boldsymbol{\eta}\, q_c - \sigma_{vo}}{N_{kt}}\right] \tag{47-b}$$

Table 5 lists the statistical characteristics of the random variables used in this study. The characteristics of the random variable $\boldsymbol{\xi}$ are given in Table 6 and Table 7 for both classification techniques used in this study, namely Robertson and Zhang and Tumay. The bias and standard deviation values were computed by determining the statistical descriptors (mean and standard deviation) for the ratio between the CPT estimates and borehole results, S_u^{CPT} / S_u^{UC}, in the database.

$$\text{bias}, \lambda_\xi = \text{mean}\left(\frac{\boldsymbol{S_u^{CPT}}}{\boldsymbol{S_u^{UC}}}\right) \tag{48}$$

$$\text{coefficient of variation}, \text{COV}(\xi) = \frac{\text{standard deviation}\left(\dfrac{\boldsymbol{S_u^{CPT}}}{\boldsymbol{S_u^{UC}}}\right)}{\text{mean}\left(\dfrac{\boldsymbol{S_u^{CPT}}}{\boldsymbol{S_u^{UC}}}\right)} = \frac{\sigma_\xi}{\lambda_\xi} \tag{49}$$

Several CPT coefficient values were considered in determining these statistical descriptors. For each value, the CPT undrained shear estimates, S_u^{CPT}, would change and cause the bias and coefficient of variation given above. The various values are needed for the optimization step that follows for determining an appropriate CPT coefficient, N_{kt}. Finally, the tip resistance uncertainty was obtained from the repeatability study presented earlier (see page 42) while the overburden pressure was taken as a deterministic quantity due to its low COV as will be seen later.

Table 5

Random variables used in reliability calibration

Variable	Mean	COV (%)	Distribution	Source
Soil Uncertainty, γ	1.0	33	Lognormal	Phoon and Kulhawy (1999)
Transformation Model, ξ	varies		Lognormal	Current Study
Tip Resistance, η	varies		Normal	Current Study
Overburden Pressure	deterministic			Current Study

Table 6

Statistical characteristics of transformation model (Robertson classification)

N_{kt}	ALL Cases		2		3		4	
	Bias	**STDEV**	**Bias**	**STDEV**	**Bias**	**STDEV**	**Bias**	**STDEV**
12	2.401	1.693	1.541	1.196	2.284	1.366	2.484	1.652
15	2.009	1.427	1.358	0.962	1.899	1.268	2.067	1.299
18	1.793	1.418	1.178	0.806	1.604	1.048	1.881	1.252
21	1.562	1.218	1.041	0.680	1.390	0.898	1.612	1.055
24	1.414	1.154	0.964	0.580	1.229	0.792	1.482	1.108
27	1.285	1.126	0.879	0.512	1.093	0.705	1.329	0.982
30	1.201	1.125	0.791	0.461	0.991	0.633	1.220	0.916
33	1.100	1.026	0.719	0.419	0.904	0.576	1.115	0.829
36	1.023	0.971	0.700	0.368	0.835	0.536	1.027	0.759
39	0.961	0.924	0.678	0.350	0.772	0.496	0.971	0.748
42	0.906	0.914	0.630	0.325	0.717	0.461	0.941	0.874
45	0.860	0.873	0.609	0.294	0.673	0.431	0.900	0.866
48	0.817	0.825	0.571	0.275	0.635	0.405	0.854	0.816
51	0.773	0.777	0.554	0.254	0.600	0.381	0.806	0.767

Table 7

Statistical characteristics of transformation model (Zhang and Tumay classification)

N_{kt}	ALL Cases		Clay > 75%		Clay = 50-75%		Clay = 25-50%	
	Bias	STDEV	Bias	STDEV	Bias	STDEV	Bias	STDEV
12	2.401	1.693	2.172	1.387	2.426	1.981	2.662	1.906
15	2.009	1.427	1.822	1.124	1.954	1.476	2.273	1.774
18	1.793	1.418	1.614	1.038	1.776	1.732	1.946	1.521
21	1.562	1.218	1.414	0.891	1.521	1.441	1.675	1.297
24	1.414	1.154	1.258	0.825	1.357	1.255	1.542	1.251
27	1.285	1.126	1.129	0.737	1.216	1.120	1.426	1.419
30	1.201	1.125	1.053	0.728	1.130	1.017	1.368	1.545
33	1.100	1.026	0.958	0.662	1.045	0.926	1.244	1.402
36	1.023	0.971	0.892	0.614	0.959	0.851	1.143	1.281
39	0.961	0.924	0.828	0.569	0.886	0.788	1.075	1.210
42	0.906	0.914	0.769	0.529	0.823	0.732	0.998	1.124
45	0.860	0.873	0.744	0.581	0.771	0.684	0.937	1.049
48	0.817	0.825	0.701	0.545	0.726	0.643	0.892	0.990
51	0.773	0.777	0.660	0.513	0.694	0.609	0.842	0.933

Chi-Square Statistical Test "Goodness of Fit"

In addition to the statistical descriptors that were determined in the previous section (bias, λ, and coefficient of variation, COV), a distribution type will be needed for the reliability study that follows. Statistical distributions are mathematical expressions that represent the frequency within a dataset continuously over the possible range for the entire population.

Any random variables can be described using different distribution types. The choice of one distribution over another is based on how well the chosen mathematical distribution *fits* the collected data (observations). Many statistical tests can be used to evaluate how well a certain distribution fits the collected data. In this study, the *Chi-Square Test* will be used. The details of how the test is conducted are given in Appendix C. The random variables in this study were tested for two possible distribution types, namely Normal and Lognormal. Details of both distributions can be found in the literature and are summarized in the Appendix for convenience. The results from conducting these tests are presented next for the two random variables that were determined in this study.

Reliability-based Calibration

Calibration of the CPT coefficient, N_{kt}, will be conducted using the LSF described earlier. The goal is to identify N_{kt} values that result in desired reliability levels, which will be measured in terms of a reliability index, β, defined as the ratio between the mean value of the LSF and its standard deviation, which was previously illustrated in Figure 26b:

$$\beta = \frac{\mu_Z}{\sigma_Z} \tag{50}$$

The reliability index, β, is related to the probability of exceedance, P_e, using the following expression:

$$P_e = \Phi(\beta) \tag{51}$$

where, $\Phi(\beta)$ is a cumulative distribution function (CDF) for a limit state function, Z. The reliability index was evaluated for each considered case. In all, a total of 672 cases were considered (14 N_{kt} values × 4 Soil Classifications × 6 σ_{vo}/q_c ratios × 2 Classification Methods). The ratio of overburden pressure to the tip resistance, σ_{vo}/q_c, in the reliability analyses was considered in the reliability study since the results should cover a wide range of possibilities (design space). The First Order Reliability Method (FORM) was used to compute β for all cases. FORM is based on a first order Taylor series expansion of the limit state function, which approximates the failure surface by a tangent plane at the point of interest. More details about FORM and the procedure used in this study are given in A B.

Table 8
Range of parameters covered in reliability study

Parameter		Range
CPT Coefficient, N_{kt}		12, 15, 18, 21, … , 39, 42, 45, 48
Ratio, σ_{vo}/q_c		0.05, 0.10, 0.20, 0.50, 0.80, 0.90
Soil Classification	Robertson	2, 3, 4, 5
	Zhang and Tumay	> 75%, 50-75%, 25-50%, < 25%

DISCUSSION OF RESULTS

Repeatability Tests

The data files obtained from the CPT tests were analyzed by running the LTRC software for analysis of CPT readings. The main parameters of interest for this repeatability study are the variables included in the limit state function to be used in the reliability calibration. These parameters are:

- tip resistance, q_c
- overburden pressure, σ_{vo}

It should be noted that the overburden pressure, σ_{vo}, is computed using the estimated unit weight of the soil, γ_T. Hence, the data for the unit weight of the soil, γ_T, was also analyzed in addition to the two aforementioned variables. Each of the three parameters was first plotted from all 16 CPT tests. Figure 28a through Figure 28c show the plots for q_c, γ_T, and σ_{vo}, respectively. The values of each parameter are plotted versus depth. As expected, it is obvious from Figure 28 that the tip resistance, q_c, shows more scatter than the other two variables. The variability in the unit weight of the soil, γ_T, is far less than it is for the tip resistance. Consequently, the variability of the overburden pressure, σ_{vo}, is also relatively less than that of the tip resistance. By comparing the plots for the γ_T and σ_{vo}, it is clear that the variability in the overburden pressure is almost negligible. This is due to the fact that the depth, h, is included in estimating the overburden pressure, σ_{vo}. Depth estimates are pretty accurate in CPT tests since they are based on pipe lengths. As the depth increases, so does the overburden pressure, σ_{vo}, and local variations in the soil unit weight, γ_T, become small compared to the total overburden pressure, σ_{vo}.

Another observation from the plots is that a major change in soil characteristics takes place somewhere in between the 40-ft. and 50-ft. depths. This is especially obvious from Figure 28 where the tip resistance suddenly shifts from values below 40 tsf to values easily exceeding 100 tsf. This observation will help explain one of the trends of uncertainty that are computed and presented in the next section.

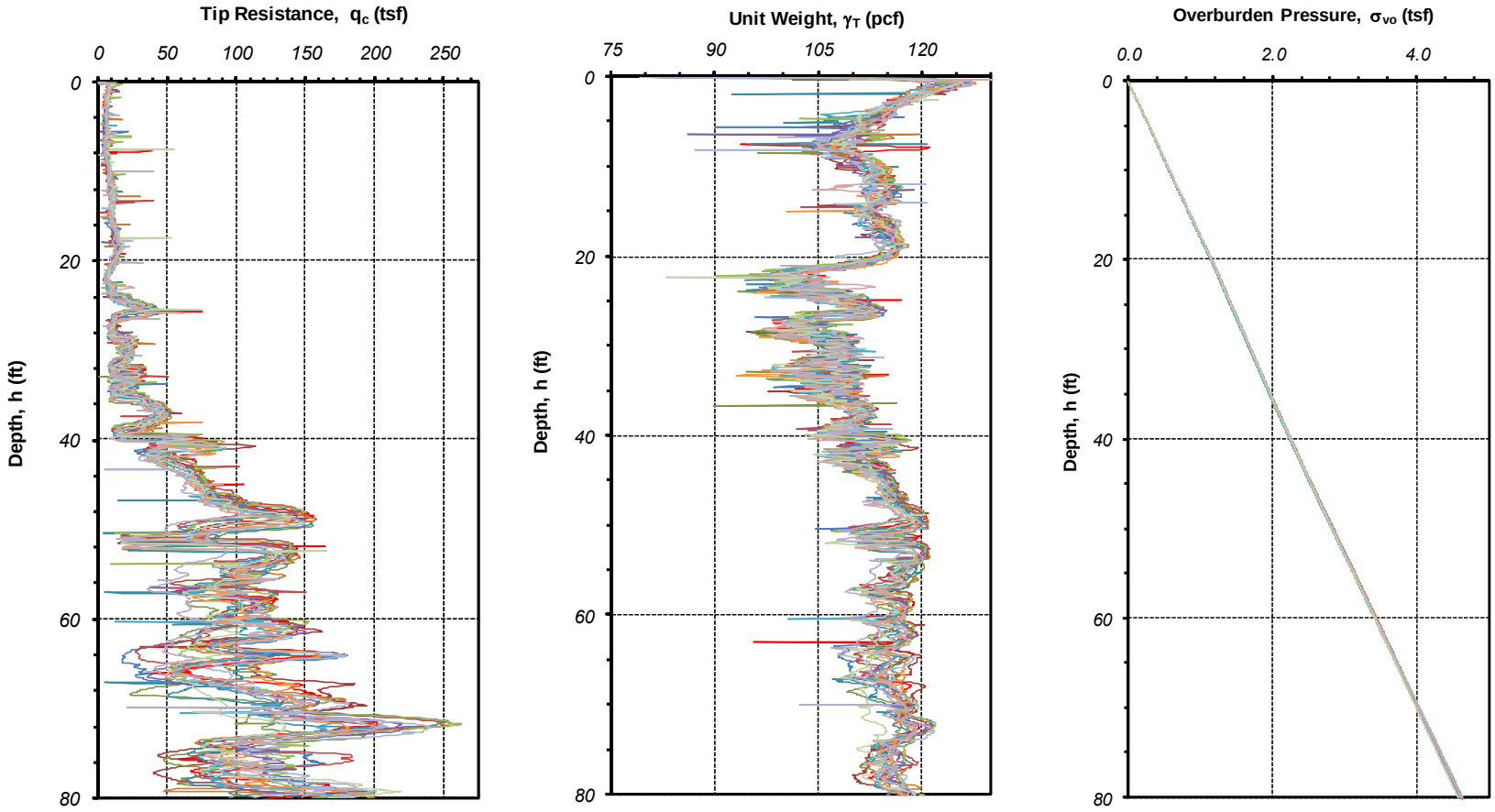

(a) Tip resistance, q_c **(b) Unit weight, γ_T** **(c) Overburden pressure, σ_{vo}**

Figure 28
Cone data from all repeatability tests

Statistical Characteristics of Repeatability Data

The data obtained from the analysis of all 16 CPT soundings were further analyzed to assess the statistical characteristics of the parameters of interest for the reliability calibration study, namely q_c, γ_T, and σ_{vo}. Two spatial variation parameters were studied to investigate whether the variability inherent in the device could be related to either of them. The two parameters are the soil depth and the soil classification.

Soil Depth. The statistical analysis focused on discrete locations along the depth of the penetration with a resolution of 5 ft. intervals. As with the other analyses, the readings were averaged for a depth equal to 10 in. (5 in. above and 5 in. below) around each of the chosen depths. Table 9 through Table 11 show the data for all three parameters. The maximum and minimum reading for each variable at each depth are identified (highlighted) in the tables. The coefficient of variation, COV, was computed for each variable at each discrete depth, which is defined as:

$$COV(X_i) = \frac{\sigma_{X_i}}{\mu_{X_i}} \tag{52}$$

where, σ_{X_i} and μ_{X_i} are the standard deviations and the mean value for the random variable, X_i, respectively. The COV is a direct measure of the scatter resulting from the CPT readings under *identical* soil conditions. A large COV indicates a wide scatter of the results and vice versa.

Table 9 through Table 11 also list the COV for all three parameters for each depth. The computed COV results also plotted in Figure 29 through Figure 31 versus depth. The average value for each of the parameters is plotted next to each of the COV plots as an indicator of the parameter's trend. Based on these plots, it can be said that there is no clear relationship between the variability inherent in the measuring device and the soil depth for the first two parameters q_c and γ_T. A trend is observed for the overburden pressure, σ_{vo}, which decreases steadily from the surface (depth = 0.0 ft.) to a depth of about 40 ft., after which the $COV(\sigma_{vo})$ is almost a constant. In both regions, it should be noted that the variability is extremely low (< 1 percent). The $COV(q_c)$, on the other hand, is higher with values close to 40 percent in some cases. On average, the COVs for three studied parameters are 19.7 percent, 1.50 percent, and 0.51 percent, respectively. These COV values will be incorporated in the limit state function for the reliability calibration to account for uncertainties inherent in the measuring device, the cone for this study.

Table 9

Discrete tip resistance, q_c, readings at 5 ft. intervals

Job #	Depth (ft)	Soil Classification	q_c CPT 1	2	3	4	5	6	7	8	9	10	11	12	13	14	15	16	COV(q_c)
Repeaibiliy (ALF)	5	4	5.4	5.6	5.8	5.8	4.9	6.1	4.8	6.4	5.2	4.6	7.1	5.8	6.0	6.3	6.9	6.4	12.3%
	10	3	7.9	5.9	9.4	8.8	7.8	8.5	8.7	6.3	8.5	7.0	9.0	9.3	8.4	7.9	9.5	11.1	15.2%
	15	3	8.6	9.6	9.1	8.3	7.9	10.8	10.3	10.6	9.3	9.8	10.5	8.5	9.9	9.4	10.6	10.1	9.4%
	20	3	10.7	10.6	13.0	12.7	13.0	10.1	11.9	12.2	10.5	12.7	12.8	13.0	10.6	11.2	12.2	13.9	9.7%
	25	5	34.6	27.5	23.8	23.5	29.3	31.8	38.5	34.8	35.4	32.6	19.8	26.9	23.5	21.3	32.5	31.8	19.3%
	30	5	16.9	23.1	22.1	24.2	24.8	17.8	15.9	16.1	16.7	21.3	21.4	24.6	23.7	25.3	17.0	16.5	17.7%
	35	4	20.7	10.6	20.3	25.1	17.6	13.4	27.5	29.4	32.0	15.3	11.5	18.1	15.6	13.2	14.8	22.7	34.0%
	40	5	55.5	50.7	25.0	20.4	32.3	48.8	53.0	63.4	68.5	49.4	44.7	24.5	29.7	19.3	49.5	56.8	36.5%
	45	5	83.8	80.5	75.9	76.9	75.7	79.0	78.5	77.2	79.2	74.9	71.4	67.6	69.8	69.5	73.6	63.2	7.2%
	50	5	75.3	79.0	135.3	135.1	124.9	89.6	64.4	62.9	69.1	72.9	74.8	100.5	110.6	98.8	74.7	49.5	29.8%
	55	5	99.8	95.0	115.4	110.0	108.8	121.8	118.8	104.3	111.0	102.9	93.5	98.0	106.0	99.2	101.6	61.9	13.3%
	60	5	114.9	113.4	80.7	94.0	98.9	104.0	90.3	100.3	127.6	104.2	99.5	97.4	110.6	103.8	87.0	66.1	14.6%
	65	5	99.2	126.8	112.2	115.1	118.7	69.9	21.8	48.3	78.3	81.4	79.6	125.6	115.0	94.3	63.2	57.1	34.9%
	70	5	170.8	180.1	140.3	120.0	131.2	147.8	131.2	121.7	145.8	148.1	120.2	151.0	169.1	139.5	91.5	121.2	16.2%
	75	5	85.6	52.7	77.3	61.5	68.0	95.0	126.8	150.2	123.4	116.9	81.3	95.8	105.9	89.6	91.7	109.2	26.9%
	80	5	144.5	163.7	121.9	142.8	102.5	137.6	136.9	130.0	183.6	183.5	159.3	188.8	184.4	150.2	199.0	139.3	17.8%

Minimum= **7.2%** Average= **19.7%** Maximum= **36.5%**

Table 10

Discrete unit weight, γ_T, results at 5 ft. intervals

Job #	Depth (ft)	Soil Classification	γ_T CPT 1	2	3	4	5	6	7	8	9	10	11	12	13	14	15	16	COV(γ_T)
Repeaibiliy (ALF)	5	4	113.2	113.6	112.6	110.1	106.6	111.7	110.0	114.6	111.0	111.5	112.3	112.4	110.9	114.5	111.0	113.5	1.80%
	10	3	114.1	108.0	114.4	112.7	112.9	114.3	113.2	110.6	113.3	111.4	111.7	114.6	110.9	113.5	113.0	112.9	1.53%
	15	3	111.8	111.8	112.3	110.0	111.7	112.7	112.8	113.0	111.9	111.9	112.2	110.7	111.8	113.3	111.1	113.0	0.79%
	20	3	113.3	114.0	115.7	112.7	115.9	113.4	114.2	115.0	113.4	114.8	114.4	116.2	109.3	115.0	114.3	115.0	1.43%
	25	5	110.6	107.6	108.2	104.4	109.6	108.2	112.0	110.6	110.4	109.4	105.4	107.8	106.9	106.3	107.9	110.6	1.94%
	30	5	107.7	108.6	105.4	107.0	108.4	109.5	108.1	107.5	107.2	107.8	107.3	106.9	108.0	107.5	107.9	109.3	0.91%
	35	4	107.3	105.2	107.7	107.3	109.4	107.3	106.1	107.8	108.3	106.6	106.5	108.5	107.4	107.2	105.5	107.3	1.00%
	40	5	109.3	109.0	111.9	110.6	108.4	108.2	112.8	111.5	115.0	109.2	107.3	109.3	108.0	106.4	107.3	111.7	2.12%
	45	5	115.8	114.7	115.2	114.9	115.5	115.0	115.8	115.8	115.7	115.0	114.4	114.4	114.6	113.4	113.0	114.0	0.73%
	50	5	116.2	118.4	120.8	120.9	120.6	120.0	113.5	112.3	113.9	117.5	117.8	119.3	120.2	118.9	117.1	112.7	2.53%
	55	5	117.0	117.8	120.1	119.9	119.2	117.6	115.8	115.7	116.4	117.0	116.8	117.9	118.3	117.9	116.4	112.8	1.52%
	60	5	115.1	114.8	115.3	115.9	116.4	117.7	116.0	116.1	117.2	116.3	116.1	117.1	117.6	117.2	115.3	111.7	1.25%
	65	5	117.5	119.5	117.1	116.7	117.6	115.6	108.9	111.0	113.7	115.9	115.7	118.0	118.6	115.2	112.6	111.3	2.62%
	70	5	118.1	117.7	116.9	116.4	115.2	118.9	116.6	117.1	118.5	117.9	117.0	117.5	119.4	117.4	112.1	114.6	1.53%
	75	5	114.5	113.1	115.7	112.8	114.1	114.7	115.6	115.7	117.4	115.9	113.6	115.1	115.7	114.5	111.4	116.3	1.32%
	80	5	118.1	117.1	116.3	115.1	116.3	116.7	115.9	116.1	118.6	118.5	116.7	117.1	118.3	115.9	117.9	118.2	0.94%

Minimum= **0.73%** Average= **1.50%** Maximum= **2.62%**

Table 11

Discrete overburden pressure readings at 5 ft. intervals

Job #	Depth (ft)	Soil Classification	σ_{vo} CPT																COV(σ_{vo})
			1	2	3	4	5	6	7	8	9	10	11	12	13	14	15	16	
Repeaibiliy (ALF)	5	4	0.30	0.30	0.30	0.30	0.29	0.30	0.30	0.30	0.30	0.30	0.29	0.30	0.29	0.30	0.30	0.30	0.87%
	10	3	0.58	0.57	0.58	0.57	0.57	0.58	0.58	0.58	0.58	0.57	0.57	0.58	0.57	0.58	0.58	0.58	0.79%
	15	3	0.87	0.86	0.87	0.86	0.86	0.87	0.87	0.87	0.87	0.86	0.86	0.87	0.85	0.87	0.87	0.87	0.65%
	20	3	1.17	1.16	1.16	1.16	1.16	1.16	1.16	1.17	1.17	1.16	1.15	1.17	1.14	1.16	1.16	1.17	0.61%
	25	5	1.44	1.42	1.43	1.43	1.42	1.43	1.43	1.44	1.43	1.43	1.42	1.44	1.41	1.43	1.43	1.44	0.58%
	30	5	1.71	1.69	1.70	1.70	1.70	1.71	1.70	1.71	1.71	1.70	1.69	1.71	1.68	1.70	1.70	1.71	0.52%
	35	4	1.98	1.97	1.97	1.97	1.97	1.98	1.97	1.98	1.98	1.97	1.96	1.98	1.95	1.97	1.97	1.99	0.47%
	40	5	2.26	2.24	2.25	2.25	2.25	2.26	2.25	2.26	2.26	2.25	2.23	2.26	2.23	2.25	2.25	2.27	0.44%
	45	5	2.55	2.54	2.54	2.53	2.54	2.55	2.54	2.55	2.55	2.54	2.52	2.54	2.51	2.54	2.53	2.56	0.45%
	50	5	2.85	2.84	2.84	2.83	2.84	2.85	2.84	2.85	2.85	2.84	2.82	2.84	2.81	2.83	2.83	2.85	0.41%
	55	5	3.15	3.14	3.14	3.14	3.13	3.15	3.14	3.15	3.15	3.13	3.12	3.14	3.11	3.13	3.12	3.14	0.37%
	60	5	3.44	3.43	3.44	3.43	3.43	3.45	3.44	3.44	3.44	3.43	3.41	3.43	3.41	3.42	3.41	3.43	0.37%
	65	5	3.74	3.73	3.73	3.73	3.72	3.74	3.72	3.73	3.74	3.73	3.70	3.73	3.70	3.72	3.70	3.71	0.36%
	70	5	4.04	4.03	4.02	4.02	4.02	4.04	4.01	4.03	4.04	4.02	4.00	4.03	4.00	4.01	3.99	4.00	0.39%
	75	5	4.34	4.33	4.32	4.31	4.31	4.34	4.31	4.33	4.34	4.32	4.30	4.33	4.31	4.31	4.28	4.30	0.42%
	80	5	4.62	4.60	4.60	4.59	4.59	4.62	4.59	4.61	4.62	4.60	4.57	4.60	4.59	4.59	4.55	4.58	0.42%

Minimum= **0.36%** Average= **0.51%** Maximum= **0.87%**

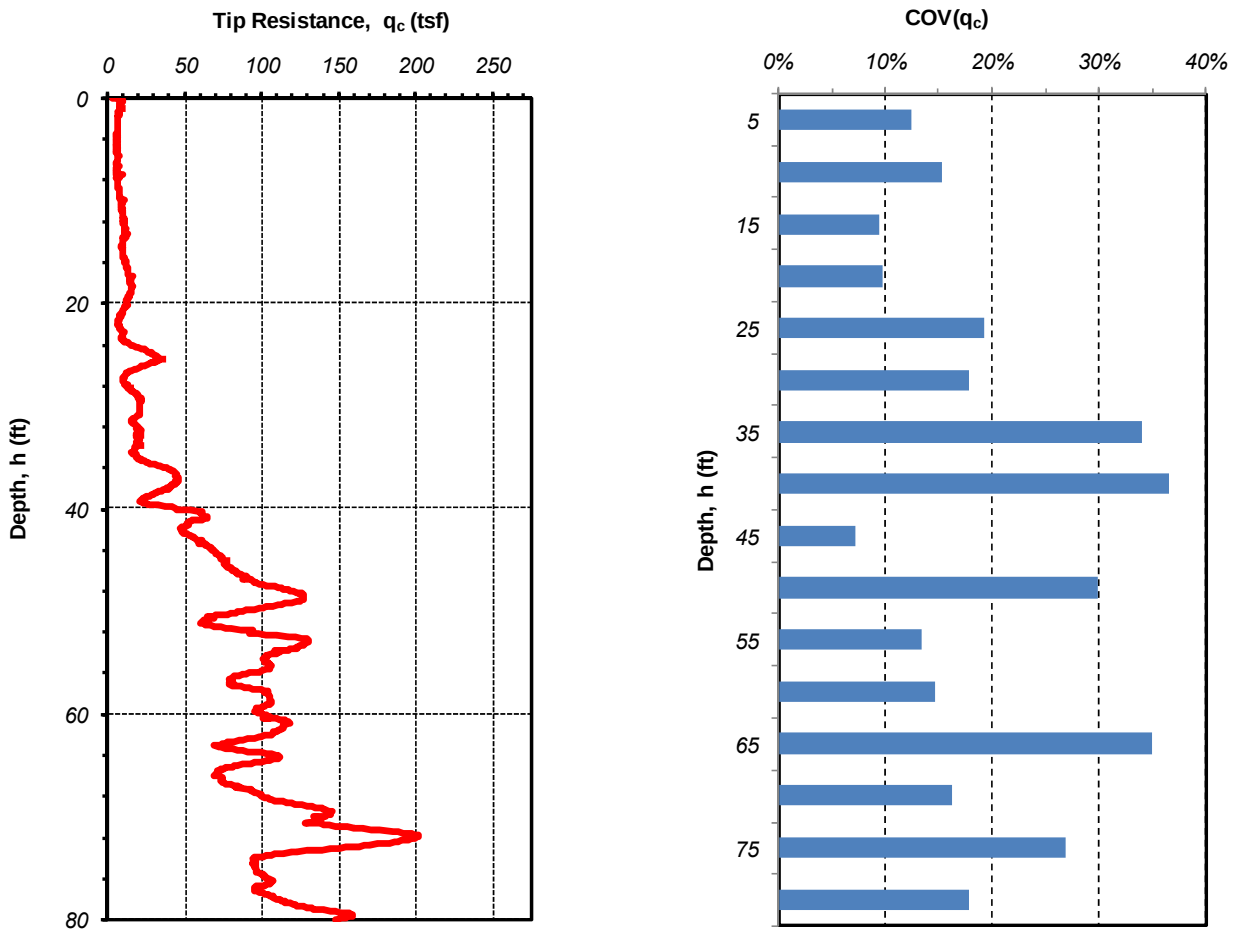

(a) Average q_c readings **(b) COV (q_c) vs. depth**

Figure 29
Analysis of repeatability data for cone tip resistance

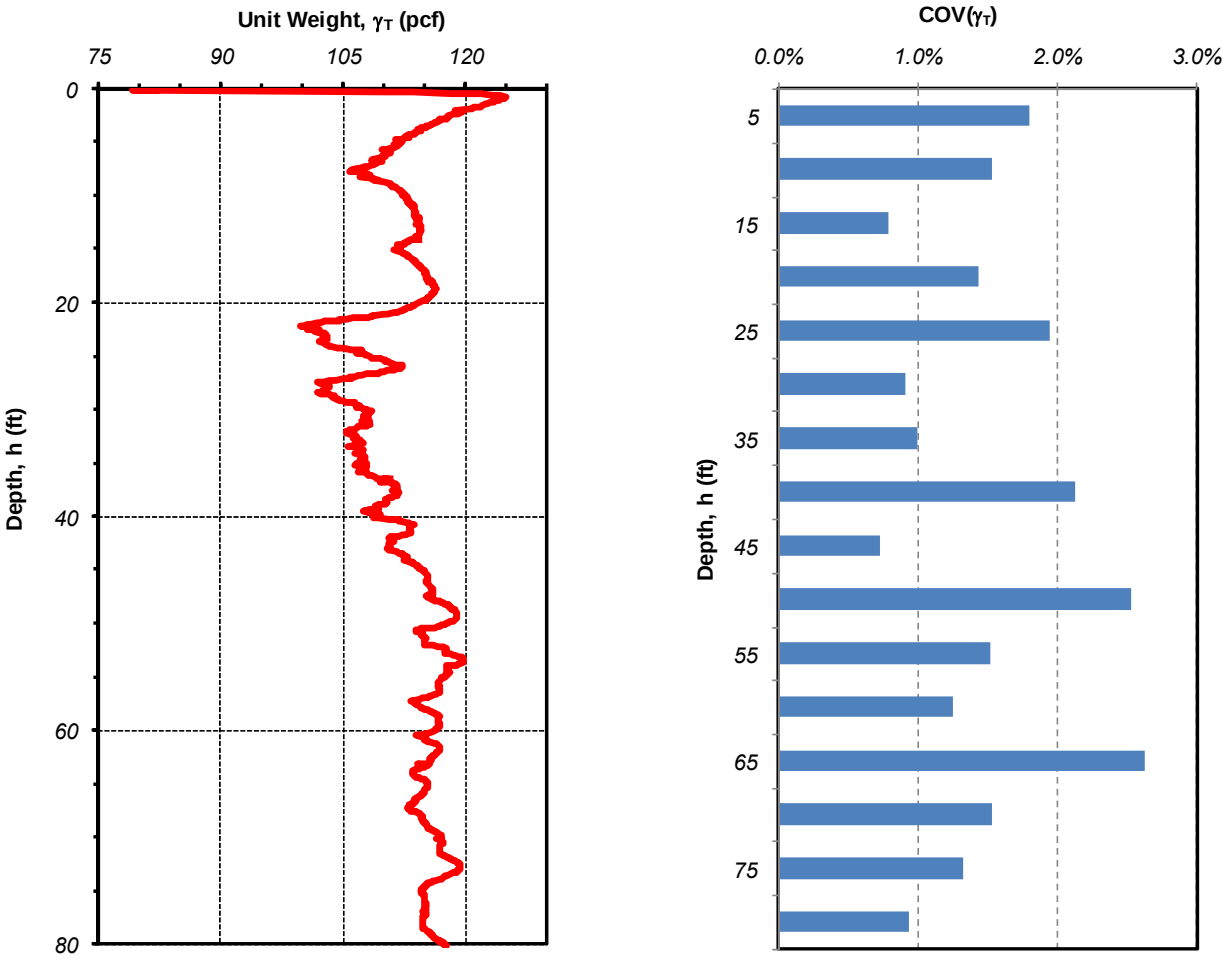

(a) Average γ_T readings **(b) COV (γ_T) vs. depth**

Figure 30

Study of unit weight data scatter from repeatability tests

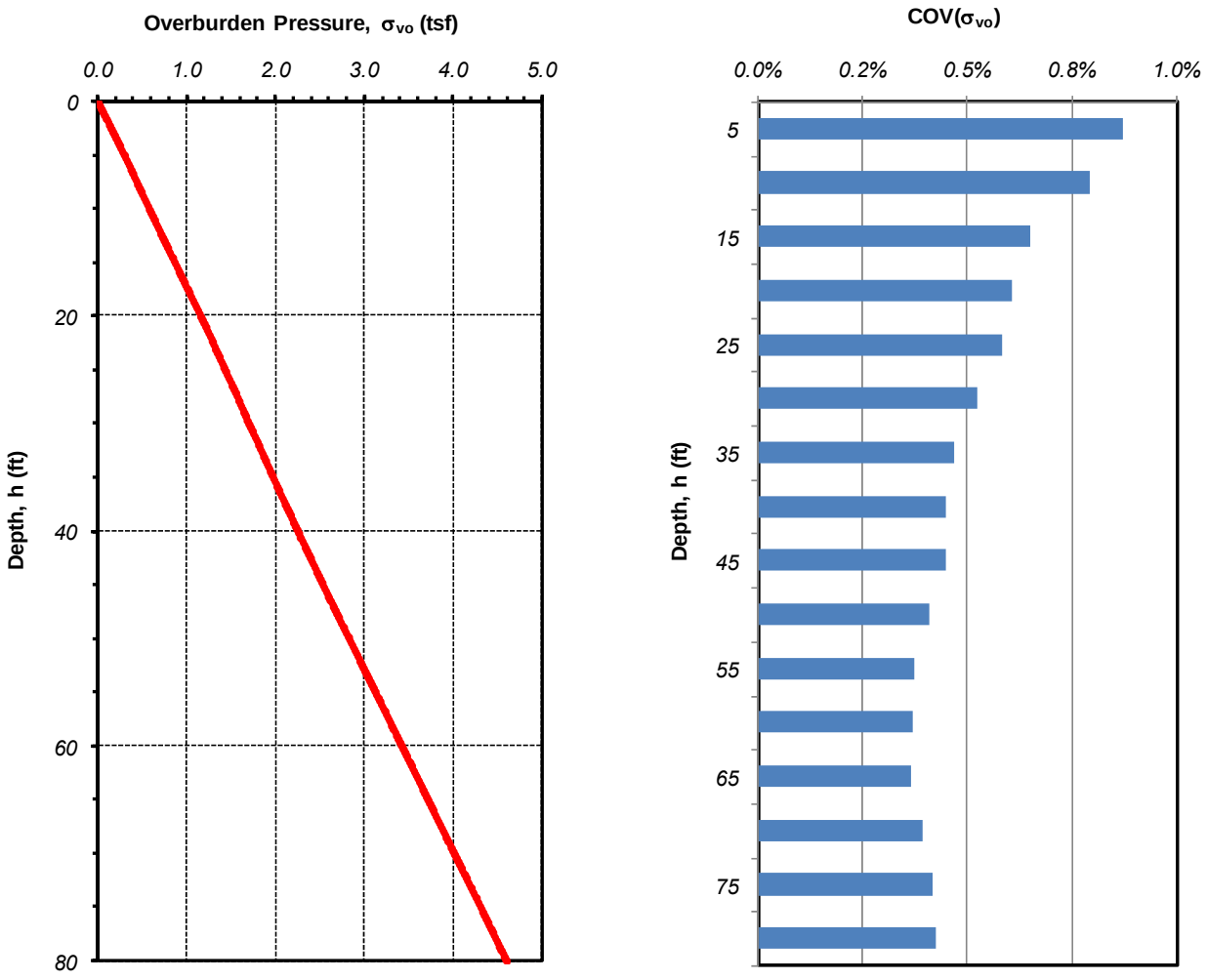

(a) Average σ_{vo} readings **(b) COV (σ_{vo}) vs. depth**

Figure 31
Study of overburden pressure data scatter from repeatability tests

Soil Classification. The same statistical results were studied by focusing on the soil classification obtained using Robertson's method [*1*].Classifications where obtained along the soil depth for all 16 CPT repeatability tests. These results are plotted in Figure 32 which shows that the first 40 ft. of the soil are classified as to be mixtures of silt and clay. The range is from clay (Classification 3) to clayey silt or silty clay (Classification 4). Some readings show silt/sand mixtures (Classification 5). Beyond the first 40 ft., an obvious change can be seen. The soil classification is mainly between Classification 5 and Classification 6 which corresponds to silt/sand mixture to clean sand, except for a thin layer around a depth of 50 ft., where it appears that more clay and silt are present. These classifications may be the

explanation why the trend for $COV(\sigma_{vo})$ changed at this juncture (h=40 ft.). It also raises interest in studying the variability of the measurements as a function of the soil classification.

Plots of the coefficient of variation, COV, for the same previous parameters are shown in Figure 33 through Figure 35 to study such an effect. By analyzing these plots, one can conclude that clays/silty clays (Classification 3) have a narrower range of COV, of the tip resistance, q_c, as compared to the same range for silt/sand mixtures (Classification 5). Similar observations may be made for the unit weight, γ_T; however, the difference is smaller. No clear trend is observed for the overburden pressure, σ_{vo}. Again, it should be noted that the COV of the unit weight, γ_T, and the overburden pressure, σ_{vo} are extremely small and that the COV of the tip resistance, q_c, will be the main source of device/procedural uncertainty in this study.

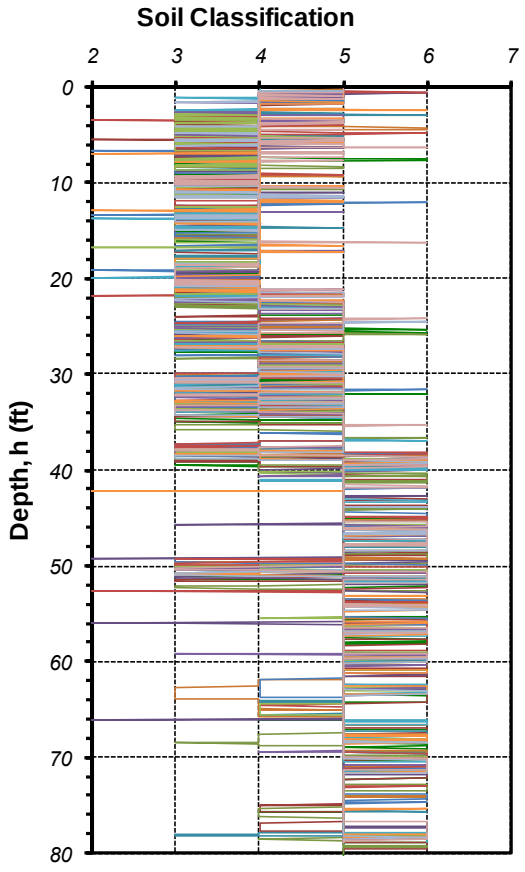

Figure 32
Tip resistance, q_c, readings from all CPT repeatability tests

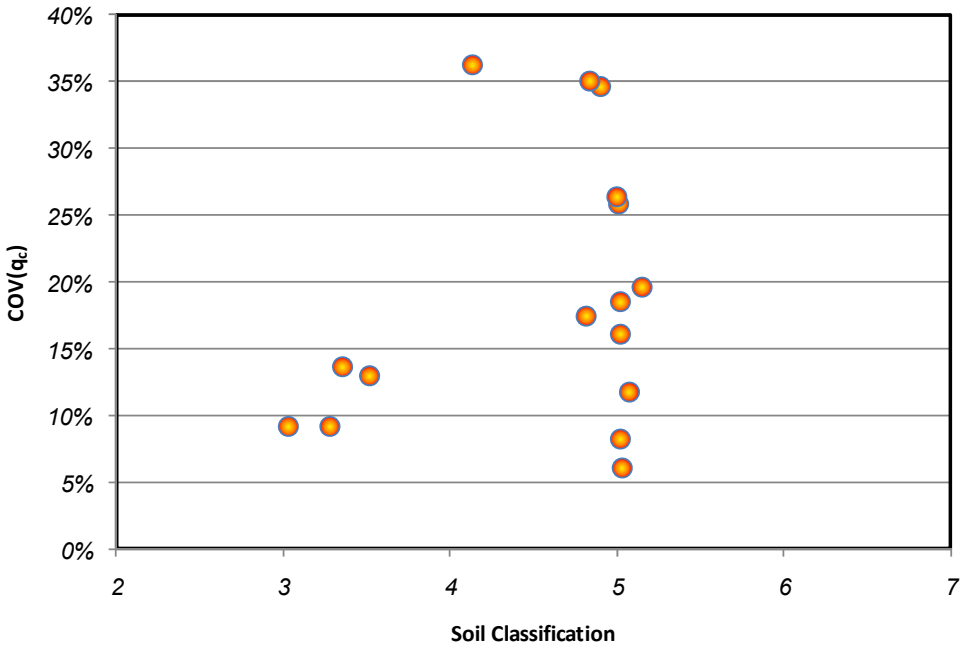

Figure 33

Study of tip resistance data scatter, COV(q_c), vs. soil classification

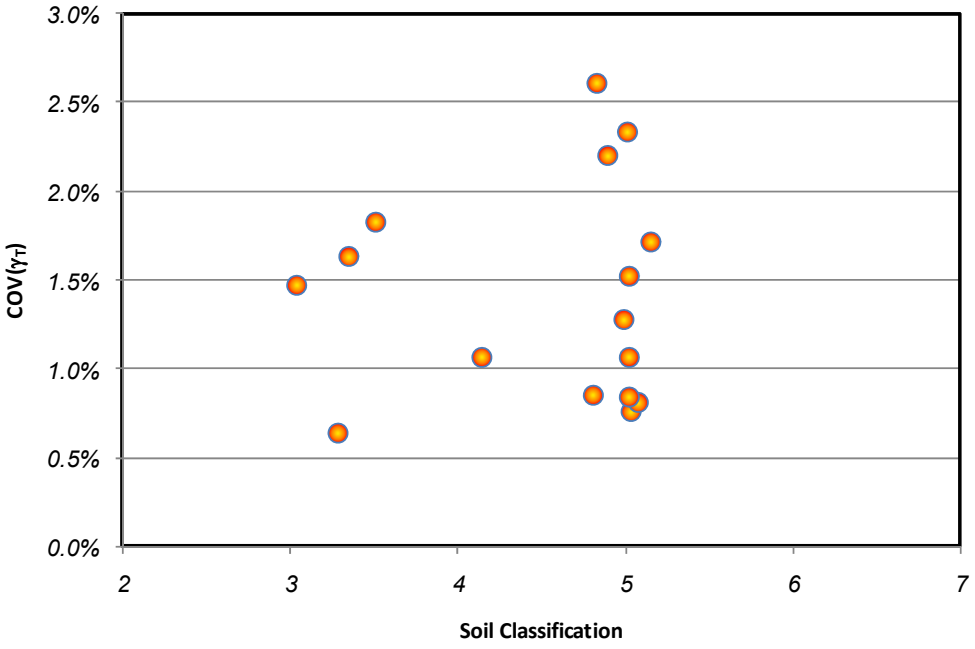

Figure 34

Study of unit weight data scatter, COV(γ_T), vs. soil classification

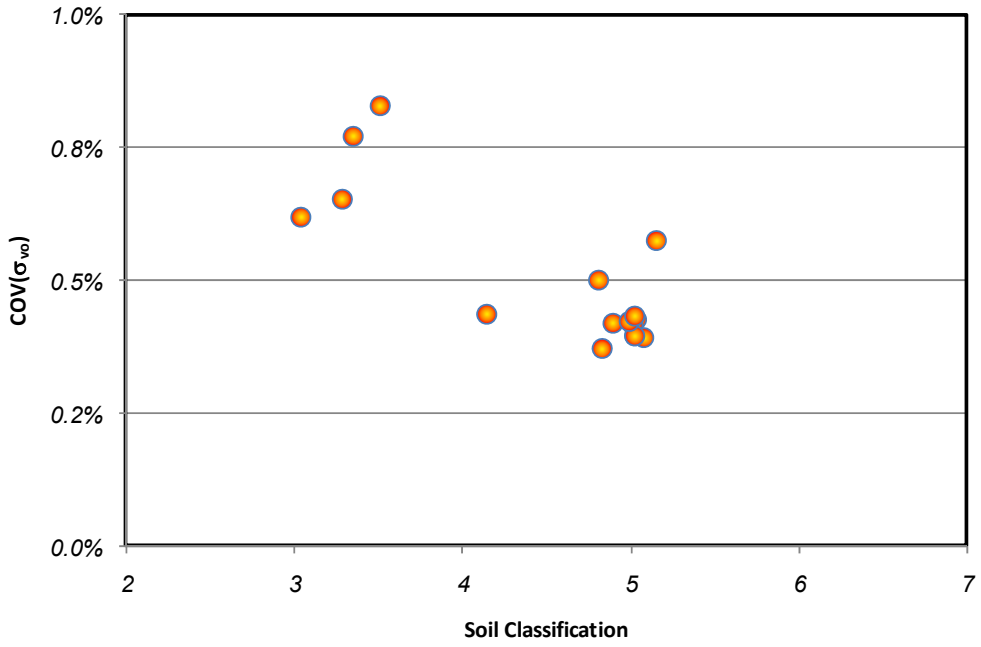

Figure 35
Study of overburden pressure data scatter, COV(σ_{vo}), vs. soil classification

Utilizing CPT for Assessment of Site Variability

Recent LRFD design codes adopt an approach where design factors are dependent on site variability. The assessment of the site variability is an important step in the overall design process as it greatly influences the outcomes. In this section, a methodology is proposed to assist geotechnical engineers in determining the site variability from CPT readings. Although the goals of this study did not include developing methods for classification of sites based on their variability, the results presented in this report may assist in achieving this goal. It is believed that based on the repeatability study, a procedure can be established for the purpose of classifying sites without the need for any subjective interference by the designer.

The underlying principal in the proposed approach is that multiple CPT soundings in a certain site can reveal the uncertainties inherent in the site. These uncertainties include those related to the device itself as well as soil variability. If we assume that the overall scatter is presented as the $COV\left(S_u^{CPT}\right)$ from multiple CPT soundings from a specific layer at the investigated site, it can be said that this scatter is caused by:

- the device uncertainty, which is mostly caused by the uncertainty in cone tip resistance and measured by $COV(\eta)$ since the variability in the overburden pressure is negligible and can be ignored, and
- the inherent variability in soil properties, which can be obtained from the literature as the coefficient of variation of the undrained shear strength for fine soils $COV(\gamma)$.

This assumption leads to the fact that the expected coefficient of variation of the undrained shear strength can be obtained as a function of the coefficient of variation for the two random variables, η and γ . Based on the coefficient of variation of the cone tip resistance that was established earlier (19.7 percent), it is possible to determine the expected coefficient of variation for the undrained shear strength for different assumed soil variabilities corresponding to low, medium, and high variability. Comparing the expected coefficient of variation, $COV\left(S_u^{CPT}\right)$, to what is actually computed from multiple CPT soundings for the soil layer of interest can be used to classify the site variability.

The proposed procedure that lays out the framework that can be refined and tested in a future research project is outlined next. For illustration purposes, the coefficient of variation, $COV(\gamma)$, is taken as 6 percent, 25 percent, and 33 percent corresponding to low, medium, and high, respectively.

1. The CPT readings for the site in question are collected and soil layers (classifications) are identified.

2. For each layer of interest (e.g., foundation level), the estimate for the design property such as undrained shear strength, S_u^{CPT} , is obtained from all CPT soundings.

3. Statistical analysis of the soil property (e.g., S_u^{CPT}) will yield a mean and standard deviation. The coefficient of variation from these results, $COV\left(S_u^{CPT}\right)$, is then computed to be used for site variability assessment.

4. By comparing $COV\left(S_u^{CPT}\right)$ to the coefficient of variation that is expected from the measuring device and the inherent soil variability, one can assess the site variability. This can be done in three groupings:
   a. measured coefficient of variation values equal to or smaller than what is

expected for the low end of inherent soil variability ($COV(\gamma) = 6$ percent); i.e., expected $COV\left(S_u^{CPT}\right) = 21$ percent, indicate that the site variability is *low*,

b. measured $COV\left(S_u^{CPT}\right)$ values corresponding to what is expected for an average inherent soil variability ($COV(\gamma) = 20$ percent); i.e., expected $COV\left(S_u^{CPT}\right) = 28$ percent, indicate that the site variability is *medium*, and

c. Higher $COV\left(S_u^{CPT}\right)$ values indicate that the site variability is *high*.

It should be noted that this approach is only valid for fine soils if consistent soil layers could be identified. In the case were soil layers cannot be identified, the site variability assessment should be automatically set to *high*.

Initial Data Analysis

General Trends

Before calibrating the CPT method for undrained shear strength results, data trends are examined to identify any possible relations. The current expression (transformation model) used for estimating the undrained shear strength is given as

$$S_u^{CPT} = \frac{q_c - \sigma_{vo}}{N_{kt}} \tag{41}$$

Figure 36 shows a preliminary comparison of the undrained shear strength as obtained from CPTs and boreholes (UC). The plot shows all 862 data points in the database. Two general conclusions may be made at this stage and these are:
The data scatter is considerably high (COV=71 percent)
CPT results are on average higher than the corresponding borehole results; i.e., S_u^{CPT} is an overestimate of S_u^{UC}.

It should be noted that these results were obtained using equation (41) assuming a N_{kt} value of 15. As will be seen later, a single N_{kt} value that is valid for all soil types is not the right approach, which has therefore contributed to the wide scatter.
An attempt was then made to assess the relationship between the undrained shear strength and each of the variables involved, q_c and σ_{vo}.

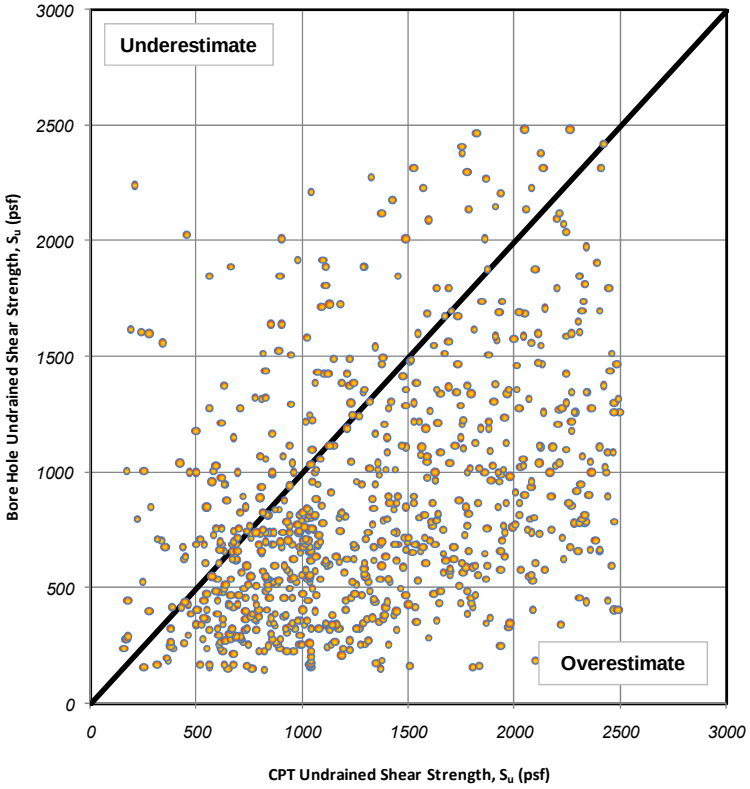

Figure 36
Comparison of undrained shear strength, S_u, from CPT and UC tests

While studying the trends in collected data, it was deemed worthy to also study the trends of the borehole undrained shear strength values, S_u^{UC}, versus various CPT readings used in this study. The purpose of this analysis is to shed some light on the performance of equation (41) in predicting the undrained shear strength and whether a different expression is needed.

In Figure 37, three plots for the relation between the undrained shear strength, S_u^{UC}, and the tip resistance, q_c, as well as the overburden pressure, σ_{vo}, and the net difference, $q_c - \sigma_{vo}$, are shown. The plots reveal that there is a rising trend in the tip resistance versus undrained shear strength values. This confirms the inclusion of the first term in equation (41) as a first order with a positive sign. Figure 37b shows that the undrained shear strength drops as the overburden pressure increases. However, this trend is not as pronounced as it is for the tip resistance, which may suggest that including both parameters, q_c and σ_{vo}, with equal slopes in equation (41) may need to be revisited. Finally, Figure 37c confirms the rising trend of undrained shear strength, S_u^{UC}, as a function of the net difference, $q_c - \sigma_{vo}$, which is a basic

variable in equation (41). The figure also shows five ideal trends obtained using equation (41) for different N_{kt} values ranging from 12 to 30. The purpose of these trends is to provide the reader with a visual representation of which N_{kt} results in a better match to the borehole results in the database. It can be seen from these trend lines in Figure 37c that a N_{kt} value of 12 is biased on one side of the dataset and that a N_{kt} value between 25 and 30 better represents the results in the database. It should be noted that these remarks are based on the entire dataset compiled in the database.

Development of a more refined expression would need to include various factors that may affect the observed trends (e.g., soil classification, depth, etc.) Several attempts were made to come up with other expressions that would better match the available data. These expressions included higher order polynomials; elimination of the overburden pressure, σ_{vo}, from the expression; and a constant to address the non-zero intersect that can be seen in the Figure 37. The conclusion from these attempts is that a better bias can be achieved (results can be better matched on average); however, the scatter is not much different, which affects the uncertainty of the transformation model. Therefore, it was decided to keep the currently used transformation model, equation (41), because of its simplicity.

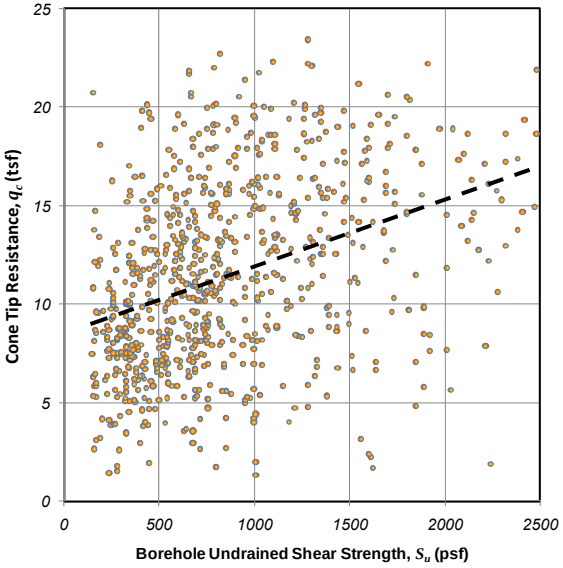

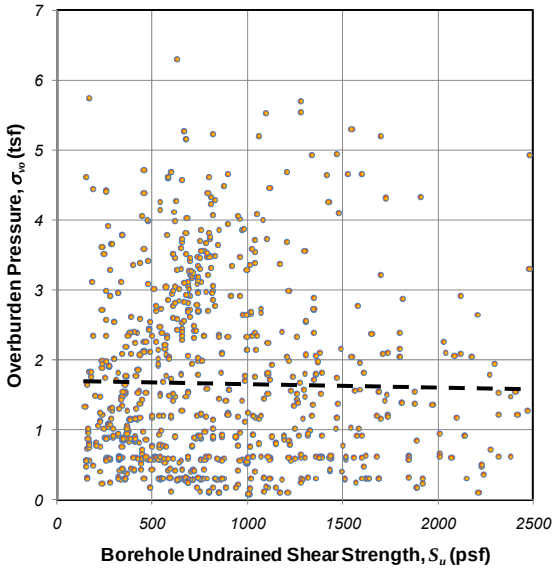

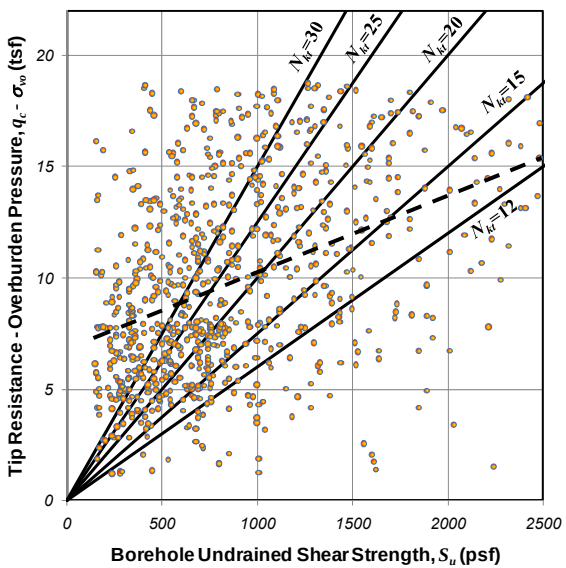

(a) cone tip resistance, q_c **(b) overburden pressure, σ_{vo}** **(c) net difference, q_c - σ_{vo}**

Figure 37

Analyzing data trends of different CPT readings versus S_u^{UC}

Specific Parameter Trends

Following the initial review of the collected data, the next phase in the study was to study the results in light of specific relevant parameters that may affect the reliability of CPT readings. This section presents the results of these analyses which include studying the following parameters:

- Soil Depth, *h*
- CPT Reading Values, ($q_c - \sigma_{vo}$)
- Soil Classification:
  - Zhang and Tumay Method (1999)
  - Robertson's Method (1990)
  - Plasticity Index

The range of each of the studied parameters was dissected into small intervals. The CPT results in the database within each of the intervals was statistically analyzed to obtain the bias, λ, and coefficient of variation, COV, of the ratio S_u^{CPT} / S_u^{UC} as described earlier. Both quantities represent how accurate the CPT results are when compared to the borehole results. Bias values close to unity (1.0) indicate an accurate method on average, whereas values below or above 1.0 mean that the CPT results are underestimating or overestimating the undrained shear strength, respectively. The scatter of the results is reflected in the COV values. The higher the COV, the more scatter in S_u^{CPT} is indicated. These results are presented next in tabular form for each of the listed parameters. They will form the basis for the reliability-based calibration study that follows this section. Also presented in the tables are the average and standard deviation for N_{kt} within each subcategory. These N_{kt} characteristics are provided for easier interpretation of the statistical parameters discussed earlier. In addition to the tabulated results, graphical plots (Figure 38 through Figure 43) of undrained shear strength estimates from CPT and boreholes are presented within each range of the chosen parameters. The purpose of these plots is to provide the reader with a sense of the extent of the scatter and the bias graphically, which may be needed for readers with little exposure to scientific literature in that area.

It should be noted that the purpose of investigating these trends is to identify any parameters that would improve CPT estimates of the undrained shear strength if included in the analysis.

The trends are determined based on the currently used value of 15. Despite the fact that this N_{kt} value is commonly used, it was picked for this part of the study as an arbitrary value. Other N_{kt} values could have been chosen without altering the observations made about the trends; N_{kt} is only a constant in any case. As will be seen later, other N_{kt} values will be determined during the calibration study.

Depth, *h*. Studying the effect of soil depth on the uncertainties inherent in CPT predicted undrained shear strength values can be viewed as part of studying the effect of spatial variations. The goal of this study is to determine whether different soil depths result in different overestimation or underestimation of the undrained shear strength. Several arbitrary depth intervals were chosen for this purpose. They represent a top layer with a 5 ft. depth followed by layers ending at 20 ft. depth intervals, i.e., *h* = 5-20, *h* = 20-40, *h* = 40-60, and *h* greater than 60 feet. It should be noted that each depth range included an acceptable number of data points that can be analyzed statistically. A higher resolution of depth ranges might be possible in the future as more CPT results are included in the database. The S_u^{CPT} / S_u^{UC} ratio within each depth interval was analyzed and the bias and COV were calculated.

Table 12 summarizes the bias and COV results for the chosen depth ranges. The results do not indicate a clear trend for any of the computed statistical descriptors. For example, the bias increases from a value of 1.473 (overestimate) at depths < 5 ft. to 2.203 for depths between 5 ft. and 20 ft. However, this trend does not continue beyond this depth range. Actually, it fluctuates around an almost constant value. Similarly, the coefficient of variation, COV, also does not seem to follow a clear trend. After dropping from 85 percent to 58 percent at depth range 40-60 ft., it increases again for higher depths.

Based on these observations, it was concluded that no clear trends can be extracted from the available dataset. As a result, the reliability-based calibration would not result in a N_{kt} factor that depends on, or is a function of, *h*.

Table 12

Effect of soil depth on uncertainty of CPT results

Depth range, h_1 : h_2 (feet)	**< 5**	**5-20**	**20-40**	**40-60**	**> 60**
Bias, λ	1.473 ↗	2.203 ↘	2.191 ↘	1.826 ↗	1.940
Standard Deviation, σ_λ	1.248 ↗	1.600 ↘	1.347 ↘	1.057 ↗	1.410
Coefficient of Variation, COV	85% ↘	73% ↘	61% ↘	58% ↗	73%
Number of Points, N	123	317	189	122	111
Average CPT Coefficient, N_{kt}	22.1	33.0	32.9	27.4	29.1
Standard Deviation, $\sigma_{N_{kt}}$	18.7	24.0	20.2	15.9	21.2

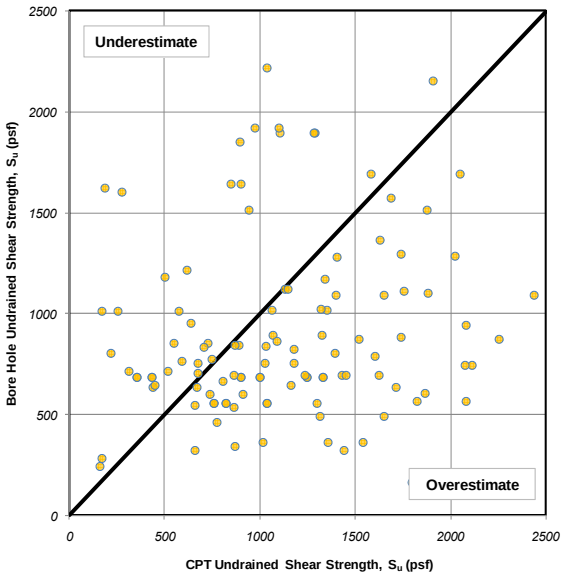

***h* < 5 ft.**

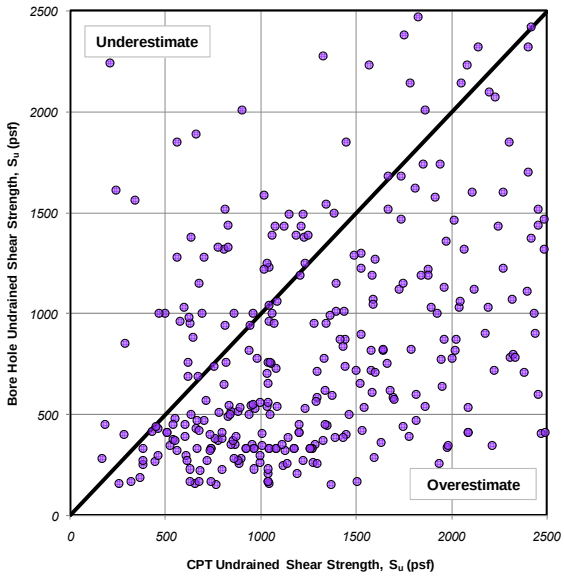

5 ft. < *h* < 20 ft.

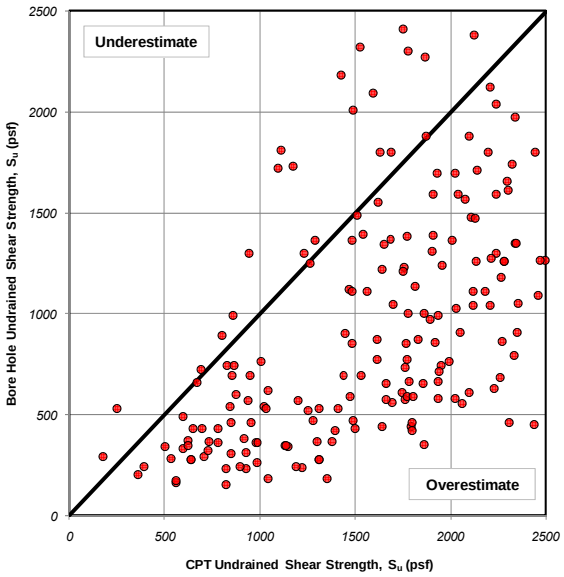

20 ft. < *h* < 40 ft.

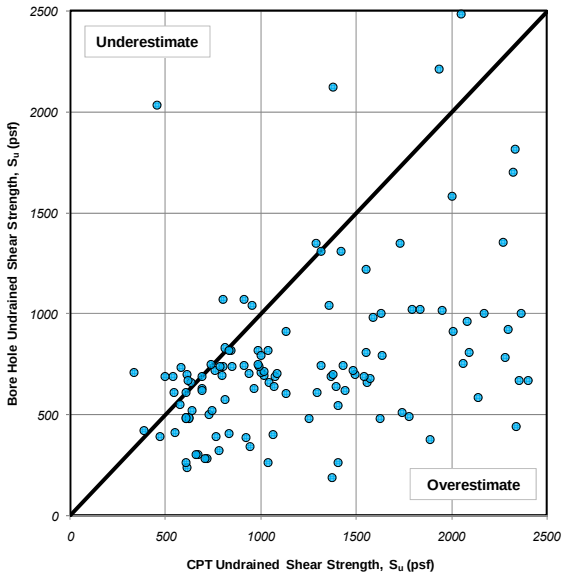

40 ft. < *h* < 60 ft.

Figure 38

Comparison of undrained shear strength, S_u, from CPT and UC tests at different depths

CPT Reading Values ($q_c - \sigma_{vo}$)

The second influence study conducted is related to the net difference between CPT readings, $q_c - \sigma_{vo}$. This difference is in the core of the CPT expression for undrained shear strength, equation (6). Studying whether the uncertainties in the CPT results are influenced by $q_c - \sigma_{vo}$ is done for the purpose of incorporating such influence in the calibration study to follow. The hypothesis is that if such a trend exists, the user can easily compute the net difference and use an appropriate N_{kt} value for undrained shear strength calculations. As with the previous parameter (soil depth), the range of $q_c - \sigma_{vo}$ was divided into several ranges. They are: less than 4 tsf, between 4 and 8 tsf, between 8 and 12 tsf, between 12 and 16 tsf, and greater than 16 tsf. The data points that fell within these ranges were statistically analyzed as before. Table 13 summarizes the results of this statistical analysis for each of the $q_c - \sigma_{vo}$ ranges.

The results show that there is a clear trend in the bias for the ratio S_u^{CPT} / S_u^{UC}. The CPT estimates are conservative on average for the $q_c - \sigma_{vo}$ below 4 tsf. However, unconservative estimates of the undrained shear strength are indicated for the higher $q_c - \sigma_{vo}$ values. This COV varies slightly about an average value of 68 percent. It appears that the net difference between the CPT readings, $q_c - \sigma_{vo}$ present the clearest parameter that influence the CPT coefficient N_{kt}. As more data become available, it may be possible to calibrate N_{kt} as a function of two parameters, one being the net difference between the CPT readings, $q_c - \sigma_{vo}$. Therefore, this information should be considered in any future research efforts that build on the findings of this study.

Table 13

Effect of net difference between CPT readings, $q_c - \sigma_{vo}$, on uncertainty of CPT results

Net Difference, $q_c - \sigma_{vo}$ (tsf)	**< 4**	**4-8**	**8-12**	**12-16**	**> 16**
Bias, λ	0.849 ↗	1.751 ↗	2.215 ↗	2.339 ↗	2.491
Standard Deviation, σ_λ	0.610 ↗	1.082 ↗	1.474 ↗	1.636 ↗	1.724
Coefficient of Variation, COV	72% ↘	62% ↗	67% ↗	70% ↘	69%
Number of Points, N	57	315	226	173	91
Average CPT Coefficient, N_{kt}	12.7	26.3	33.2	35.1	37.4
Standard Deviation, $\sigma_{N_{kt}}$	9.2	16.2	22.1	24.5	25.9

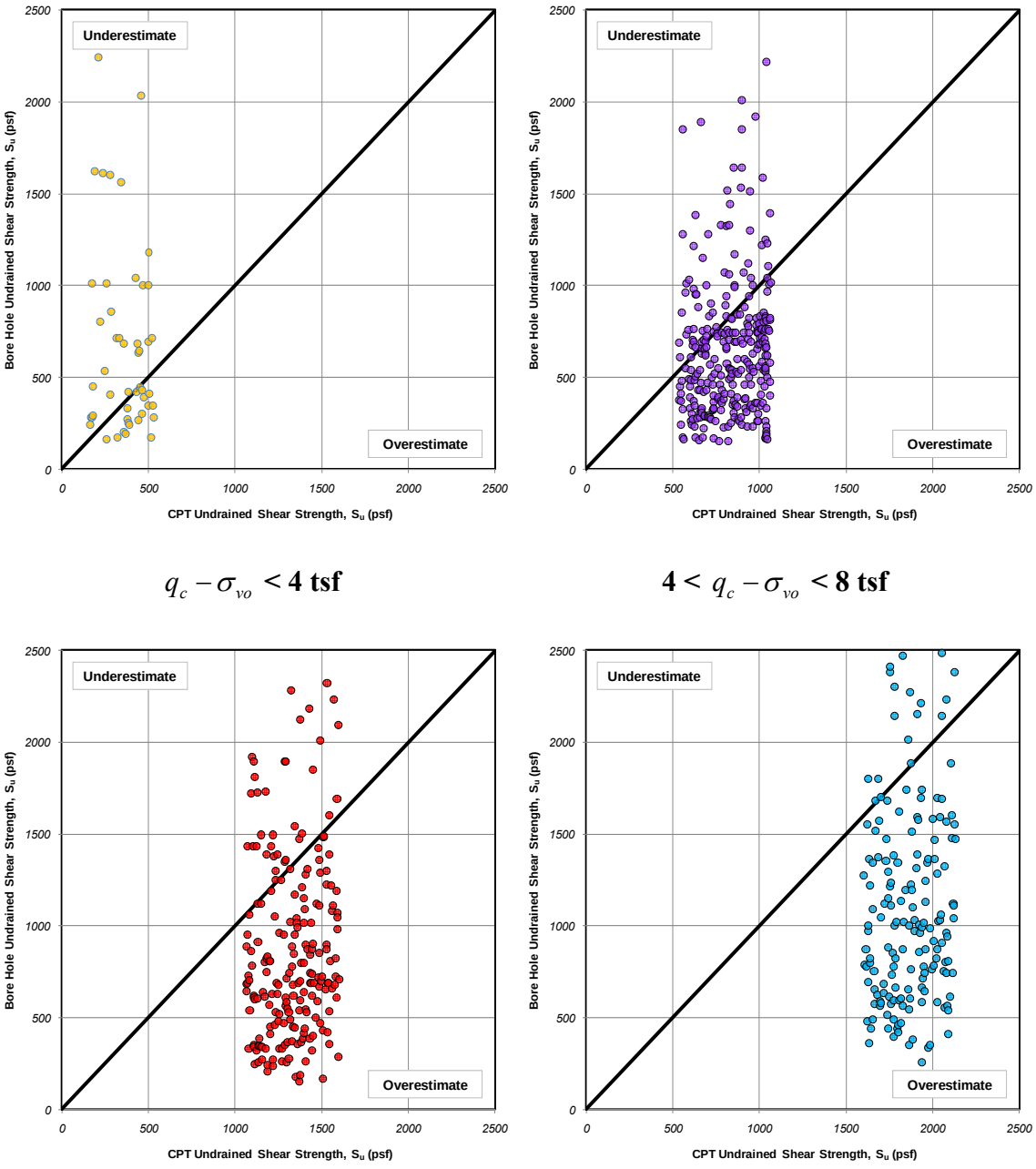

$q_c - \sigma_{vo} < 4$ tsf

$4 < q_c - \sigma_{vo} < 8$ tsf

$8 < q_c - \sigma_{vo} < 12$ tsf

$12 < q_c - \sigma_{vo} < 16$ tsf

Figure 39

Comparison of undrained shear strength, S_u, from CPT and UC tests at different CPT readings net difference, $q_c - \sigma_{vo}$, values

Soil Classification. Three soil classification methods were investigated to study the uncertainty in CPT undrained shear strength estimates:

- Zhang and Tumay Method (1999)
- Robertson's Method (1990)
- Plasticity Index (PI)

The first method is implemented in the LADOTD's software for CPT data analysis. It provides the probability of existence of three soil types, namely, clay, silt, and sand. The focus of this project is on the undrained shear strength that is related to clayey soils. Therefore, the predicted probability of clay percentage is chosen as the classification parameter. The second method by Robertson (1990) provides soil classifications as one of six possible types: two for organic soils and peats, three for clays (silty clay to clays), four for silt mixtures (clayey silt to silty clay), five for sand mixtures (silty sand to sandy silt), six for sands (clean sand to silty sand), and seven for gravelly sand to dense sand. The classifications of interest to this study are two through four where the undrained shear strength is relevant. Finally, the plasticity index, which is equal to Liquid Limit (LL) minus the plastic Limit (PL) is also investigated as a possible soil classification method by studying its correlation to CPT undrained shear strength estimates. The results from studying these three parameters are described next.

Zhang and Tumay Method. This classification approach provides the user with the probability of existence of clay, silt, and sand from CPT readings. Its major advantage in the context of this study is that no borehole results will be needed to assist in estimating the undrained shear strength, unlike the Plasticity Index for example where such information will be necessary. The data points were grouped twice based on: (1) the probability of existence of clay and (2) the probability of existence of clay plus silt combined. The probability of existence of sand was not considered since it is not related to the undrained shear strength. The results from the two groupings are presented next.

Table 14 lists the results for the first grouping of probability of existence of clay in the tested soil. Both silt and sand are excluded in this grouping. Four ranges of probability of clay existence were chosen for this study. They are less than 25 percent, between 25 and 50 percent, between 50 and 75 percent and greater than 75 percent. Data points falling

within each range were analyzed statistically as before. The bias, standard deviation, and coefficient of variation are given in Table 14. It can be seen that after an initial increase in the bias and coefficient of variation for the first two ranges (< 25 percent and 25-50 percent), a clear declining trend is noticed. This implies that as the probability of clay existence increases, the CPT becomes a more reliable tool for estimating the undrained shear strength. This is expected because the undrained shear strength is a quantity that describes soils with high clay contents and the existence of coarser materials in the soil adversely affects the CPT readings for undrained shear strength calculations.

Table 15 lists the results from the same classification method; however, the probabilities of existence of clay and silt are combined. Four ranges were chosen for the investigation. They are less than 80 percent, between 80 and 90 percent, between 90 and 97.5 percent and greater than 97.5 percent. The statistical results for the data points within each range showed trend similar to when only clay was considered. An initial rise for the bias between the first and second range was noticed followed by a consistent drop from one range to the other for subsequent ranges. The coefficient of variation's trend was not as clear. The first two ranges (< 80 percent and 80 – 90 percent) had a similar coefficient of variation (68 percent), followed with a rise in the third range to 83 percent and then a drop to 65 percent in the fourth range. This indicates that relying on the existence of clay might be a better solution in future calibration efforts due to the clearer trends it offers.

Table 14
Effect of soil classification on uncertainty of CPT results
(Zhang and Tumay – clay only)

Clay Percentage (%)	**< 25**		**25-50**		**50-75**		**> 75**
Bias, λ	2.112	↗	2.273	↘	1.954	↘	1.822
Standard Deviation, σ_λ	1.422	↗	1.774	↘	1.476	↘	1.124
Coefficient of Variation, COV	67%	↗	78%	↘	76%	↘	62%
Number of Points, N	171		210		128		353
Average CPT Coefficient, N_{kt}	31.7		34.1		29.3		27.3
Standard Deviation, $\sigma_{N_{kt}}$	21.3		26.6		22.1		16.9

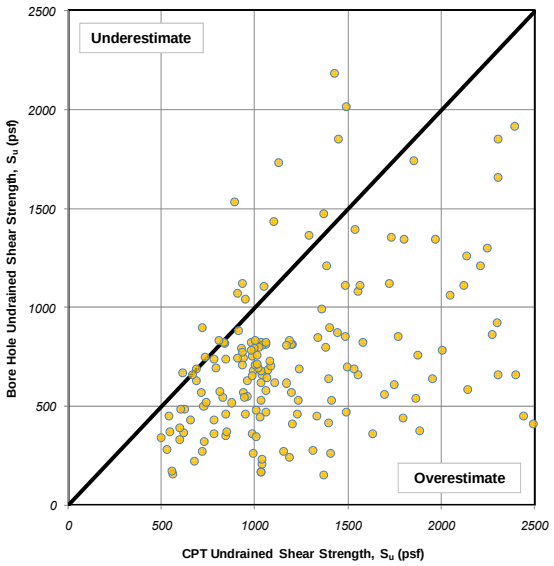

Clay < 25%

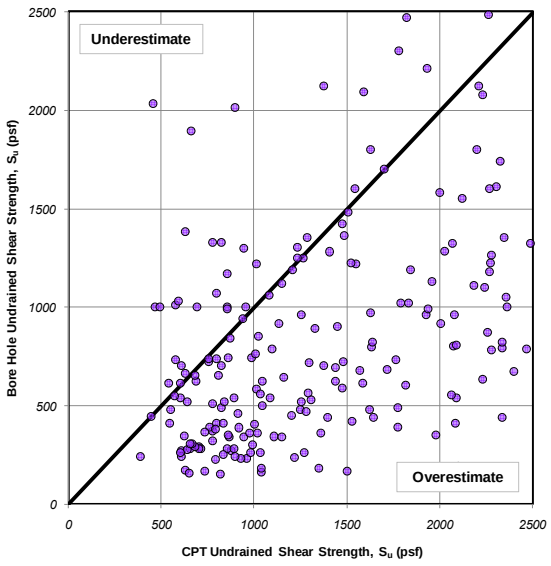

25 % < Clay < 50%

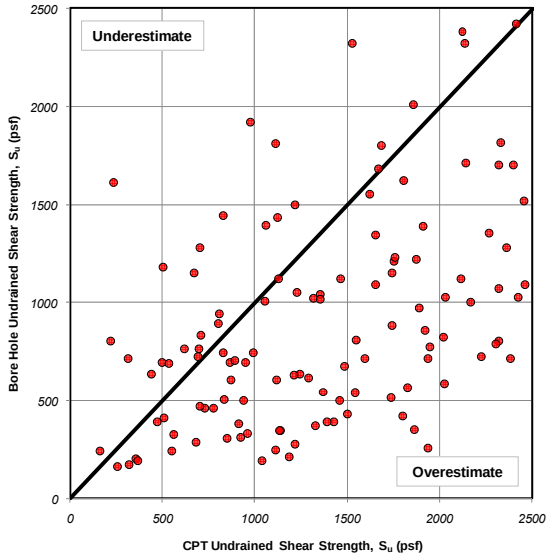

50 % < Clay < 75%

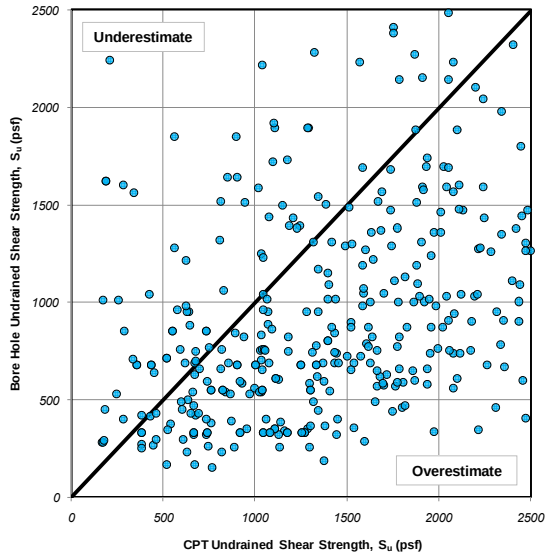

Clay > 75%

Figure 40

Comparison of undrained shear strength, S_u, from CPT and UC tests for different soil classifications (Zhang and Tumay – clay only)

Table 15
Effect of soil classification on uncertainty of CPT results
(Zhang and Tumay – clay and silt)

Clay and Silt Percentage (%)	**< 80**	**80-90**	**90-97.5**	**> 97.5**
Bias, λ	2.168	2.207	2.203	1.853
Standard Deviation, σ_{λ}	1.478	1.505	1.825	1.212
Coefficient of Variation, COV	68%	68%	83%	65%
Number of Points, N	105	132	156	469
Average CPT Coefficient, N_{kt}	32.5	33.1	33.0	22.8
Standard Deviation, $\sigma_{N_{kt}}$	22.2	22.6	27.4	18.2

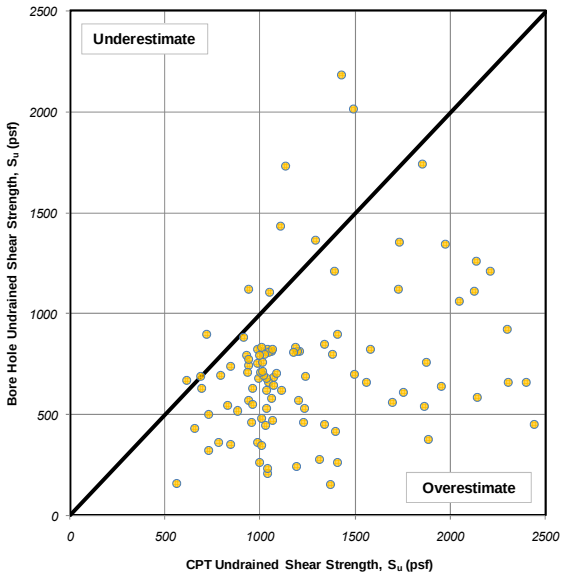

Clay and Silt < 80%

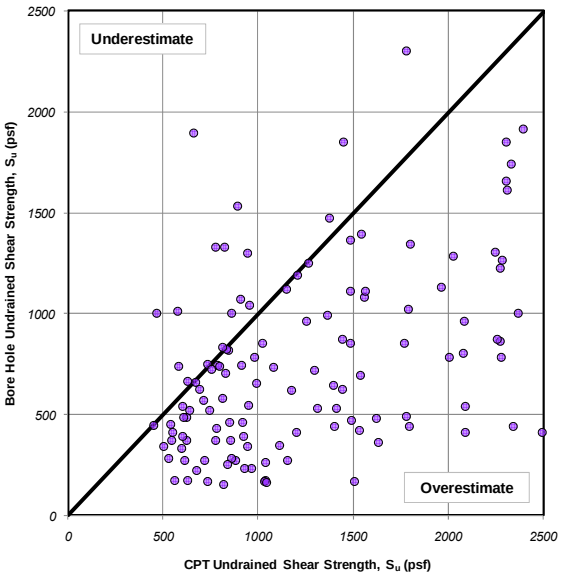

80 % < Clay and Silt < 90%

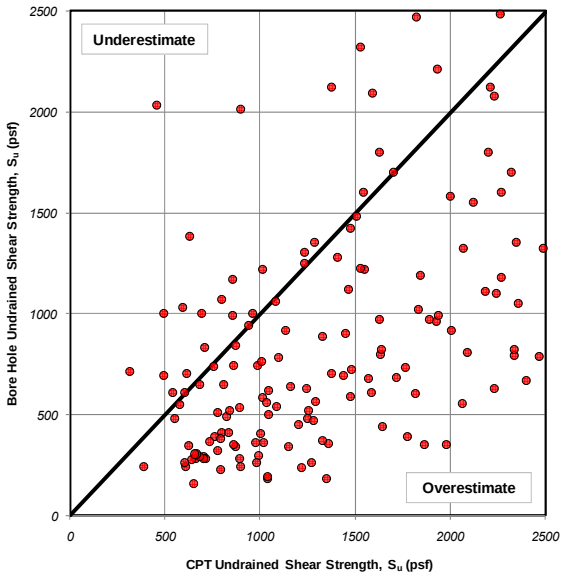

90% < Clay and Silt < 97.5%

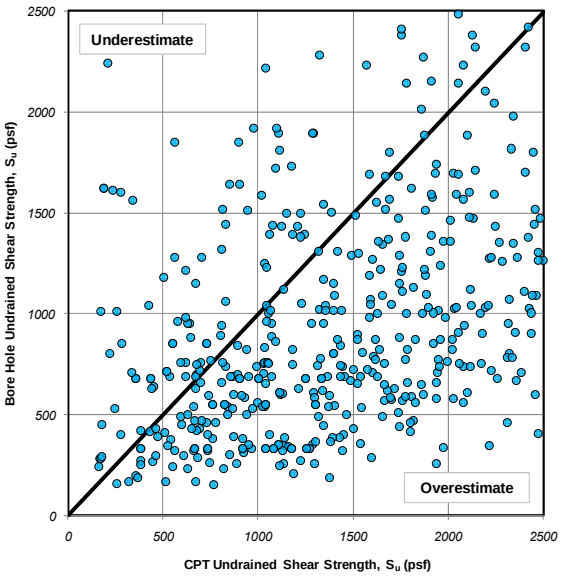

Clay and Silt > 97.5%

Figure 41

Comparison of undrained shear strength, S_u, from CPT and UC tests for different soil classifications (Zhang and Tumay – clay and silt)

Robertson's Method. The first four soil types [two for organic soils and peats, three for clays (silty clay to clays), four for silt mixtures (clayey silt to silty clay), and five for sand mixtures (silty sand to sandy silt)] are analyzed in this study. The remaining two classifications [six for sands (clean sand to silty sand) and seven for gravelly sand to dense sand)] were not included in this analysis because of the irrelevance of undrained shear strength to these soil types. The same can be said about Soil Type 5. It is, however, included in the analysis. Table 16 lists the summary of the results that show a consistent trend of a rising bias and a dropping coefficient of variation for the most relevant soil types (2, 3, and 4). This indicates that the CPT overestimates the undrained shear strength at a lower rate for Soil Type 2 than Type 3, which is also lower than Type 4. This method shows a good potential for inclusion in future CPT calibration efforts because it only relies on CPT data (no boreholes are needed) similar to the previous classification technique (Zhang and Tumay).

Table 16
Effect of soil classification on uncertainty of CPT results (Robertson)

Soil classification	**2**	**3**	**4**	**5**
Bias, λ	1.358 ↗	1.899 ↗	2.067 ↗	2.643
Standard Deviation, σ_λ	0.962 ↗	1.268 ↗	1.299 ↗	2.292
Coefficient of Variation, COV	71% ↘	67% ↘	63% ↗	87%
Number of Points, N	33	478	258	87
Average CPT Coefficient, N_{kt}	20.4	28.5	31.0	39.6
Standard Deviation, $\sigma_{N_{kt}}$	14.4	19.0	19.5	34.4

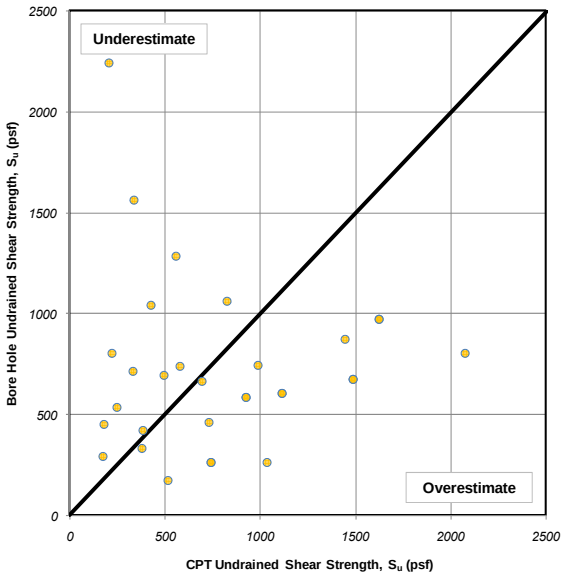

Classification 2

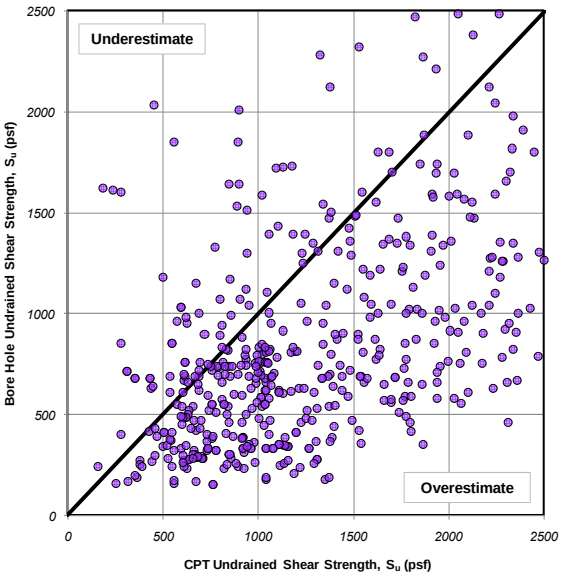

Classification 3

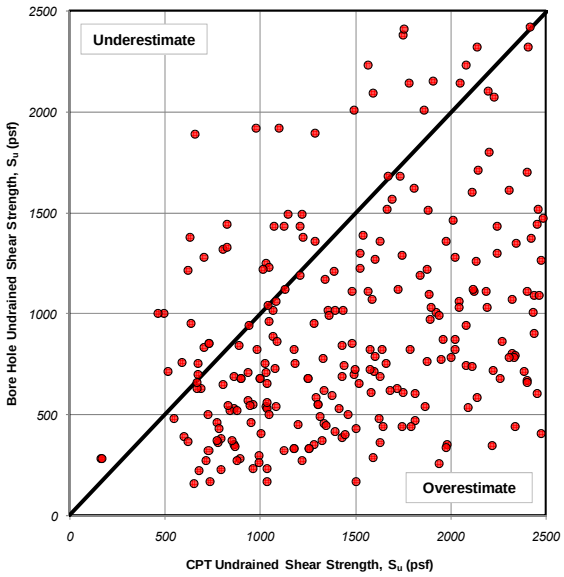

Classification 4

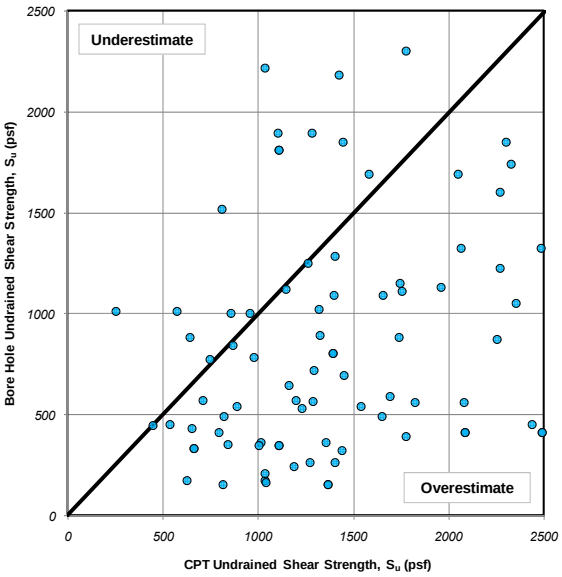

Classification 5

Figure 42

Comparison of undrained shear strength, S_u, from CPT and UC tests for different soil classifications (Robertson)

Plasticity Index. The Plasticity Index (PI) was also analyzed as a classification technique in an attempt to relate the accuracy of CPT undrained shear strength estimates to this quantity. Unlike the previous classification techniques, the PI would require results from boreholes if it were to be used in interpreting CPT test readings. This approach eliminates the possibility of using the CPT as an independent testing tool. Five ranges of PI were chosen for the study, namely, less than 20, between 20 and 30, between 30 and 40, between 40 and 50, and greater than 50. The results of the statistical analysis for the accuracy of CPT undrained shear estimates with respect to borehole results are summarized in Table 17 for each of the studied ranges. There is no clear trend for the bias or the coefficient of variation. Therefore, it can be concluded that there is no justification for including the plasticity index in subsequent calibration studies.

Table 17
Effect of Plasticity Index on uncertainty of CPT results

PI range	**< 20**	**20-30**	**30-40**	**40-50**	**> 50**
Bias, λ	2.195 ↘	1.912 ↘	1.871 ↗	2.010 ↘	1.726
Standard Deviation, σ_λ	1.585 ↘	1.580 ↘	1.041 ↘	0.968 ↘	0.941
Coefficient of Variation, COV	72% ↗	83% ↘	56% ↘	48% ↗	55%
Number of Points, N	214	148	137	69	132
Average CPT Coefficient, N_{kt}	32.9	28.7	28.1	30.2	25.9
Standard Deviation, $\sigma_{N_{kt}}$	23.8	23.7	15.6	14.5	14.1

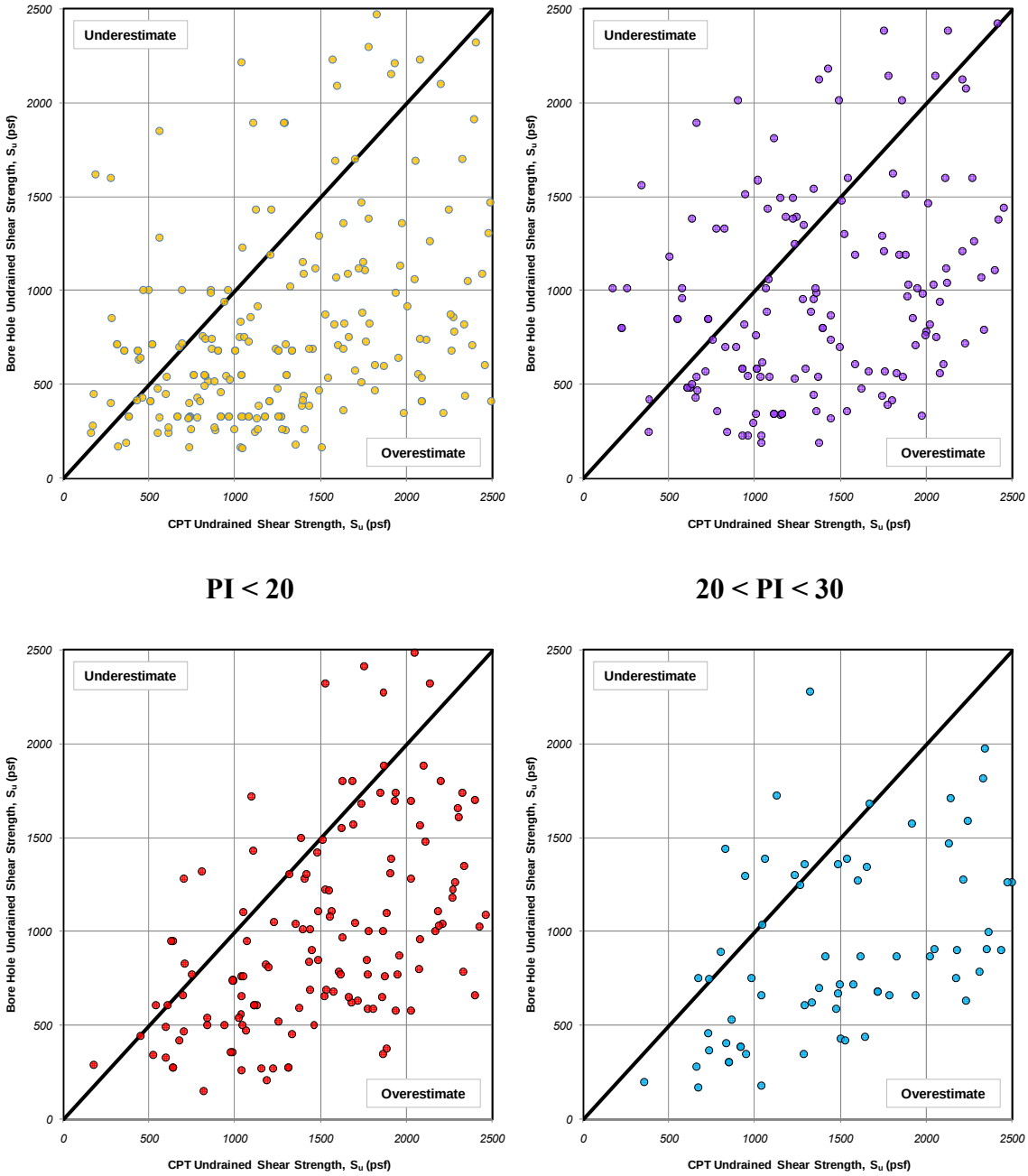

PI < 20 **20 < PI < 30**

30 < PI < 40 **40 < PI < 50**

Figure 43

Comparison of undrained shear strength, S_u, from CPT and UC tests for different Plasticity Index values

Chi-Square Results

Transformation Model, S_u^{CPT} / S_u^{UC} **.** A Chi-Square test was conducted on the transformation model results, i.e., the ratio S_u^{CPT} / S_u^{UC} , following the procedure described in Appendix C. Figure 44 shows a plot of the observed data (862 points) and theoretical lognormal and normal values. It can be seen that the lognormal distribution fits the observed data better. The Chi Square test revealed that the summation $\sum_{i=1}^{m} \frac{(n_i - e_i)^2}{e_i}$ is equal to 9.115 for the lognormal distribution and 268.190 for the normal distribution. According to Table 36, the lognormal distribution passes the test, which requires the summation to be less than 10.64 for 6 degrees of freedom ($f = m - 1 - k$ = 9-1-2 = 6) with a significance level of α =10 percent ($1 - \alpha = 0.900$). The normal distribution fails this test.

Similar tests were conducted for the data subsets according to Robertson classification of soils. The conclusions were identical to those obtained from the whole dataset, except for Soil Classification 2 where both normal and lognormal distribution passed the test, however, at a lower significance level (5 percent).

Table 18
Summary of chi-square test results for transformation model

Dataset	Count	$\sum_{i=1}^{m} \frac{(n_i - e_i)^2}{e_i}$	
		Lognormal	**Normal**
All data points	862	9.115	268.190
Soil Classification 2	33	11.730	11.074
Soil Classification 3	478	8.487	142.681
Soil Classification 4	258	6.057	66.195

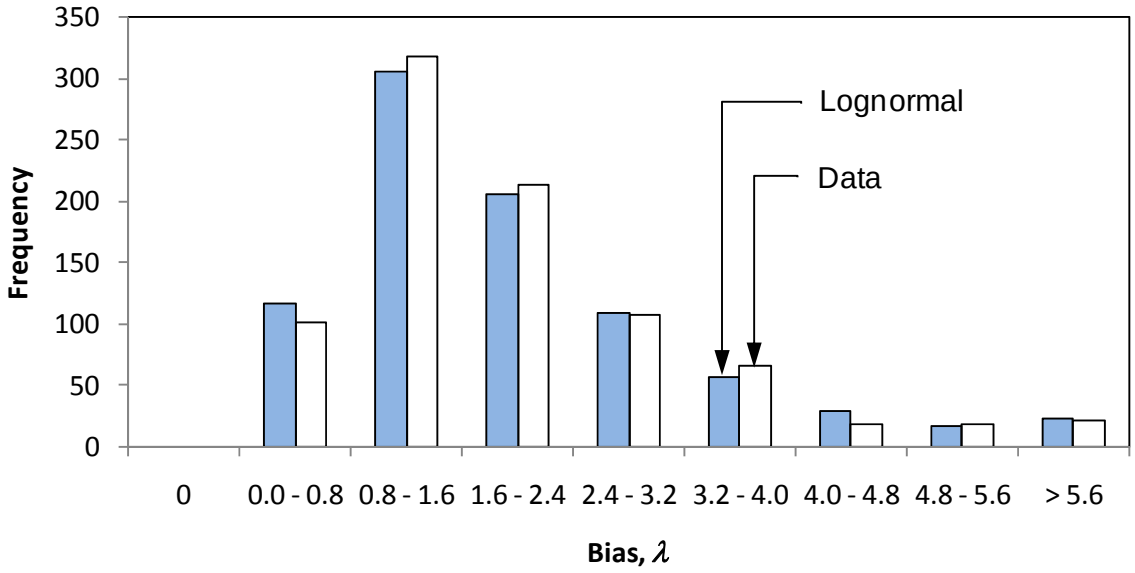

(a) Lognormal

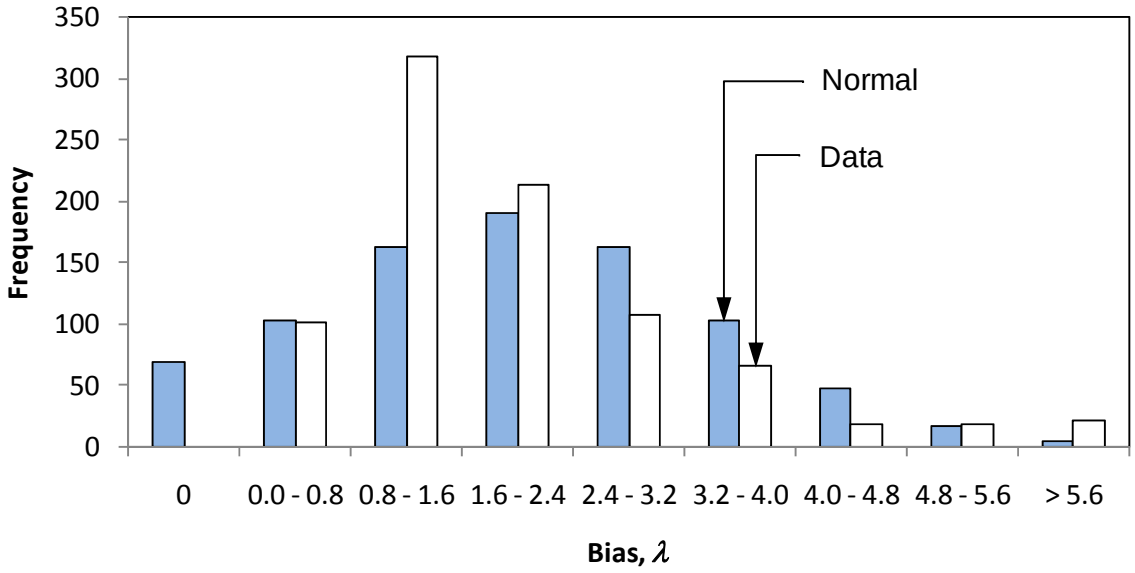

(b) Normal

Figure 44
Chi square test results for transformation model (all data points)

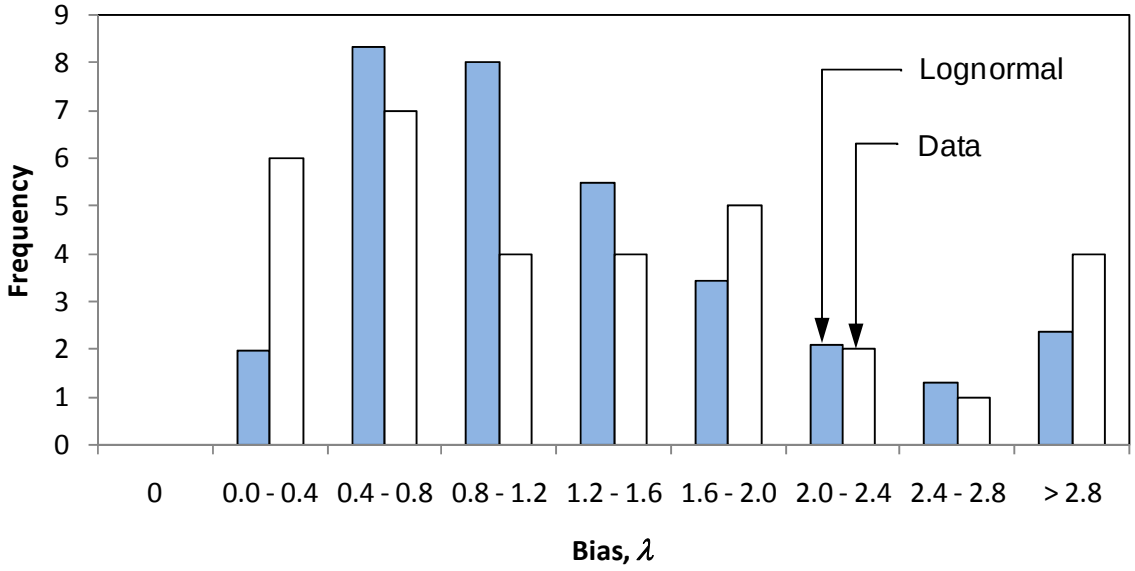

(a) Lognormal

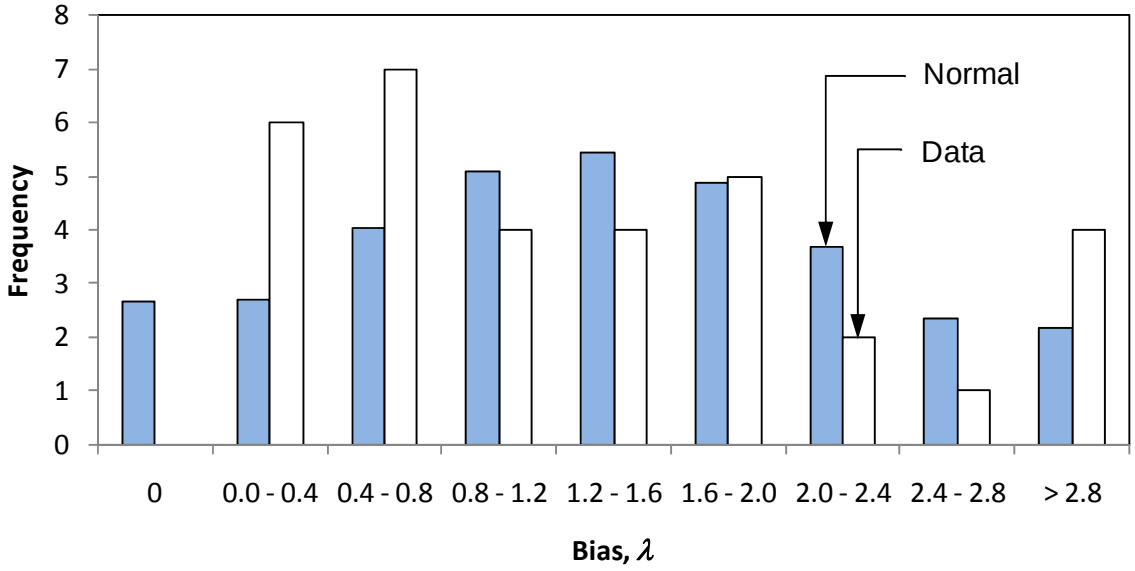

(b) Normal

Figure 45
Chi square test results for transformation model (Soil Classification 2)

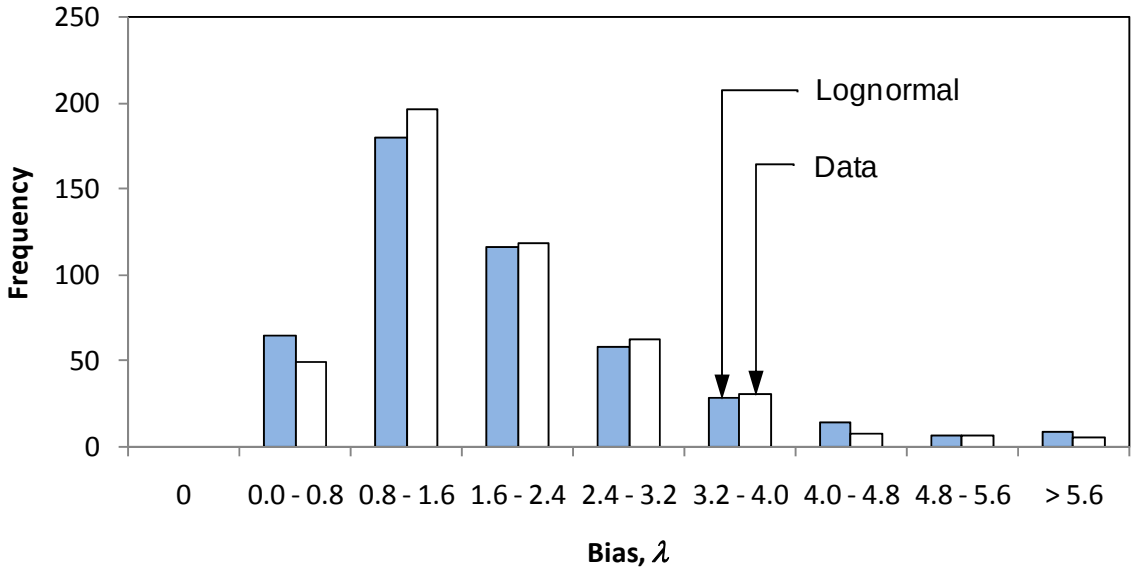

(a) Lognormal

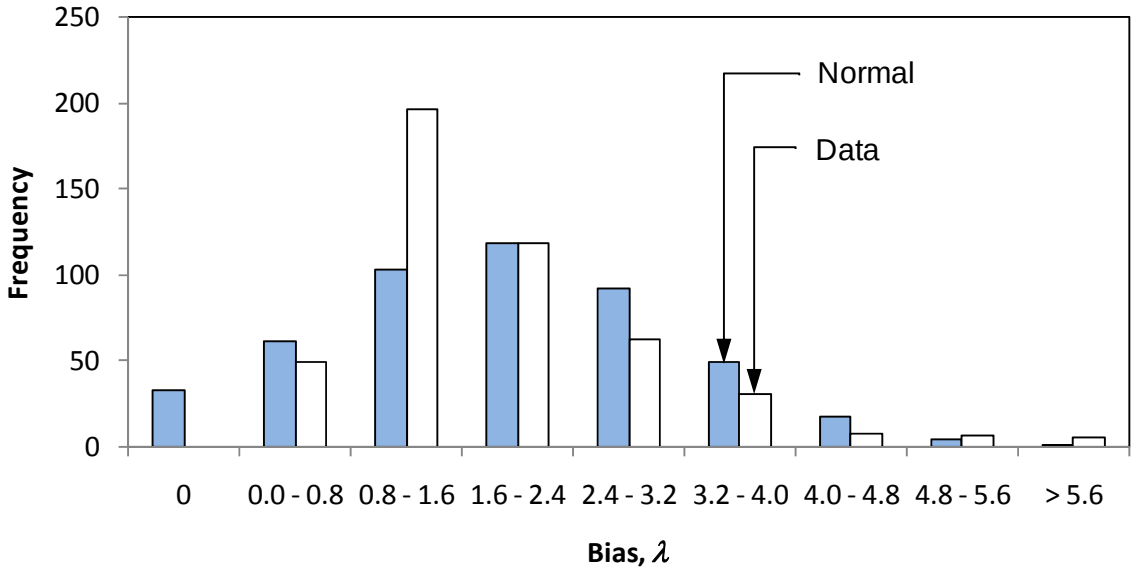

(b) Normal

Figure 46
Chi square test results for transformation model (Soil Classification 3)

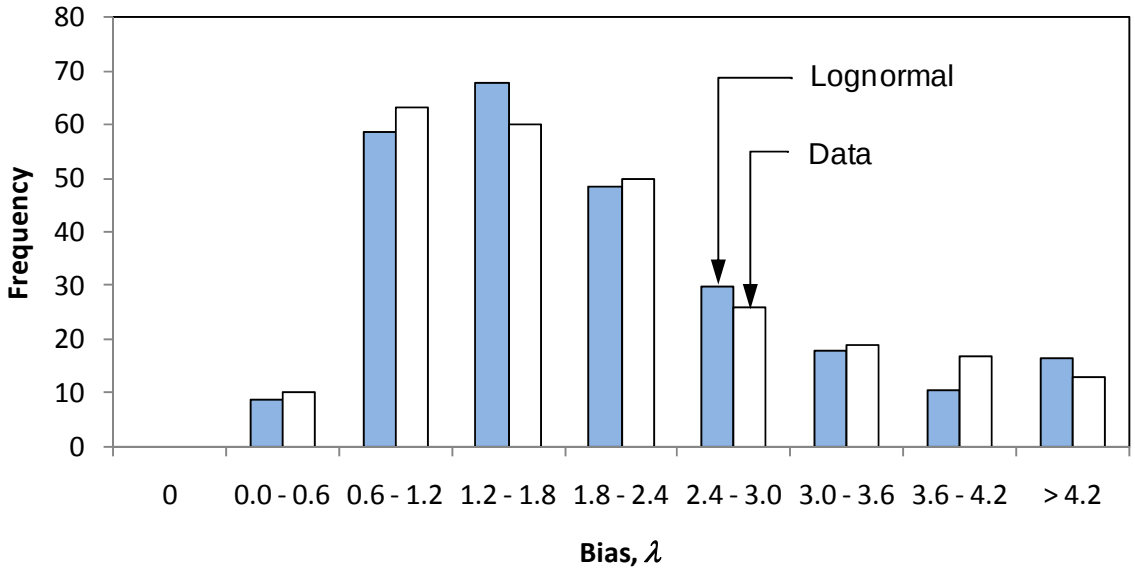

(a) Lognormal

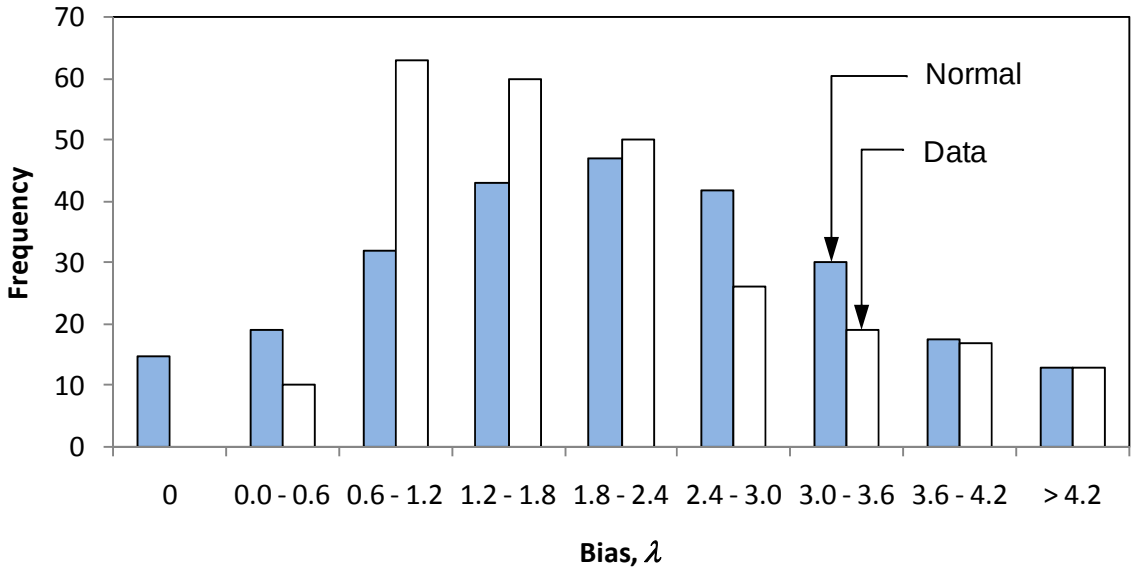

(b) Normal

Figure 47
Chi square test results for transformation model (Soil Classification 4)

Repeatability of Tip Resistance, q_c. The other random variable that is determined from this study is that related to the inherent uncertainty in the device measurements. The repeatability results (see on Page 59) were used to choose an appropriate distribution for this random variable. The results are plotted in Figure 48 for both distribution types. The summation $\sum_{i=1}^{m} \frac{(n_i - e_i)^2}{e_i}$ was equal to 56.879 for the lognormal distribution and 11.814 for the normal distribution. This means that a normal distribution fits this random variable better as it passes the Chi-Square test at a significance level, α, equal to 5percent ($1-\alpha = 0.950$).

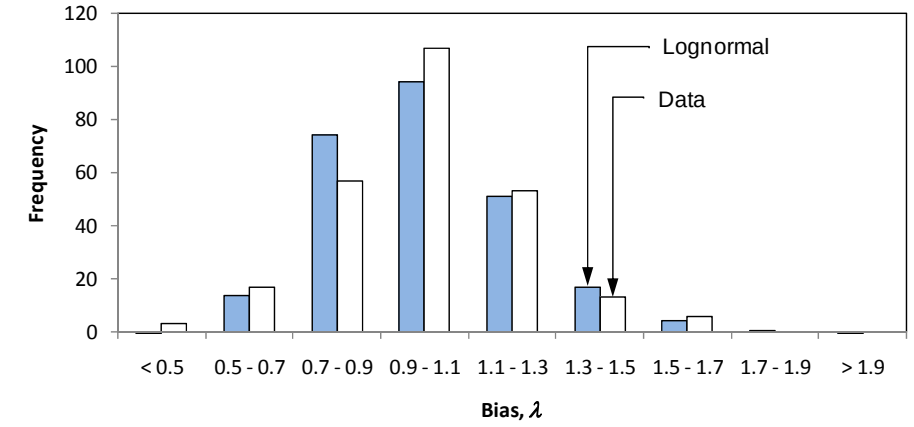

(a) Lognormal

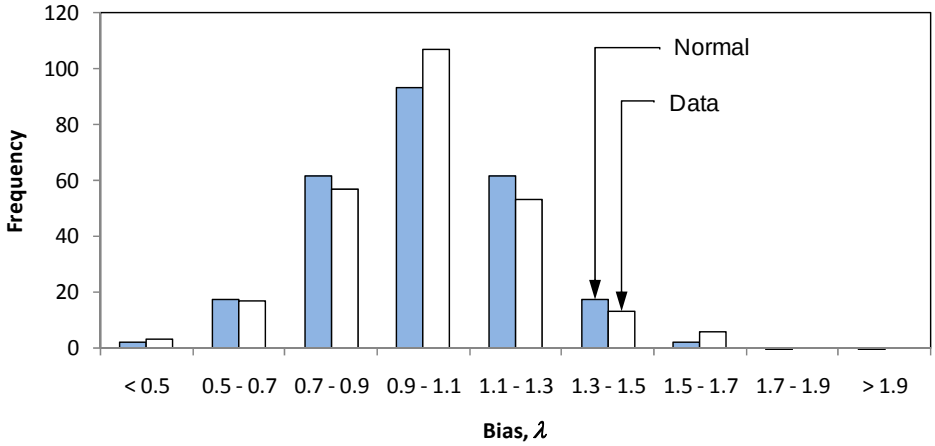

(b) Normal

Figure 48
Chi square test results for device uncertainty

Calibration of CPT Coefficient for Undrained Shear Strength

N_{kt} Calibration–1st Approach

As described earlier, the 1st approach adopted in this study for calibrating the CPT coefficient, N_{kt}, is straightforward and relies on direct correlation between undrained shear strength obtained from CPT and boring results. For the 862 points available in the database, N_{kt} values were computed. Figure 49 shows a histogram of the N_{kt} values computed using equation (42). It can be seen that a wide range of N_{kt} resulted from the data. To illustrate how this plot can be used, a N_{kt} value of 15 is chosen. For this value, it can be seen that the shear strength for 80.7 percent of the points in the database will be overestimated.

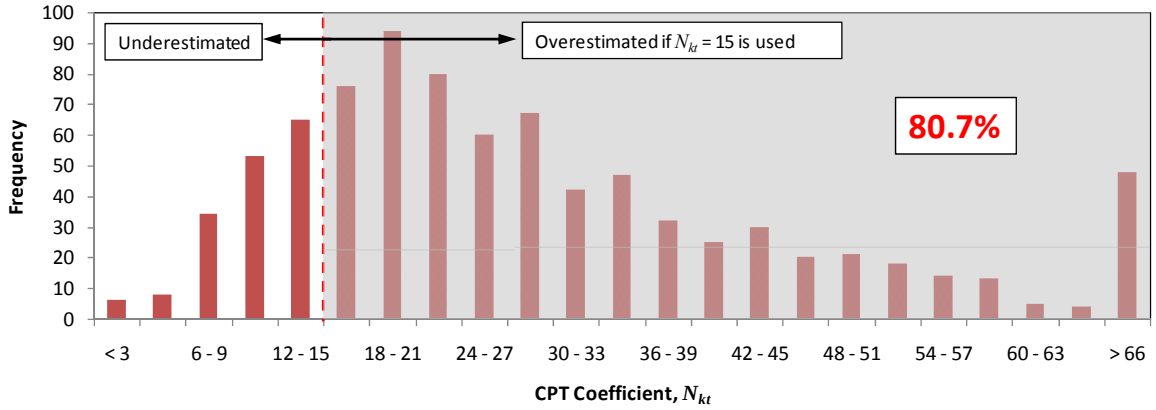

Figure 49

Histogram of N_{kt} –values obtained from equation (42) –all data points

To simplify this plot in such a way that can be used to determine N_{kt} values for target probabilities of exceedance, the cumulative distribution function (CDF) of the data is constructed and plotted in Figure 50. This plot can be used to determine the probability of exceedance for any N_{kt} value. For example, the figure shows that if N_{kt} is set to 15, the probability of exceedance is equal to 19 percent (1.00 – 81). Alternatively, N_{kt} can be determined for a given target probability of exceedance. In the same figure, a N_{kt} value can be determined for a desired target probability of exceedance (40 percent in this illustration)

can be easily determined to be 21. Similar plots can be generated for different soil classifications. Table 19 lists N_{kt} value obtained for probability of exceedance, P_e, equal to 50 percent, 55 percent, and 66.7 percent, which will be the target values throughout this study.

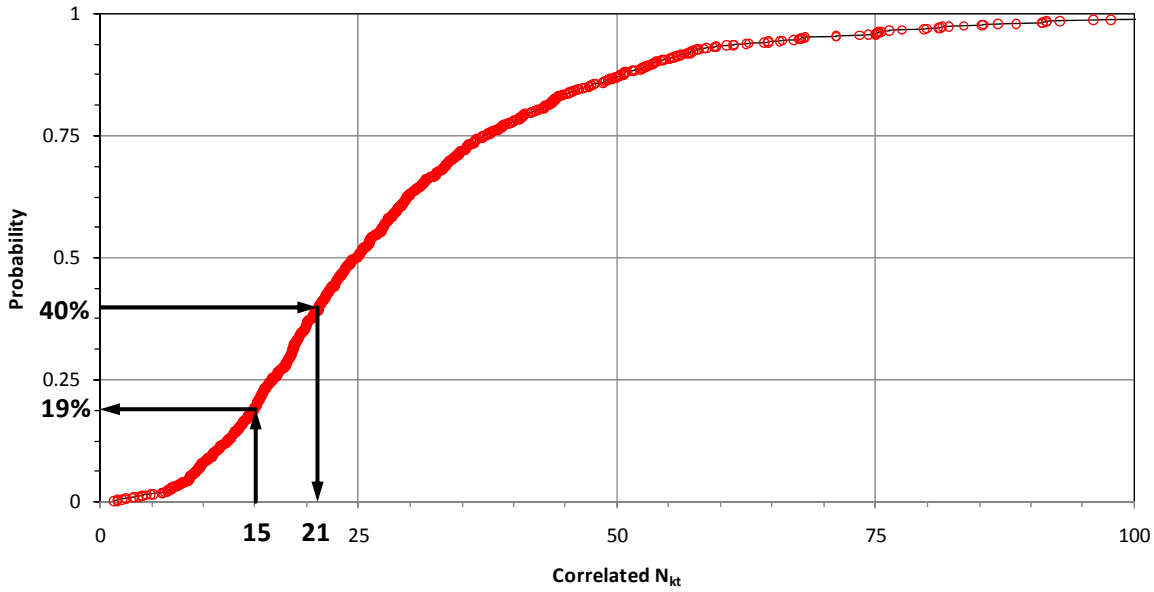

Figure 50
Cumulative distribution function (CDF) for N_{kt} –values [all data points]

Table 19
Calibrated N_{kt} values for different probability of exceedance, P_e, values

Probability of Exceedance, P_e	**CPT Coefficient, N_{kt}**
50.0%	24.879
55.0%	26.914
66.7%	32.285

Plots similar to the histogram seen in Figure 49 can be generated for any subgroup of data points. For example, Figure 51 and Figure 52 show the histograms for each soil classification using both methods investigated in this study, namely Robertson (1990) and Zhang and Tumay (1999). It can be seen from the plots that the decrease in clay content (lower classification number in Robertson's method and higher percentage in Zhang and Tumay method) is translated into an increase in N_{kt} value. This is illustrated with the shift in the histogram to higher N_{kt} values. Plots similar to the CDF shown in Figure 50 can also be generated for each soil classification. However, due to the limited number of data points, a smooth S-curve such as the one seen in Figure 50 is not achievable. As more data points become available, the development of these charts will be trivial.

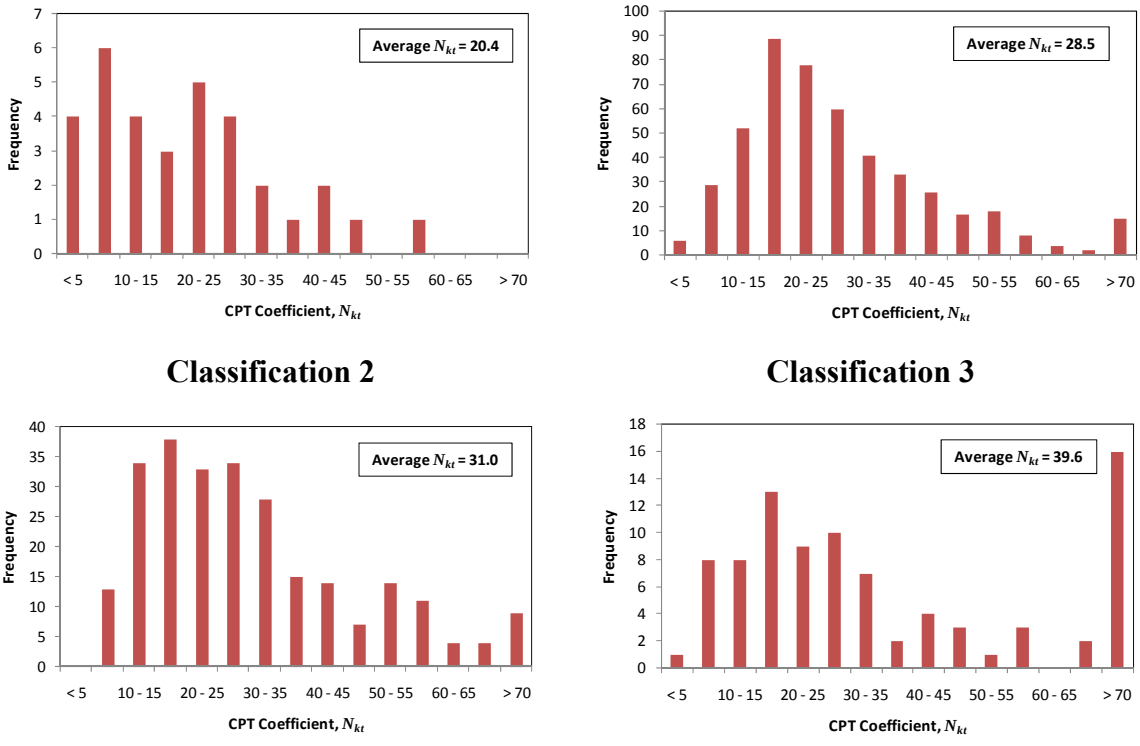

Figure 51

Histogram of N_{kt} –values obtained from equation (42) (by Robertson soil classification)

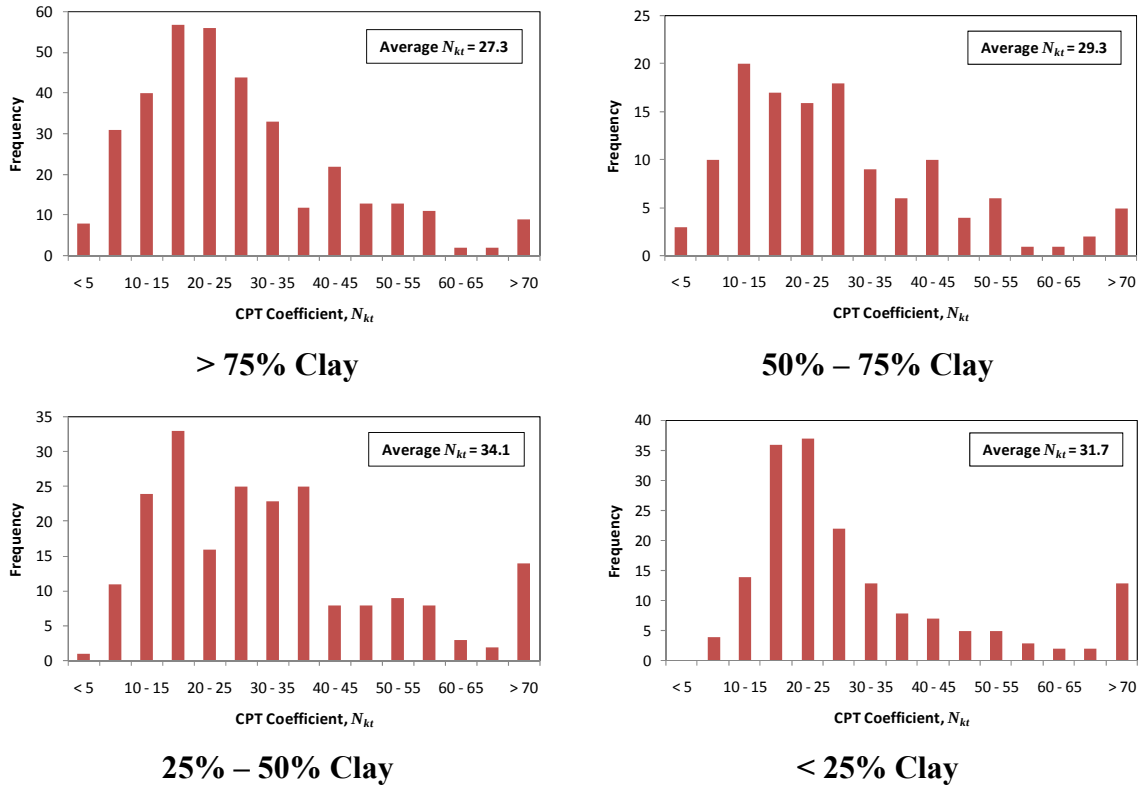

Figure 52
Histogram of N_{kt} –values obtained from equation (42)
(by Zhang and Tumay's soil classification)

It should be emphasized that this approach does not account for the variability inherent in soil properties or measuring device. In other words, each of the N_{kt} values is obtained using one CPT sounding and one unconfined compression test. In real life, different CPT soundings will result in different readings as was demonstrated by the repeatability study. Also, variations in soil properties are the norm and should be accounted for. If these sources of uncertainty are not accounted for at this level (soil property), proper care should be taken when using these properties in the next level of engineering computations (foundation design).

N_{kt} Calibration–2nd Approach

The 2nd approach for calibration of the CPT coefficient, N_{kt}, accounts for all uncertainties identified in this study using the limit state function equation (47-b), and applying the First Order Reliability Method (FORM) described in Appendix B. The results from this study are presented next.

Table 20 through Table 22 show the results for a series of computations considering σ_{vo}/q_c = 0.10 and relying on Robertson's classification. The choice to present the results for a σ_{vo}/q_c ratio equal to 0.10 was based on the average σ_{vo}/q_c ratio of data points included in the database, which is 0.14. Furthermore, a sensitivity study was conducted, and it was determined that the σ_{vo}/q_c ratio does not impact the reliability results except for high end values, e.g., σ_{vo}/q_c = 0.80. The tables also show the term $(\beta - \beta_T)^2$, which will be used in the optimization of N_{kt}. The three tables correspond to the three chosen target probability of exceedance levels, namely 50 percent (β_T = 0.0), 55 percent (β_T = 0.1257), and 66.7 percent (β_T = 0.4308). As can be seen, targeting higher β values requires higher N_{kt} values so the term $(\beta - \beta_T)^2$ is equal to zero. An exact zero value cannot always be achieved due to the discrete N_{kt} values chosen in this study. Therefore, finding an optimum N_{kt} is achieved as can be seen in Figure 53 where the minimum value of the plot of $(\beta - \beta_T)^2$ versus N_{kt} corresponds to the desired value.

Table 20

Reliability results (β_T = 0.0, σ_{vo}/q_c = 0.10, Robertson classification)

N_{kt}	ALL Cases		2		3		4	
	β	$(\beta-\beta_T)^2$	β	$(\beta-\beta_T)^2$	β	$(\beta-\beta_T)^2$	β	$(\beta-\beta_T)^2$
12	-0.971	0.944	-0.324	0.105	-1.116	1.245	-1.102	1.215
15	-0.727	0.529	-0.214	0.046	-0.731	0.534	-0.897	0.804
18	-0.491	0.241	-0.033	0.001	-0.505	0.255	-0.708	0.502
21	-0.329	0.108	0.125	0.016	-0.303	0.092	-0.502	0.252
24	-0.176	0.031	0.214	0.046	-0.124	0.015	-0.294	0.086
27	-0.021	0.000	0.350	0.122	0.049	0.002	-0.157	0.025
30	0.091	0.008	0.515	0.265	0.190	0.036	-0.036	0.001
33	0.188	0.035	0.665	0.442	0.325	0.106	0.079	0.006
36	0.277	0.077	0.712	0.507	0.444	0.197	0.185	0.034
39	0.352	0.124	0.767	0.589	0.559	0.313	0.273	0.074
42	0.431	0.186	0.891	0.794	0.668	0.446	0.369	0.136
45	0.489	0.239	0.963	0.928	0.762	0.580	0.430	0.185
48	0.544	0.295	1.077	1.159	0.848	0.719	0.488	0.238
51	0.603	0.363	1.146	1.314	0.933	0.870	0.552	0.305

Table 21

Reliability results (β_T = 0.1257, σ_{vo}/q_c = 0.10, Robertson classification)

N_{kt}	ALL Cases		2		3		4	
	β	$(\beta-\beta_T)^2$	β	$(\beta-\beta_T)^2$	β	$(\beta-\beta_T)^2$	β	$(\beta-\beta_T)^2$
12	-0.971	1.204	-0.324	0.202	-1.116	1.541	-1.102	1.508
15	-0.727	0.727	-0.214	0.115	-0.731	0.733	-0.897	1.045
18	-0.491	0.381	-0.033	0.025	-0.505	0.397	-0.708	0.695
21	-0.329	0.206	0.125	0.000	-0.303	0.184	-0.502	0.394
24	-0.176	0.091	0.214	0.008	-0.124	0.062	-0.294	0.176
27	-0.021	0.021	0.350	0.050	0.049	0.006	-0.157	0.080
30	0.091	0.001	0.515	0.152	0.190	0.004	-0.036	0.026
33	0.188	0.004	0.665	0.290	0.325	0.040	0.079	0.002
36	0.277	0.023	0.712	0.344	0.444	0.101	0.185	0.004
39	0.352	0.051	0.767	0.412	0.559	0.188	0.273	0.022
42	0.431	0.093	0.891	0.586	0.668	0.294	0.369	0.059
45	0.489	0.132	0.963	0.701	0.762	0.405	0.430	0.093
48	0.544	0.175	1.077	0.905	0.848	0.522	0.488	0.131
51	0.603	0.227	1.146	1.042	0.933	0.651	0.552	0.182

Table 22

Reliability results (β_T = 0.4308, σ_{vo}/q_c = 0.10, Robertson classification)

N_{kt}	ALL Cases		2		3		4	
	β	$(\beta-\beta_T)^2$	β	$(\beta-\beta_T)^2$	β	$(\beta-\beta_T)^2$	β	$(\beta-\beta_T)^2$
12	-0.971	1.966	-0.324	0.570	-1.116	2.392	-1.102	2.350
15	-0.727	1.341	-0.214	0.415	-0.731	1.349	-0.897	1.762
18	-0.491	0.850	-0.033	0.215	-0.505	0.875	-0.708	1.297
21	-0.329	0.577	0.125	0.094	-0.303	0.539	-0.502	0.871
24	-0.176	0.368	0.214	0.047	-0.124	0.308	-0.294	0.525
27	-0.021	0.204	0.350	0.007	0.049	0.146	-0.157	0.346
30	0.091	0.116	0.515	0.007	0.190	0.058	-0.036	0.217
33	0.188	0.059	0.665	0.055	0.325	0.011	0.079	0.124
36	0.277	0.024	0.712	0.079	0.444	0.000	0.185	0.060
39	0.352	0.006	0.767	0.113	0.559	0.017	0.273	0.025
42	0.431	0.000	0.891	0.212	0.668	0.056	0.369	0.004
45	0.489	0.003	0.963	0.283	0.762	0.109	0.430	0.000
48	0.544	0.013	1.077	0.417	0.848	0.174	0.488	0.003
51	0.603	0.030	1.146	0.512	0.933	0.252	0.552	0.015

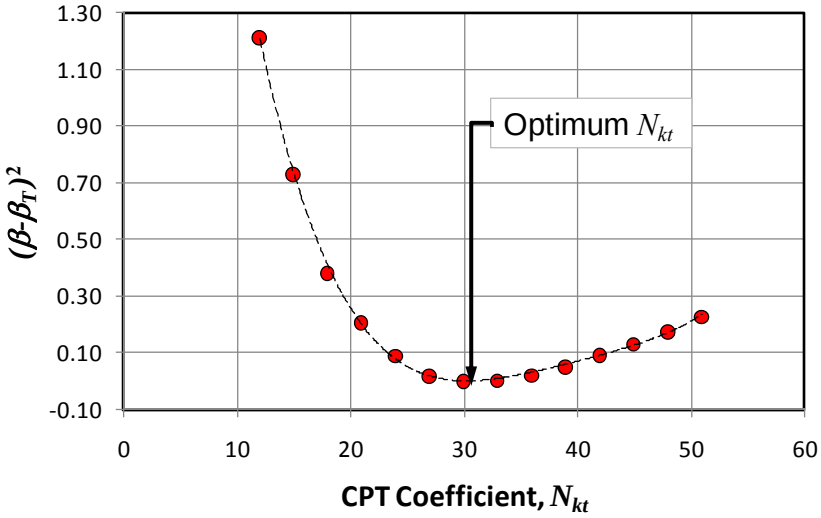

(a) All data

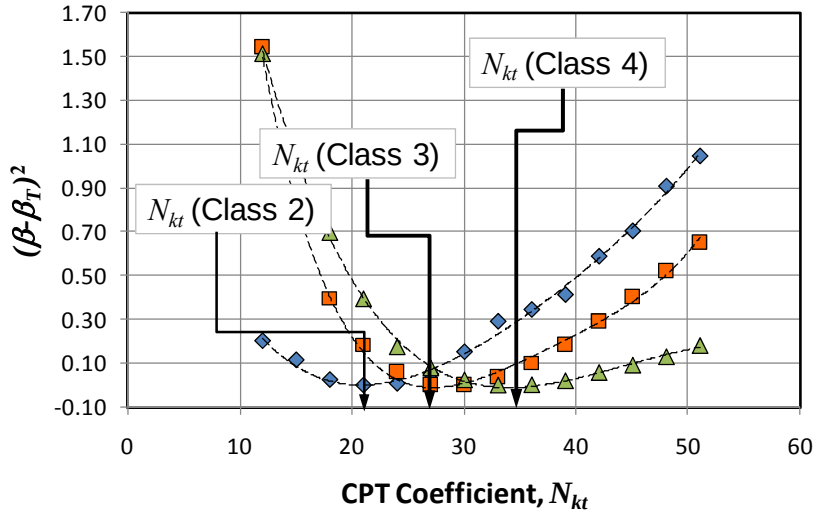

(b) by Robertson's classification

Figure 53

Determining optimum N_{kt} values (β_T = 0.1257, σ_{vo}/q_c = 0.05)

This optimization procedure was repeated for all studied cases, and the results are summarized in Table 23 through Table 25.

Table 23

Optimum N_{kt} values (β_T = 0.0, Robertson classification)

σ_{vo}/q_c	Classification			
	ALL	**2**	**3**	**4**
0.05	27.559	18.630	26.150	30.933
0.1	27.557	18.630	26.151	30.933
0.2	27.557	18.630	26.149	30.933
0.5	27.555	18.632	26.150	30.932
0.8	27.542	18.631	26.145	30.927
0.9	27.528	18.628	26.132	30.918

Table 24

Optimum N_{kt} values (β_T = 0.1257, Robertson classification)

σ_{vo}/q_c	Classification			
	ALL	**2**	**3**	**4**
0.05	31.064	21.016	28.630	34.311
0.1	31.075	21.022	28.633	34.320
0.2	31.107	21.036	28.642	34.343
0.5	31.326	21.145	28.713	34.505
0.8	32.783	21.986	29.231	35.631
0.9	36.084	24.167	30.574	38.475

Table 25

Optimum N_{kt} values (β_T = 0.4308, Robertson classification)

σ_{vo}/q_c	Classification			
	ALL	**2**	**3**	**4**
0.05	41.941	28.458	35.657	44.992
0.1	41.982	28.470	35.672	45.033
0.2	42.137	28.500	35.709	45.133
0.5	43.228	28.721	35.985	45.862
0.8	49.973	30.297	37.970	50.411
0.9	N/A	38.159	42.805	N/A

Table 26 through Table 31 list the reliability calibration results for Zhang and Tumay soil classification method that were obtained by repeating the procedure described above. It can be seen that the optimum N_{kt} values are also affected by the type of soil (clay content). Nevertheless, the differences between N_{kt} values for difference soil types are smaller than those obtained using the Robertson soil classification.

Table 26

Reliability results (β_T = 0.0, σ_{vo}/q_c = 0.10, Zhang and Tumay classification)

N_{kt}	ALL Cases		> 75%		50% - 75%		25% - 50%	
	β	$(\beta - \beta_T)^2$	β	$(\beta - \beta_T)^2$	β	$(\beta - \beta_T)^2$	β	$(\beta - \beta_T)^2$
12	-0.971	0.944	-0.931	0.867	-0.837	0.701	-1.092	1.193
15	-0.727	0.528	-0.710	0.505	-0.638	0.407	-0.800	0.640
18	-0.491	0.241	-0.506	0.256	-0.322	0.104	-0.604	0.364
21	-0.328	0.108	-0.331	0.110	-0.169	0.029	-0.422	0.178
24	-0.176	0.031	-0.143	0.021	-0.055	0.003	-0.286	0.082
27	-0.021	0.000	0.006	0.000	0.068	0.005	-0.068	0.005
30	0.091	0.008	0.125	0.016	0.142	0.020	0.047	0.002
33	0.188	0.035	0.253	0.064	0.227	0.052	0.142	0.020
36	0.277	0.077	0.350	0.122	0.328	0.108	0.226	0.051
39	0.352	0.124	0.451	0.203	0.421	0.178	0.290	0.084
42	0.431	0.186	0.552	0.305	0.508	0.258	0.365	0.134
45	0.489	0.239	0.609	0.371	0.584	0.340	0.428	0.183
48	0.543	0.295	0.685	0.469	0.654	0.427	0.475	0.226
51	0.603	0.363	0.761	0.579	0.706	0.498	0.534	0.285

Table 27

Reliability results (β_T = 0.1257, σ_{vo}/q_c = 0.10, Zhang and Tumay classification)

N_{kt}	ALL Cases		> 75%		50% - 75%		25% - 50%	
	β	$(\beta - \beta_T)^2$	β	$(\beta - \beta_T)^2$	β	$(\beta - \beta_T)^2$	β	$(\beta - \beta_T)^2$
12	-0.971	1.204	-0.931	1.117	-0.837	0.927	-1.092	1.483
15	-0.727	0.727	-0.710	0.699	-0.638	0.583	-0.800	0.857
18	-0.491	0.381	-0.506	0.399	-0.322	0.201	-0.604	0.532
21	-0.328	0.206	-0.331	0.209	-0.169	0.087	-0.422	0.300
24	-0.176	0.091	-0.143	0.072	-0.055	0.033	-0.286	0.169
27	-0.021	0.021	0.006	0.014	0.068	0.003	-0.068	0.038
30	0.091	0.001	0.125	0.000	0.142	0.000	0.047	0.006
33	0.188	0.004	0.253	0.016	0.227	0.010	0.142	0.000
36	0.277	0.023	0.350	0.050	0.328	0.041	0.226	0.010
39	0.352	0.051	0.451	0.106	0.421	0.087	0.290	0.027
42	0.431	0.093	0.552	0.182	0.508	0.146	0.365	0.058
45	0.489	0.132	0.609	0.234	0.584	0.210	0.428	0.091
48	0.543	0.175	0.685	0.312	0.654	0.279	0.475	0.122
51	0.603	0.227	0.761	0.404	0.706	0.337	0.534	0.167

Table 28

Reliability results (β_T = 0.4308, σ_{vo}/q_c = 0.10, Zhang and Tumay classification)

N_{kt}	ALL Cases		> 75%		50% - 75%		25% - 50%	
	β	$(\beta - \beta_T)^2$	β	$(\beta - \beta_T)^2$	β	$(\beta - \beta_T)^2$	β	$(\beta - \beta_T)^2$
12	-0.971	1.966	-0.931	1.855	-0.837	1.607	-1.092	2.319
15	-0.727	1.340	-0.710	1.302	-0.638	1.141	-0.800	1.515
18	-0.491	0.850	-0.506	0.877	-0.322	0.567	-0.604	1.070
21	-0.328	0.576	-0.331	0.580	-0.169	0.360	-0.422	0.727
24	-0.176	0.368	-0.143	0.330	-0.055	0.236	-0.286	0.514
27	-0.021	0.204	0.006	0.180	0.068	0.131	-0.068	0.249
30	0.091	0.116	0.125	0.093	0.142	0.083	0.047	0.147
33	0.188	0.059	0.253	0.031	0.227	0.041	0.142	0.083
36	0.277	0.024	0.350	0.007	0.328	0.011	0.226	0.042
39	0.352	0.006	0.451	0.000	0.421	0.000	0.290	0.020
42	0.431	0.000	0.552	0.015	0.508	0.006	0.365	0.004
45	0.489	0.003	0.609	0.032	0.584	0.023	0.428	0.000
48	0.543	0.013	0.685	0.064	0.654	0.050	0.475	0.002
51	0.603	0.030	0.761	0.109	0.706	0.076	0.534	0.011

Table 29

Optimum N_{kt} values (β_T = 0.0, Zhang and Tumay classification)

σ_{vo}/q_c	Classification (clay probability)				
	ALL	**> 75%**	**50% - 75%**	**25% - 50%**	**< 25%**
0.05	27.557	26.874	25.332	28.780	31.536
0.1	27.557	26.874	25.332	28.780	31.536
0.2	27.557	26.874	25.332	28.779	31.536
0.5	27.554	26.874	25.331	28.774	31.535
0.8	27.540	26.871	25.320	28.742	31.526
0.9	27.527	26.869	25.305	28.710	31.515

Table 30

Optimum N_{kt} values (β_T = 0.1257, Zhang and Tumay classification)

σ_{vo}/q_c	Classification (clay probability)				
	ALL	**> 75%**	**50% - 75%**	**25% - 50%**	**< 25%**
0.05	31.063	30.002	29.307	32.476	35.291
0.1	31.075	30.015	29.324	32.486	35.302
0.2	31.106	30.049	29.367	32.511	35.331
0.5	31.326	30.284	29.670	32.694	35.534
0.8	32.784	31.749	31.465	34.072	37.613
0.9	36.081	35.268	34.799	37.543	41.498

Table 31

Optimum N_{kt} values (β_T = 0.4308, Zhang and Tumay classification)

σ_{vo}/q_c	Classification (clay probability)				
	ALL	**> 75%**	**50% - 75%**	**25% - 50%**	**< 25%**
0.05	41.939	38.343	39.278	45.127	50.877
0.1	41.984	38.398	39.326	45.194	50.936
0.2	42.136	38.540	39.449	45.365	N/A
0.5	43.228	39.505	40.298	46.563	N/A
0.8	49.976	45.618	45.800	N/A	N/A
0.9	N/A	N/A	N/A	N/A	N/A

Correlation Between Unit Weight, γ_T, from CPT and Boring Data

As a byproduct of this study, the correlation between unit weight estimates obtained from CPT and boring data was also investigated. Equation (33) was used to compute the unit weight from CPT readings, while direct unit weight values were available from boring data. A plot of this correlation can be seen in Figure 54. Unlike the undrained shear strength plots

presented earlier, this plot shows better correlation between unit weight estimates from CPT and boring data. As before, the bias (λ) and COV of the ratio, $\gamma_T^{CPT} / \gamma_T^{UC}$, were computed to assess the accuracy of the CPT unit estimates. The results showed that the bias is equal to 0.98, which indicates that the CPT slightly underestimated the unit weight on average. The COV of the same ratio is computed to be 12.4 percent indicating a scatter in the results, which can be seen in Figure 55. However, it should be noted that these results are substantially better than those presented earlier for the undrained shear strength estimates ($\lambda = 2.01$ and COV = 71 percent for $N_{kt} = 15$). In summary, it can be said that the CPT is a valid testing tool for estimating the unit weight of Louisiana soils.

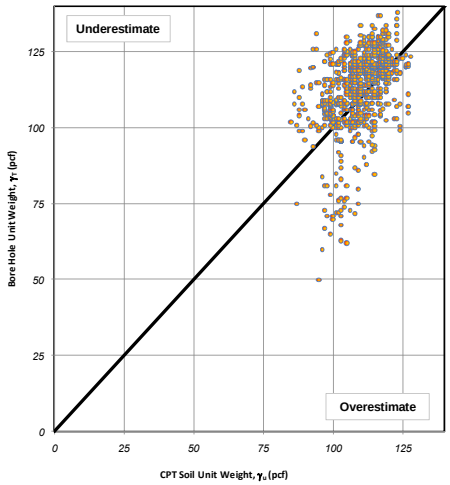

Figure 54

Unit weight correlation γ_T (CPT vs. boring results)

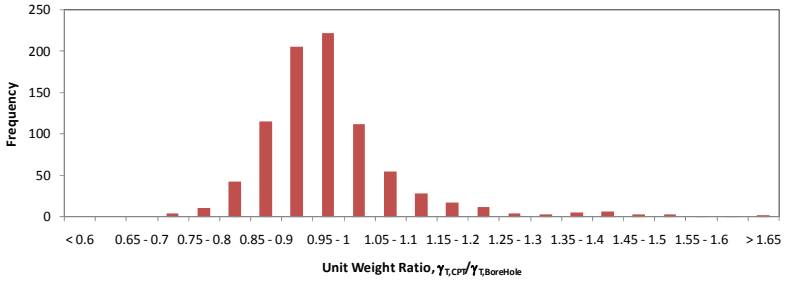

Figure 55

Histogram of unit weight ratio $\gamma_{T,\mathrm{CPT}} / \gamma_{T,\mathrm{BoreHole}}$

SUMMARY AND CONCLUSIONS

Summary

The purpose of this study is to update the correlations between cone penetration and boring log data. A thorough literature review was first conducted. An extensive database of CPT results from projects in Louisiana was collected and processed. This database was merged into a GIS software package to facilitate future retrieval of information generated from this study. A total of 752 CPT points were documented of which 503 were matched with adjacent boreholes and 249 did not have adjacent borehole data available. The CPT data was used to predict soil undrained shear strength, bulk density, and classification according to the Robertson (Robertson 1990) and Zhang and Tumay (1999) methods. A reliability based calibration of the CPT results with respect to borehole data as benchmarks was then conducted. The calibration considered the uncertainties known to be associated with soil properties, namely, inherent soil variability, device measurement, and analytical expression (transformation model). Finally, recommendations for future research and an implementation statement were suggested based on the findings of this research.

Conclusions

The conclusions from this study can be summarized in the following:

1. A single N_{kt} value that is valid for all soil types is unwarranted as it will lead to acceptable results for some soil conditions and unacceptable results for others, which can be unconservative.
2. Two approaches for the calibration of the CPT coefficient, N_{kt}, were presented in this study. The first approach is a direct correlation between undrained shear strength results in the assembled database from CPT and boring data. The second approach utilizes the First Order Reliability Method (FORM) and accounts for all sources of uncertainty (soil properties, device measurement, and transformation model) as compared to the first approach, which only accounts for uncertainties in the transformation model, equation (41).
3. Based on the first approach, a value of 25 should be used for the CPT coefficient, N_{kt}, to achieve a 50 percent probability of exceedance, i.e., β_T = 0.0. Safer designs will

need higher probability of exceedance values (higher β_T), which results in N_{kt} equal to 27 and 32 for target β_T values equal to 0.1257 (55 percent) and 0.4308 (66.7 percent), respectively.

4. The second approach yielded N_{kt} values equal to 27.5, 31.0, and 42.0 for target β_T values equal to 0, (0 percent), 0.1257 (55 percent) and 0.4308 (66.7 percent), respectively. The difference in N_{kt} values obtained from both methods is attributed to the fact that the first approach does not account for the uncertainties inherent in soil properties and the measuring device. Both uncertainties add to the overall confidence in the soil property, which was captured by the FORM analysis (2nd approach) but cannot be captured using the first approach.
5. The N_{kt} results presented above are based on the entire dataset compiled for this study. The dataset was further analyzed by grouping data points in subgroups based on different parameters associated with each point. The parameters considered in this study for grouping the data are: (1) depth, (2) soil classification (three different methods), and (3) CPT readings. It was determined that the soil classification is the only parameter showing clear trends that affect CPT estimates of the undrained shear strength. Therefore, further calibrations were warranted taking into account the soil type. Values of N_{kt} for each soil type based on the Robertson (1990) classification and the Zhang and Tumay (1999) classification were obtained. The following tables summarize the recommended N_{kt} values obtained from the FORM analysis for both soil classification techniques. It is obvious that the N_{kt} coefficient for soils with higher clay content is lower than those with less clay content.
6. Results obtained from this study also showed that the unit weight estimates from CPT readings using equation (33) are in good agreement with borehole results. The expression in equation (33) slightly underestimates the unit weight on average by 2 percent. The scatter of the results is also limited (COV = 12.4 percent) compared to the undrained shear strength discussed earlier.

Table 32

Recommended N_{kt} values using 2nd approach (Robertson classification)

Probability of Exceedance	N_{kt} values for different soil Classifications			
	ALL	**2**	**3**	**4**
50% (β_T = 0.0)	27.5	18.6	26.2	30.9
55% (β_T = 0.1257)	31.1	21.0	28.6	34.3
66.7% (β_T = 0.4308)	42.0	28.5	35.7	45.0

Table 33

Recommended N_{kt} values using 2nd approach (Zhang and Tumay classification)

Probability of Exceedance	N_{kt} values for different soil classifications (clay probability)				
	ALL	**> 75%**	**50% - 75%**	**25% – 50%**	**< 25%**
50% (β_T = 0.0)	27.5	26.9	25.3	28.8	31.5
55% (β_T = 0.1257)	31.1	30.0	29.3	32.5	35.3
66.7% (β_T = 0.4308)	42.0	38.4	39.3	45.2	50.1

7. A procedure for classifying projects based on the site variability was proposed. The procedure builds on the results from the repeatability study conducted in this project. It can be used to obtain a non-subjective classification for site variability of a certain project (e.g., low, medium, or high) by studying the coefficient of variation of the CPT undrained shear strength estimates from multiple sounding at the project site. This classification can then be used in conjunction with AASHTO-LRFD design code to use appropriate design coefficients.

RECOMMENDATIONS

The research team recommends promoting the developed database to LADOTD staff to use it before sending the drilling crew to the field. In some regions, there are a large number of borehole and CPT data files which can prove useful for future projects.

The research team also recommends expanding the GIS database when future measurements become available. The following procedure describes the steps to add more data, i.e., preparing a table of the new data points where each row of the table represents one CPT sounding. The column headers should be similar to the ones in the original database, i.e., Job Number, Location, Station, Date, latitude, longitude, etc.; the table should also include the location of the PDF and Excel files of the CPT soundings. This table can then be imported into ArcMap by using the "Add Data" function. Once the table is added to ArcMap, the new data can be displayed on the map by selecting the "Add X, Y data" option. This will prompt the user to select the columns where the latitude and longitude are located in the table. After selecting the column where the coordinates are located, the points will appear on the map. At this point, the data can be converted into a shape file to be saved and used in ArcMap. Finally, the "join" function can be used to add the new points to the original database.

Based on the statistical studies performed in this research effort, it is recommended that the LADOTD starts adopting the updated CPT coefficient in conjunction with borehole results for a transition period until the proposed values are validated. Updates of the CPT coefficient are also prudent as more CPT data becomes available, which mentioned earlier, should be added to the developed database.

ACRONYMS, ABBREVIATIONS, AND SYMBOLS

α	Significance level
a	Cone area ratio
AASHTO	The American Association of State Highway and Transportation Officials
A_c	The projected area of the cone
ACI	American Concrete Institute
A_f	Skempton's pore pressure parameter at failure
ALF	LTRC's Accelerated Loading Facility
A_s	The surface area of the sleeve
A_s	Friction sleeve surface area
A_{sb}	Cross sectional area at the bottom of the friction sleeve
ASD	Allowable Stress Design
A_{st}	Cross sectional area at the top of the friction sleeve
B_q	The pore pressure ratio
B	Angle of plastification
β	Reliability Index
B_q	Pore water pressure index
c_v	Coefficient of consolidation
$c1$	Model uncertainty
c_1, c_2, and c_3	Constants dependent on the compressibility
COV	The coefficient of variation
CPT	Cone Penetration Test
CRR	Cyclic resistance ratio
CSR	Cyclic stress ratio
D_{50}	Mean particle size
D_i	Distance between CPT and borehole

DOQQ	Digital orthophoto quarter quad images
D_r	Relative density
Dr_L, Dr_M, Dr_H	Relative densities corresponding to low, medium, and high compressibility conditions
Δu	Excess pore water pressure
e	Void ratio
E_t	Initial tangent modulus
E_s	Secant modulus at 50 percent failure
e_{max}, e_{min}	The maximum and minimum void ratios
ϕ	Resistance factor
f_t	The corrected sleeve friction
FC	Fines content
FORM	The First Order Reliability Method
F_s	The force acting on the friction sleeve
f_s	The sleeve friction
φ`	Friction angle
ft.	Feet
γ_i	The load factor
γ_T	Soil unit weight
GIS	Geographic information system
h	Depth in feet
HPC	highly probable clay
HPM	highly probable mixed
HPS	highly probable sand
I_c	Soil classification index
In.	Inch
IR	Rigidity index

k	Adjustment factor (function of soil type and properties)
K_o	Earth pressure coefficient at rest
kPa	Kilo Pascal
λ	The bias
LADOTD	Louisiana Department of Transportation and Development
LRFD	Load and Resistance Factor Design
LSD	Limit State Design
LTRC	Louisiana Transportation Research Center
μ_{X_i}	The mean
MPa	Mega Pascal
N_c, N_k, N_{kt}, N_c', $N_{\Delta u}$	Theoretical cone factor
NCHRP	The National Cooperative Highway Research Program
OCR	over-consolidation ratio
p_a	Atmospheric pressure
PCPT	Piezo-Cone Penetration Test
PDF	Portable document format
PI	Plasticity index
psf	Pounds per square foot
q	Weighted average
q_E	Effective tip resistance parameter
Q_i	The demand due to applied loads (dead, live, etc.)
Q_A	Aging factor
Q_c	The total force acting on the cone
q_c	The cone resistance
Q_F	Empirical constant of the least-square regression
q_t	Cone resistance corrected for unequal end area effects
$q_{t\text{-}net}$	Net tip resistance

R_n	The nominal capacity of the designed member
R_f	Friction ratio
σ_{ho}	Horizontal pressure
σ_{mean}	Mean stress
σ_{vo}	total overburden stress
$\sigma`_p$	Pre-consolidation pressure
σ_{X_i}	Standard deviation
S_u^{UC}	Unconfined compression undrained shear strength
S_u^{CPT}	Undrained shear strength calculated from CPT data
SBPMT	Self-boring Pressuremeter Test
SPT	Standard penetration test
SPT-N	Number of blows in SPT for 300 mm penetration
STE	Soil Testing Engineers, Inc.
S_u	Undrained shear strength
θ	Semi-apex angle
tsf	Tons per square foot
U	soil classification index
u_1	Pore water pressure at the tip of the cone
u_2	Pore water pressure behind the cone
u_3	Pore water pressure behind the friction sleeve
u_o	Hydrostatic or initial in-situ pore pressure
USCS	Unified Soil Classification System
V_s	Shear wave velocity
W_L, W_M, and W_H	Weight factors
X_i	Random variable

REFERENCES

1. Robertson, P.K. (1990), "Soil Classification Using the Cone Penetration Test." Canadian Geotechnical Journal, Vol. 27, No. 1. pp. 151-158.

2. Zhang, Z. and Tumay, M.T. (1999), "Statistical to Fuzzy Approach Toward CPT Soil Classification." Journal of Geotechnical and Geoenvironmental Engineering, Vol. 125 (3), pp. 179-186.

3. Villet, W.C.B and Mitchell, J.K. (1981), "Cone Resistance, Relative Density and Friction Angle." Cone Penetration Testing and Experience; Session at the ASCE National Convention, St. Louis, 178-207, American Society of Engineers (ASCE).

4. Robertson, P.K. and Campanella, R.G. (1983a), "Interpretation of Cone Penetrometer Test: Part I: Sand." Canadian Geotechnical Journal, 20(4), pp.718-33.

5. Robertson, P.K. and Campanella, R.G. (1983b), "Interpretation of Cone Penetrometer Test: Part II: Clay." Canadian Geotechnical Journal, 20(4), pp. 734-45.

6. Meigh, A. C. (1987), "Cone penetration testing." CIRIA Rep., Butterworth's, London, U.K.

7. Vermeiden, J. (1948), "Improved Sounding Apparatus as Developed in Holland since 1936." Proceedings of the Second International Conference on Soil Mechanics and Foundation Engineering, Rotterdam, 1, pp. 280-7.

8. Plantema, G. (1948), "Construction and Method of Operating a New Deep Sounding Apparatus." Proceedings of the 2nd International Conference on Soil Mechanics and Foundation Engineering, Rotterdam, 1, pp. 277-9.

9. Begemann, H.K.S. Ph. (1953), "Improved Method for Determining Resistance to Adhesion by Sounding Through a Loose Sleeve Placed Behind the Cone." Proceedings of the 3rd International Conference on Soil Mechanics and Foundation Engineering, Zurich, 1, pp. 213-17.

10. Sanglerat, G. (1972), “The Penetrometer and Soil Exploration.” Elsevier, Amsterdam, 464 pp.

11. Lunne, T.; Robertson, P.K.; and Powell J.J.M. (1997), “Cone Penetration Testing in Geotechnical Practice.” Blackie Academic, EF Spon/Routledge Publishers, New York, 312 pp.

12. Kurup, P. U.; Voyiadjis, G. Z.; and Tumay, M. T. (1994), “Calibration Chamber Studies of Piezocone Test in Cohesive Soils.” J. Geotechnical Engineering, American Society of Civil Engineers (ASCE), 120(1), pp. 81-107.

13. Schaap, L.H.J. and Zuidberg, H.M. (1982), “Mechanical and Electrical Aspects of the Electric Cone Penetrometer Tip.” Proceedings of the 2nd European Symposium on Penetration Testing, ESOPT-II, Amsterdam, 2, 841-51 Balkema Pub. Rotterdam.

14. Sandven, R.; Senneset, K.; and Janbu, N. (1988), “Interpretation of Piezocone Tests in Cohesive Soils.” Proceedings of the International Symposium on Penetration Testing, ISOPT-1, Orlando, 2, 939-53, Balkema Pub., Rotterdam.

15. Begemann, H.K.S. Ph. (1965), “The Friction Jacket Cone an Aid in Determining the Soil Profile.” Proceedings of the 6th International Conference on Soil Mechanics and Foundation Engineering, Montréal, 1, 17-20.

16. Sanglerat, G.; Nhim, T. V.; Sejourne, M.; and Andina, R. (1974), “Direct Soil Classification by Static Penetrometer with Special Friction Sleeve.” Proceedings of the First European Symposium on Penetration Testing, ESOPT-1, June 5-7, Stockholm, Vol. 2.2, pp. 337-344.

17. Schmertmann, J.H. (1970), “Static Cone to Compute Static Settlement Over Sand.” Journal of the Soil Mechanics and Foundations Division, American Society of Civil Engineers (ASCE), 96(SM3), pp. 1011-43.

18. Douglas, B.J. and Olsen, R.S. (1981), “Soil Classification Using Electric Cone Penetrometer. Cone Penetration Testing and Experience.” Proceedings of the ASCE National Convention, St. Louis, American Society of Civil Engineers (ASCE), pp. 209-27.

19. Robertson, P.K.; Campanella, R.G.; Gillespie, D.; and Greig, J. (1986), "Use of Piezometer Cone Data." Proceedings of the ASCE Specialty Conference In Situ '86: Use of In Situ Tests in Geotechnical Engineering, Blacksburg, American Society of Civil Engineers (ASCE), pp. 1263-80.

20. Olsen, R.S. and Farr, J.V. (1986), "Site Characterization Using the Cone Penetration Test." Proceedings of the ASCE Specialty Conference In Situ '86: Use of In Situ Tests in Geotechnical Engineering, Blacksburg, American Society of Civil Engineers (ASCE), pp. 854-68.

21. Lunne, T.; Eidsmoen, T.; Gillespie, D.; and Howland, J.D. (1986), "Laboratory and Field Evaluation of Cone Penetrometers." Proceedings of the ASCE Specialty Conference In Situ '86: Use of In Situ Tests in Geotechnical Engineering, Blacksburg, American Society of Civil Engineers (ASCE), pp. 714-29.

22. Gillespie, D.G. (1990), "Evaluating Velocity and Pore Pressure Data from the Cone Penetration Test." Ph.D. thesis, Department of Civil Engineering, University of British Columbia, Vancouver, BC.

23. Jones G.A. and Rust, E. (1982), "Piezometer Penetration Testing, CUPT." Proceedings of the Second European Symposium on Penetration Testing, ESOPT-2, Amsterdam, May 24-27, Vol. 2, pp. 607-614.

24. Baligh, M.M.; Vivatrat, V.; and Ladd, C.C. (1980), "Cone Penetration in Soil Profiling." Journal of the Geotechnical Engineering Division, American Society of Civil Engineers (ASCE), 106(GT4), pp. 447-61.

25. Senneset K. and Janbu, N. (1985), "Shear Strength Parameters Obtained from Static Cone Penetration Tests In Situ Measurements." Symposium, San Diego, 1984, American Society for Testing and Materials (ASTM) special technical publication, STP 883, pp. 41-54.

26. Eslami, A. and Fellenius, B.H. (1997), "Pile Capacity by Direct CPT and CPTu methods applied to 102 Case Histories." Canadian Geotechnical Journal, Vol. 34, No. 6, pp. 880-898.

27. Fellenius, B.H. and Eslami, A. (2000), “Soil Profile Interpreted from CPTu data.” Year 2000 Geotechnics, Geotechnical Engineering Conference, Asian Institute of Technology, Bangkok, Thailand, November 27-30, 2000, 18 pp.

28. Kaufmann, A. (1975), “Introduction to the Theory of Fuzzy Subsets, I: Fundamental Theoretical Elements.” Academic Press, New York.

29. Brown, C.B.; Chameau, J.L.; Palmer, R.; and Yao, J.T.P. (1985). Proceedings, NSF Workshop on Civil Engineering Applications of Fuzzy Sets, Purdue University, West Lafayette, IN.

30. Hill, R. (1950), “The Mathematical Theory of Plasticity.” Oxford University Press, Oxford, England.

31. Vesic, A.S., (1972), “Expansion of Cavities on the Infinite Soil Masses.” Journal of the Soil Mechanics and Foundation Division, American Society of Civil Engineers (ASCE), Vol. 98, SM3, pp. 265-290.

32. Baligh, M.M. (1985), “Strain path method.” Journal of the Geotechnical Engineering Division, American Society of Civil Engineers (ASCE), 111(GT9), pp. 1108-36.

33. Teh, C.I. and Houlsby, G.T. (1991), “An Analytical Study of the Cone Penetration Test in Clay.” Geotechnique, 41(1), pp. 17-34.

34. Abu-Farsakh, M.Y.; Voyiadjis, G.Z; and Tumay, M.T. (1998), “Numerical Analysis of the Miniature Piezocone Penetration Tests (PCPT) in Cohesive Soils.” International Journal for Numerical and Analytical Methods in Geomechanics. Vol. 22 (10), pp. 791-818.

35. Terzaghi, K. (1943), “Theoretical soil mechanics.” John Wiley and Sons, New York, 510 pp.

36. Caquot, A. and Kerisel, J. (1956), “Traité de Mécanique des Sols.” Gauthier-Villars, Paris.

37. Meyerhof, G.G. (1951), “The Ultimate Bearing Capacity of Foundations. Géotechnique.” 2(4), pp. 301-2.

38. De Beer, E.E. (1977), "Static Cone Penetration Testing in Clay and Loam." Sondeer Symposium, Utrecht.

39. Skempton, A.W. (1951), "The Bearing Capacity of Clays." Proceedings of the Building Research Congress, London, Division I, 180-9.

40. Gibson, R.E. (1950), Discussion: G. Wilson. "The bearing capacity of screw piles and concrete cylinders." Journal of the Institution of Civil Engineers, 34, 382.

41. Baligh, M.M. (1975), "Theory of Deep Site Static Cone Penetration Resistance." Massachusetts Institute of Technology, Department of Civil Engineering, Cambridge, Mass., Publication No. R75-56.

42. Ladanyi, B. (1967), "Deep Punching of Sensitive Clays." Proceedings of the Third Oan American Conference on Soil Mechanics and Foundation Engineering, Caracas, 1, pp. 533-46.

43. Teh, C.I. (1987), "An Analytical Study of the Cone Penetration Test". D.Phil. thesis, Oxford University.

44. Lunne, T. and Kleven, A. (1981), "Role of CPT in North Sea Foundation Engineering." Session at the ASCE National Convention: Cone Penetration Testing and Materials, St. Louis, American Society of Civil Engineers (ASCE), pp. 76-107.

45. Kjekstad, O.; Lunne, T.; and Clausen, C.J.F. (1978), "Comparison Between In Situ Cone Resistance and Laboratory Strength for Overconsolidated North Sea Clays." Marine Geotechnology, 3(1), pp. 23-36.

46. Aas, G.; Lacasse, S.; Lunne, T.; and Hoeg, K. (1986), "Use of In Situ Tests for Foundation Design on Clay." Proceedings of the ASCE Specialty conference In Situ '86: Use of In Situ Tests in Geotechnical Engineering, Blacksburg, American Society of Civil Engineers (ASCE), pp. 1-30.

47. La Rouchelle, P.; Zebdi, P.M.; Leroueil, S.; Tavenas, F.; and Virely, D. (1988), "Piezocone Tests in Sensitive Clays of Eastern Canada." Proceedings of the International Symposium on Penetration Testing, ISOPT-1, Orlando, 2 pp. 831-41, Balkema Pub., Rotterdam.

48. Rad, N.S. and Lunne, T. (1988), “Direct Correlations Between Piezocone Test Results and Undrained Shear Strength of Clay.” Proceedings if The International Symposium on Penetration Testing ISOPT-1, Orlando, 2, 911-17, Balkema Pub., Rotterdam.

49. Senneset, K.; Janbu, N.; and Svanǿ, G. (1982), “Strength and Deformation Parameters from Cone Penetration Tests.” Proceedings of the 2nd European Symposium on Penetration Testing, ESOPT-II, Amsterdam, 2, 863-70, Balkema Pub., Rotterdam.

50. Lunne, T.; Christopherson, H.P.; and Tjelta, T.I. (1985), “Engineering Use of Piezocone Data in North Sea Clays.” Proceedings of the 11th International Conference on Soil Mechanics and Foundation Engineering, San Francisco, 2, 907-12, Balkema Pub., Rotterdam.

51. Campanella, R.G. and Robertson, P.K. (1988), “Current Status of the Piezocone Test.” Proceedings of the International Symposium on Penetration Testing, ISOPT-1, Orlando, 1, 93-116, Balkema Pub., Rotterdam.

52. Battaglio, M.; Jamiolkowsi, M.; Lancellotta, R.; and Maniscalco, R. (1981), “Piezometer Probe Test in Cohesive Deposits. Cone Penetration Testing and Experience.” Proceedings of the Session ASCE National Convention, St. Louis, pp. 264-302.

53. Randolph, M.F. and Wroth, C.P. (1979), “An Analytical Solution for the Consolidation Around a Driven Pile.” Proceedings of the International Journal for Numerical and Analytical Methods in Geomechanics, 3(3), 217-29.

54. Henkel, D.J. and Wade, N.H. (1966), “Plane Strain on a Saturated Remolded Clay.” ASCE-J, Vol. 92, No. 6.

55. Massarsch, K.R. and Broms, B.B. (1981), “Pile Driving in Clay Slopes.” Proceedings of the 10th International Conference on Soil Mechanics and Foundation Engineering, Stockholm, 3, 469-74, Balkema Pub., Rotterdam.

56. Keaveny, J.M. and Mitchell, J.K. (1986), “Strength of Fine-Rained Soils Using the Piezocone.” Proceedings of the ASCE Specialty Conference in Situ ’86: Use of In Situ Tests in Geotechnical Engineering, Blacksburg, 668-85, American Society of Civil Engineers (ASCE).

57. Lunne, T., Lacasse, S. and Rad, N.S. (1989), "SPT, CPT, Pressuremeter Testing and Recent Developments on In Situ Testing of Soils." General report from the 12th International Conference on Soil Mechanics and Foundation Engineering, Roi de Janeiro, 4, 2339-403, Balkema Pub., Rotterdam.

58. Senneset, K.; Sandven, R.; and Janbu, N. (1989), "The Evaluation of Soil Parameters from Piezocone Tests." Transportation Research Record, No. 1235, pp. 24-37.

59. Sully, J.P.; Campanella, R.G.; and Robertson, P.K. (1988), "Overconsolidation Ratio of Clays From Penetration Pore Water Pressures." Journal of Geotechnical Engineering, ASCE, 114(2), pp. 209-15.

60. Mayne, P.W. (1991), "Determination of OCR in Clays by Piezocone Tests using Cavity Expansion and Critical State Concepts." Soils and Foundations, 31(2), pp. 65-76.

61. Mayne, P.W., "CPT-Based Prediction of Footing Response. Measured & Predicted Behavior of Five Spread Footings on Sand (GSP 41)." ASCE, Reston, Virginia, 1994, pp. 214-218.

62. Mayne, P.W. (2006), "The 2nd James K. Mitchell Lecture: Undisturbed Sand Strength from Seismic Cone Tests." Geomechanics & Geoengineering, Taylor & Francis Group, London, Vol. 1, No. 4, 2006.

63. Chen, B.S-Y. and Mayne, P.W. (1996), "Statistical Relationships between Piezocone Measurements and Stress History of Clays." Canadian Geotechnical Journal, Vol. 33, pp. 488-498.

64. Mayne, P.W. (2001), "Stress-Strain-Strength-Flow Parameters from Enhanced In-Situ Tests." Proceedings, International Conference on In-Situ Measurement of Soil Properties and Case Histories, Bali, Indonesia, pp. 27-48.

65. Juang, C.H.; Huang, X.H.; Holtz, R.D.; and Chen, J.W. (1996), "Determination of Relative Density from CPT Using Fuzzy Sets." J. Geotechnical Engineering, American Society of Civil Engineers (ASCE), 122(1).

66. Baldi, G.; Bellotti, R.; Ghionna, V.; Jamiolkowski, M.; and Pasqualini, E. (1986), "Interpretation of CPTs and CPTUs; 2nd part: Drained Penetration of Sands." Proceedings of the Fourth International Geotechnical Seminar, Singapore, pp. 143-56.

67. Kulhawy, F.H. and Mayne, P.H. (1990), "Manual on Estimating Soil Properties for Foundation Design." Electric Power Research Institute, EPRI, August, 1990.

68. Jamiolkowski, M.; Swets, Zeitlinger and Lisse. (2001), "Where Are We Going." Pre-Failure Deformation Characteristics of Geomaterials, Vol. 2 (Proc. Torino '99), pp. 1251-1262.

69. Juang, C. H.; Fang, S. Y.; and Khor, E. H. (2006). "First-Order Reliability Method for Probabilistic Liquefaction Triggering Analysis Using CPT," Journal of Geotechnical and Geoenvironmental Engineering, Vol. 132, No. 3, pp. 337-350.

70. Meigh, A.C. and Nixon, I.K. (1961), "Comparison of In-Situ Tests for Granular Soils." Proc. 5th International Conference on Soil Mechanics and Foundation Engineering, Paris, 1961, Vol. 1, pp. 499-507.

71. Thornburn, S. (1970), "Proc. Conference on Behavior of Piles." Institution Civil Engineers, London, pp. 53-54.

72. Burland, J.B. and Burbridge, M.C. (1985), "Settlement of Foundations on Sand and Gravel." Proceedings of the Institution of Civil Engineers. December 1985 78 (Part 1), pp. 1325-1381.

73. Jefferies, M.G. and Davies, M.P. (1993), "Use of CPTu to estimate equivalent SPT N60." Geotechnical Testing Journal, GTJODJ, Vol. 15, No. 4, December 1993, pp. 458-468.

74. AASHTO (2004). LRFD Bridge Design Specifications. American Association of State Highway and Transportation Officials, Washington, D.C.

75. Hansen, B. (1956). "Limit Design and Safety Factors in Soil Mechanics." Bulletin No. 1, Danish Geotechnical Institute, Copenhagen, Denmark.

76. Hansen, B. (1966). "Code of Practice for Foundation Engineering." Bulletin No. 22, Danish Geotechnical Institute, Copenhagen, Denmark.

77. Tang, W. (1993). “Recent Developments in Geotechnical Reliability.” Proceedings, Conference on Probabilistic Methods in Geotechnical Engineering, Balkema, Rotterdam, The Netherlands, Canberra, Australia, pp. 3-28.

78. Hamilton, J. and Murff, J. (1992). “Selection of LRFD Resistance Factors for Pile Foundation Design.” Proceedings, Structures Congress, American Society of Civil Engineers, San Antonio, TX.

79. Kulhawy, F. and Phoon, K. (1996). “Engineering Judgment in the evolution from Deterministic to Reliability-Based Foundation Design.” Proceedings, 1996 Conference on Uncertainty in the Geologic Environment, UNCERTAINTY '96, American Society of Civil Engineers, NY, Madison, WI, pp. 29-48.

80. Barker, R. M.; Duncan, J. M.; Rojiani, K. B.; Ooi, P. S. K.; Tan, C. K.; and Kim, S. G. (1991). “Manuals for the Design of Bridge Foundations: Shallow Foundations, Driven Piles, Retaining Walls and Abutments, Drilled Shafts, Estimating Tolerable Movements, and Load Factor Design Specifications and Commentary.” NCHRP Report No. 343, TRB, National Research Council, Washington, D.C.

81. O'Neill, M. (1995). “LRFD Factors for Deep Foundations through Direct Experimentation.” Proceedings, US/Taiwan Geotechnical Engineering Collaboration Workshop, Taipei, Taiwan, pp. 100-114.

82. AASHTO (1994). LRFD Bridge Design Specifications. American Association of State Highway and Transportation Officials (AASHTO), Washington, D.C.

83. D'Appolonia (1998). “LRFD Specifications for Retaining Walls.” NCHRP Project 20-07 (Task 88), TRB, National Research Council, Washington, D.C.

84. Withiam, J. L. (2004). “Load and Resistance Factors for Earth Pressures on Bridge Substructures and Retaining Walls.” NCHRP Project 12-55, TRB, National Research Council, Washington, D.C.

85. Paikowsky, S. G.; Birgisson, B.; McVay, M.; Nguyen, T.; Kuo, C.; Baecher, G.; Ayyub, B.; Stenersen, K.; O'Malley, K.; Chernauskas, L.; and O'Neill, M. (2004). “Load and

Resistance Factor Design (LRFD) for Deep Foundations." NCHRP Report No. 507, TRB, National Research Council, Washington, D.C.

86. Allen, T. M. (2005). "Development of Geotechnical Resistance Factors and Downdrag Load Factors for LRFD Foundation Strength Limit State Design." FHWA-NHI-05-052, Federal Highway Administration, Washington, D.C.

87. Phoon, K. K.; Kulhawy, F. H.; and Grigoriu, M. D. (2003). "Multiple Resistance Factor Design for Shallow Transmission Line Structure Foundations," Journal of Geotechnical and Geoenvironmental Engineering, Vol. 129, No. 9, 807-+ pp.

88. Phoon, K. K.; and Kulhawy, F. H. (2005). "Characterisation of Model Uncertainties for Laterally Loaded Rigid Drilled Shafts," Geotechnique, Vol. 55, No. 1, pp. 45-54.

89. Abd Alghaffar, M. A. and Dymiotis-Wellington, C. (2005). "Reliability Analysis of Retaining Walls Designed to British and European Standards," Structure and Infrastructure Engineering, TAYLOR & FRANCIS LTD, Vol. 1, No. 4, pp. 271-284.

90. Low, B. K. (2005). "Reliability-Based Design Applied to Retaining Walls," Geotechnique, Vol. 55, No. 4, pp. 343.

91. Goh, A. T. C. and Kulhawy, F. H. (2005). "Reliability Assessment of Serviceability Performance of Braced Retaining Walls Using a Neural Network Approach," International Journal for Numerical and Analytical Methods in Geomechanics, Vol. 29, No. 6, pp. 627-642.

92. Fenton, G. A.; Griffiths, D. V.; and Williams, M. B. (2005). "Reliability of Traditional Retaining Wall Design," Geotechnique, Vol. 55, No. 1, pp. 55-62.

93. Kulhawy, F. H. and Phoon, K. K. (2002). "Observations on Geotechnical Reliability-Based Design Development in North America." Proceedings, Foundation Design Codes and Soil Investigation in View of International Harmonization and Performance Based Design, Balkema, Lisse, Netherlands, pp. 31-48.

94. Phoon, K. K. and Kulhawy, F. H. (1999a). "Characterization of Geotechnical Variability," Canadian Geotechnical Journal, Vol. 36, No. 4, pp. 612-624.

95. Phoon, K. K. and Kulhawy, F. H. (1999b). "Evaluation of Geotechnical Property Variability," Canadian Geotechnical Journal, Vol. 36, No. 4, pp. 625-639.

96. McVay, M. C.; Birgisson, B.; Zhang, L.; Perez, A.; and Putcha, S. (2000). "Load and Resistance Factor Design (LRFD) for Driven Piles Using Dynamic Methods-A Florida Perspective," Geotechnical Testing Journal, American Society for Testing and Materials, Vol. 23, No. 1, pp. 55-66.

97. Titi, H. H.; Mahamid, M.; Abu-Farsakh, M. Y.; and Elias, M. (2004). "Evaluation of CPT Methods for Load and Resistance Factor Design of Driven Piles."Geotechnical Engineering for Transportation Projects: Proceedings of Geo-Trans 2004, American Society of Civil Engineers, Reston, VA 20191-4400, United States, Los Angeles, CA, United States, pp. 687-696.

98. Babu, G. L. S.; Srivastava, A.; and Murthy, D. S. N. (2006). "Reliability Analysis of the Bearing Capacity of a Shallow Foundation Resting on Cohesive Soil," Canadian Geotechnical Journal, Vol. 43, No. 2, pp. 217-223.

99. Abu-Farsakh, M. Y. and Nazzal, M. D. (2005). "Reliability of Piezocone Penetration Test Methods for Estimating the Coefficient of Consolidation of Cohesive Soils," Geology and Properties of Earth Materials 2005, No. 1913, pp. 62-76.

100. Roy, D.; Hughes, J. M. O.; and Campanella, R. G. (1999). "Reliability of Self-Boring Pressuremeter in Sand," Canadian Geotechnical Journal, Vol. 36, No. 1, pp. 102-110.

101. Liu, C. N. and Chen, C. H. (2006). "Mapping Liquefaction Potential Considering Spatial Correlations of CPT Measurements," Journal of Geotechnical and Geoenvironmental Engineering, Vol. 132, No. 9, pp. 1178-1187.

102. Hegazy, Y.A and Mayne, P.W. (1995). "Statistical Correlations Between Vs and CPT Data for Different Soil Types." Proceedings, Cone Penetration Testing (CPT '95), Linkoping, Swedish Geotechnical Society, pp. 173-178.

APPENDIX A

List of Projects Included in Database

Table 34
Projects with CPT and borehole data

Job Number	District	Parish Name	Date	Job Location
700-44-0005	Dist 02	St. Bernard	10/1/2006	LA 46 St Bernard
006-05-0076	Dist 02	Orleans	2/1/2005	Rigolets Pass Bridge & approaches
845-09-0008	Dist 02	St. Charles	12/23/2004	LA 632 Main Canal Bridge
005-07-0057	Dist 02	Lafourche	12/22/2004	Drain Canal Bridge on LA 182
700-26-0229	Dist 02	Jefferson	11/19/2003	Causeway Boulevard
700-18-0014	Dist 02	Jefferson	11/13/2003	Huey P. Long Bridge
700-30-0068	Dist 02	Lafourche	8/20/2002	T-Bois Bridge
700-36-0146	Dist 02	Orleans	1/9/2002	US 90 @ Rigolets @ Pass
424-04-0034	Dist 03	Iberia	5/18/2005	US 90 Interchange @ LA 675
857-02-0006	Dist 03	Vermilion	8/17/2004	LA 332 Maree Michel Canal Bridge
700-23-0208	Dist 03	Iberia	5/28/2003	US 90 Iberia Parish
700-23-0205	Dist 03	Iberia	8/28/2002	US 90 @ LA 83
424-05-78	Dist 03	St marys	9/29/1992	Mac drv over mopac rr
380-02-0007	Dist 03	St. Landry	1/26/2005	LA 363 Drainage Canal
427-01-0029	Dist 04	Caddo	9/8/2005	LA 3132 @ LA 526
700-08-0110	Dist 04	Bossier	1/28/2004	LA 154
700-09-0125	Dist 04	Caddo	12/17/2003	LA 523 @ Bayou Pierre
700-09-0123	Dist 04	Caddo	3/26/2003	US 80
700-08-0001	Dist 04	Bossier	3/25/2003	Benoit Bridge
700-09-0134	Dist 04	Caddo	10/1/2002	LA 511

001-04-0029	Dist 04	Webster	8/7/2002	US 80 @ Dixie Inn
010-05-0027	Dist 04	Bossier	12/8/1999	US 71 @ KCS RR
742-37-0010	Dist 05	Ouachita	5/2/2000	N. 18 St. Ext Seg 2
069-03-0018	Dist 05	Union	12/25/2004	LA 33 Creek Bridge
700-37-0115	Dist 05	Ouachita	1/27/2004	Route US 80
700-33-0101	Dist 05	Madison	1/30/2002	Madison Parish
043-01-0017	Dist 05	Jackson	7/10/2001	LA 147
700-25-0024	Dist 05	Jackson	10/25/2000	Chaptham-Eros
713-58-94	Dist 05	La Salle	6/28/1995	Lat. 314724 Long.920509
126-01-0017	Dist 05	Jackson	6/27/1995	JCT la 34 Jackson ph-line
700-17-61	Dist 05	Ouachita	10/26/1994	Forsythe Ave
700-29-0069	Dist 08	Sabine	4/17/2001	Zwolle-noble
700-30-0035	Dist 08	Rapides	8/5/2002	Susek Dr. Pineville
362-01-0009	Dist 08	Natchitoches	8/10/2004	LA 491 str # 08353620105301
700-35-0121	Dist 08	Natchitoches	4/8/2003	str #08350420510011
700-58-0115	Dist 08	Vernon	3/19/2003	Bayou Zourie
700-35-0108	Dist 08	Natchitoches	3/29/2000	Black Lake LA 9
700-30-0281	Dist 08	Rapides	8/19/1998	LA 488 Bayou Boeuf
022-03-34	Dist 08	Winn	10/4/1995	Dugdemona Relief
713-58-63	Dist 08	Grant	4/12/1994	Flag on Bayou Grant ph
126-02-12	Dist 08	Winn	3/31/1993	LA 499
023-01-41	Dist 08	Rapides	12/15/1992	Red River Bridge Appro
022-03-34	Dist 08	Rapides	12/14/1992	Red River Bridge Appro
023-01-41	Dist 08	Rapides	12/14/1992	Red River Bridge Appro
700-30-0311	Dist 58	La Salle	4/2/2003	Hemps Creek West Bridge
344-02-07	Dist 58	Franklin	12/13/1994	Bayou Macon

700-17-0159	Dist 61	E. Baton Rouge	5/10/2004	Perkins Rd. \ LA 427
424-06-06	Dist 61	Assumption	6/12/1996	Bayou Boeuf
454-04-0038	Dist 62	St. Tammany	6/7/2005	LA1088 at I-12
454-02-0035	Dist 62	Livingston	4/21/2005	I-12 @ Juban Road
262-31-0016	Dist 62	Livingston	12/28/2004	LA 64 Amite River Bridge
452-90-17	Dist 62	Tangipahoa	11/9/1994	Ward Line Road

Table 35
Projects with CPT data without borehole data

Job Number	District	Parish Name	Date	Job Location
450-15-0100	Dist 02	Jefferson	3/3/2003	US 190 St. Landry
283-08-0143	Dist 02	Orleans	2/12/2003	LA 158 Bayou Grappe
700-26-0252	Dist 02	Jefferson	3/22/2000	Bayou Teche
283-08-0146	Dist 02	Orleans	10/31/2000	US 71/1 6 7
700-55-0100	Dist 02	Terrebonne	6/13/2006	LA 2 @ Sterlington
700-36-0129	Dist 02	Orleans	8/4/2004	Causeway Interchange Phase 1
424-07-21	Dist 02	Terrebonne	11/22/2005	Bayou Liberty
700-30-0254	Dist 03	St. Landry	10/29/2005	Russell Cemetery Road
700-49-0106	Dist 03	St. Landry	10/29/2005	Philadelphia Road
713-28-0104	Dist 03	Lafayette	10/28/2005	Red Cut Loop Road
380-03-0013	Dist 03	St. Landry	10/28/2005	Bayou Oaks Drive
700-01-0101	Dist 03	Acadia	10/26/2005	Emmanuel road @ mill bayou
700-23-0200	Dist 03	Iberia	10/25/2005	Mosswood Drive
427-01-0035	Dist 04	Caddo	10/24/2005	Hapsburg lane of US 167 Lafayette
700-09-0152	Dist 04	Caddo	4/20/2005	Creek Bridge of US 80
085-01-0017	Dist 04	Caddo	1/26/2005	LA 103 Bayou Courtableau
427-01-17	Dist 04	Caddo	1/25/2005	US 165 Oakdale to Glenmora
427-01-16	Dist 04	Caddo	12/26/2004	LA 4 Biles Branch Bridge
070-06-0022	Dist 05	Ouachita	12/25/2004	LA 577 Creek Bridge
713-37-0134	Dist 05	Ouachita	12/19/2004	Camp Street
713-37-0135	Dist 05	Ouachita	12/14/2004	Inner Loop Extension
001-09-0068	Dist 05	Ouachita	3/26/2004	Inner Loop Extension
068-03-0017	Dist 05	Jackson	11/4/2004	Fremeaux Interchange- US190b

185-03-0025	Dist 05	W. Carroll	8/11/2004	la 1220 little river bridge
700-56-0104	Dist 05	Union	6/16/2004	Drain Canal Bridge on LA 45
700-56-0102	Dist 05	Union	6/15/2004	Tchoupitoulas to South Peters
713-31-0100	Dist 05	Lincoln	4/15/2004	US190 @ LA 415
700-56-0101	Dist 05	Union	3/23/2004	Oakland Rd @ Bayou D'Loutre Bridge
332-04-0005	Dist 05	W. Carroll	2/4/2004	LA 98
700-27-10	Dist 05	Richland	7/1/2003	LA 182
713-10-0106	Dist 07	Calcasieu	4/1/2003	Bridge over Bayou D'Arbonne
0014-04-0032	Dist 07	Allen	3/18/2003	LA 468
700-02-0101	Dist 07	Allen	3/5/2003	dollar road
LA 158 bayou grappe	Dist 08	Grant	2/11/2003	LA 127 drain bridge
us 71/1 6 7	Dist 08	Rapides	1/29/2002	Cypress Creek
713-35-0123	Dist 08	Natchitoches	1/29/2002	Lion Creek Bridge
713-40-0128	Dist 08	Rapides	10/2/2001	LA 530
713-35-0122	Dist 08	Natchitoches	3/13/2001	Loreauville Canal
361-01-0008	Dist 08	Natchitoches	1/4/2001	LA 1153 Allen Ph
700-58-0102	Dist 08	Vernon	12/18/2000	LA 572 @ Bayou Macon
700-01-0018	Dist 08	Vernon	5/8/2000	Bayou Macon LA 585
014-06-25	Dist 08	Rapides	11/18/1998	Black Jack Branch
455-05-62	Dist 08	Rapides	11/2/1998	I-10 Lake Pont
455-05-45	Dist 08	Rapides	8/26/1998	I-10 relief canal
700-30-0310	Dist 58	La Salle	11/8/1995	Bayou L'ourse
700-21-0102	Dist 58	Franklin	2/9/1994	Brookwood Drive
008-01-0044	Dist 61	West Baton Rouge	2/7/1994	Richland Parish Road #12
852-21-0024	Dist 62	St. Tammany	5/4/1993	Inner Loop over W70 ST

700-18-0053	Dist 62	St. Tammany	4/29/1993	Inner Loop over Ellerb
713-59-0220	Dist 62	Washington	11/18/1992	Red River bridge app
700-26-0058	Dist 62	St. John the Baptist	11/17/1992	Alex Urban sec I49

APPENDIX B

First Order Reliability Method (FORM)

FORM is based on a first order Taylor Series expansion of the limit state function that approximates the failure surface by a tangent plane at the point of interest. It is not always possible to find a closed form solution for a non-linear limit state function or a function including more than two random variables. Hence, to convert a non-linear limit state function into simple polynomials, Taylor series, equation (53) is used. The expansion of a function, $f(X)$, at a certain point "a" is given by:

$$f(X) = f(a) + (X-a)f'(a) + \frac{(X-a)^2}{2} f''(a) + \ldots\ldots\ldots\ldots + \frac{(X-a)^n}{n!} f^n(a) \qquad (53)$$

FORM uses this expansion to simplify the limit state function, $g(Z_1, Z_2, \ldots\ldots, Z_n)$ by considering the expansion of the Taylor series after truncating terms higher than the first order. The expansion is done at the actual design point X^*. The design point is a point on the failure surface $g(Z_1, Z_2, \ldots\ldots, Z_n)$ as shown in Figure 56 for the case of two variables in a non-linear limit state function.

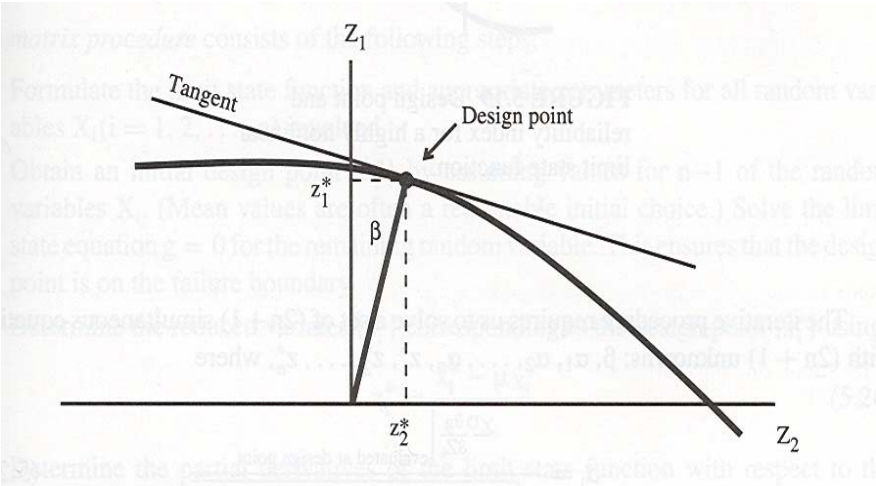

Figure 56
Reliability index evaluated at design point (Nowak and Collins 2000)

To locate this point on the design space of $g(Z_1, Z_2, ..., Z_n) = 0$, an iterative process is needed (Nowak and Collins 2000). For the convergence of a design point through iterative procedure requires solving of a set of (2*n* + 1) simultaneous equation with (2*n* + 1) unknowns $\beta, \alpha_1, \alpha_2, \ldots, \alpha_n, Z_1^*, Z_2^*, \cdots, Z_n^*$:

$$\alpha_i = \frac{-\left.\frac{\partial g}{\partial Z_i}\right|_{evaluated\ at\ design\ point}}{\sqrt{\sum_{k=1}^{n}\left(\left.\frac{\partial g}{\partial Z_k}\right|_{evaluated\ at\ design\ point}\right)^2}} \tag{54}$$

$$\frac{\partial g}{\partial Z_i} = \frac{\partial g}{\partial X_i}\frac{\partial X_i}{\partial Z_i} = \frac{\partial g}{\partial X_i}\sigma_{X_i} \tag{55}$$

$$\sum_{i=1}^{n}(\alpha_i)^2 = 1 \tag{56}$$

$$Z_i^* = \beta\alpha_i \tag{57}$$

$$g(Z_1^*, Z_2^*, \cdots, Z_n^*) = 0 \tag{58}$$

where, α_i is a unit vector in the direction of a design point from the origin, and Z_i^* is the design point in transformed space. Equation (58) is a mathematical statement of the requirement that the design point must be on the failure boundary.

This procedure was derived with the assumption that the involved random variables are normally distributed. When the probability distributions for the variables involved in the limit state function are not normally distributed, it is required to calculate the "equivalent normal" values of the mean and standard deviation for each non-normal random variable. To obtain the equivalent normal mean, μ_X^e, and standard deviation, σ_X^e, the CDF and PDF of the actual function should be equal to normal CDF and normal PDF at the value of the variable X^* on the failure boundary described by $g = 0$. Mathematically it can be expressed asp

$$F_X(X^*) = \Phi\left(\frac{X^* - \mu_X^e}{\sigma_X^e}\right) \tag{59}$$

$$f_X\left(X^*\right)=\frac{1}{\sigma_X^e}\phi\left(\frac{X^*-\mu_X^e}{\sigma_X^e}\right) \tag{60}$$

where, X is a random variable with mean μ_X and standard deviation σ_X and is described by a CDF $F_X(X)$ and a PDF $f_X\left(X\right)$. Where, $\Phi(.)$ is the CDF for the standard normal distribution and $\phi(.)$ is the PDF for the standard normal distribution. Expressions for μ_X^e and σ_X^e can be obtained as follows:

$$\mu_X^e = X^* - \sigma_X^e\left[\Phi^{-1}\left(F_X\left(X^*\right)\right)\right] \tag{61}$$

$$\sigma_X^e = \frac{1}{f_X\left(X^*\right)}\phi\left[\Phi^{-1}\left(F_X\left(X^*\right)\right)\right] \tag{62}$$

The basic steps in the iteration procedure (Nowak and Collins 2000) to obtain β are as follows:

1. Formulate the limit state function. Determine the probability distributions and appropriate parameters for all random variables, $X_i\left(i=1,2,\cdots,n\right)$ involved.
2. Obtain an initial design point, $\left\{X_i^*\right\}$, by assuming values for n-1 of the random variables. (Mean values are a reasonable choice.) Solve the limit state equation $g=0$ for the remaining random variable which ensures that the design point is on the failure boundary.
3. Equivalent normal mean, μ_X^e and standard deviation, σ_X^e is determined using equations (61) and (62) for design values corresponding to a non-normal distribution. Determine the reduced variables $\left\{Z_i^*\right\}$ corresponding to the design point $\left\{X_i^*\right\}$ using

$$Z_i^* = \frac{X_i^* - \mu_{X_i}^e}{\sigma_{X_i}^e} \tag{63}$$

4. Determine the partial derivatives of the limit state function with respect to the reduced variables; $\{G\}$ is a column vector whose elements are the partial derivatives equation (55), multiplied by -1.

$$\{G\} = \begin{Bmatrix} G_1 \\ G_2 \\ \vdots \\ G_n \end{Bmatrix} \qquad \text{where, } G_i = -\left.\frac{\partial g}{\partial Z_i}\right|_{\textit{evaluated at design point}} \tag{64}$$

5. Estimate of β is then calculated using

$$\beta = \frac{\{G\}^T \{Z^*\}}{\sqrt{\{G\}^T \{G\}}} \qquad \text{where, } \{Z^*\} = \begin{Bmatrix} Z_1^* \\ Z_2^* \\ \vdots \\ Z_n^* \end{Bmatrix} \tag{65}$$

6. The direction cosines for the design point to be used in the subsequent iteration are then calculated using

$$\{\alpha\} = \frac{\{G\}}{\sqrt{\{G\}^T \{G\}}} \tag{66}$$

7. Determine a new design point for n-1 of the variables using

$$Z_i^* = \alpha_i \beta \tag{67}$$

8. Determine the corresponding design point values in original coordinates for the n-1 values in Step 7 by

$$X_i^* = \mu_{X_i}^e + Z_i^* \sigma_{X_i}^e \tag{68}$$

9. Determine the value of the remaining random variable by solving the limit state function $g = 0$.

10. Repeat Steps 3 to 10 until β and $\{X_i^*\}$ converge.

APPENDIX C

Chi-Square Statistical Test: Goodness-of-fit Test

The Chi-Square test is often used to assess the goodness-of-fit between an obtained set of frequencies in a random sample and what is expected under a given statistical hypothesis. To be able to decide which distribution is better for a particular random variable, the difference between actual observation values (observed frequencies) and theoretical distribution values (theoretical frequencies) is quantified. The steps to determine the probability distribution of a random variable are given below.

1. Divide the observed data range into equal intervals.
2. Find the number of observations (Observed Frequency, n_i) within each interval which do not depend on the distribution type.
3. Assume different distribution types that will represent the random variable and find the theoretical distribution values (Theoretical Frequency, e_i) within each interval for the respective distributions. If a random variable, X, lies in an interval *a* to *b* such that $a < X \le b$, then the Theoretical Frequency, e_i, for a certain distribution type is given by

   $$e_i = P(a < X \le b) * N \tag{69}$$

   where, *N* is the total number of observation (data points), and

   $$P(a < X \le b) = P(X \le b) - P(X < a) \tag{70}$$

   The probability of X less than *a* or *b*, $P(X < a)$, and $P(X \le b)$ is found using the CDF for the respective distribution. The CDF for different distribution types can be obtained from the literature.
4. For each interval, compute the difference between n_i and e_i, (squared) as a ratio of e_i.
5. Compute the summation of differences (squared) as a ratio of e_i which is given as

   $$\sum_{i=1}^{m} \frac{(n_i - e_i)^2}{e_i} \tag{71}$$

   where, *m* is the total number of intervals.

6. Calculate the degree of freedom, *f*, for the Chi-Square test, which is given by
$$f = m - 1 - k$$
where, *k* is the number of parameters required to describe a particular distribution. In this study, Normal and Lognormal distribution types are used for these types, $k = 2$.

7. The summation evaluated in Step 5 is compared to the Chi-Square distribution for a certain significance level, α , which is always taken between 1 and 10 percent.

8. If $\sum_{i=1}^{m} \frac{(n_i - e_i)^2}{e_i} < C_{\alpha,f}$, then the assumed distribution is fitting statistical data well enough. $C_{\alpha,f}$ values are given in Table 36.

Table 36
CDF of the chi-square distribution (Nowak and Collins 2000)

Table of the CDF of the Chi-Square Distribution with *f* Degrees of Freedom

$$P(C \le c_{\alpha,f}) = \int_0^{c_{\alpha,f}} \frac{1}{2^{f/2}\Gamma(f/2)} s^{(f/2)-1} e^{-s/2} ds$$

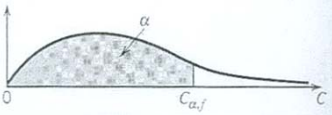

f \ α	0.001	0.005	0.010	0.025	0.050	0.100	0.900	0.950	0.975	0.990	0.995	0.999
1	1.57e–06	3.93e–05	1.57e–04	9.82e–04	3.93e–03	1.58e–02	2.706	3.841	5.024	6.635	7.879	10.83
2	2.00e–03	1.00e–02	0.0201	0.0506	0.1026	0.2107	4.605	5.991	7.378	9.210	10.60	13.82
3	2.43e–02	7.17e–02	0.1148	0.2158	0.3518	0.5844	6.251	7.815	9.348	11.34	12.84	16.27
4	9.08e–02	0.2070	0.2971	0.4844	0.7107	1.064	7.779	9.488	11.14	13.28	14.86	18.47
5	0.2102	0.4118	0.5543	0.8312	1.145	1.610	9.236	11.07	12.83	15.09	16.75	20.51
6	0.3810	0.6757	0.8721	1.237	1.635	2.204	10.64	12.59	14.45	16.81	18.55	22.46
7	0.5985	0.9893	1.239	1.690	2.167	2.833	12.02	14.07	16.01	18.48	20.28	24.32
8	0.8571	1.344	1.647	2.180	2.733	3.490	13.36	15.51	17.53	20.09	21.95	26.12
9	1.152	1.735	2.088	2.700	3.325	4.168	14.68	16.92	19.02	21.67	23.59	27.88
10	1.479	2.156	2.558	3.247	3.940	4.865	15.99	18.31	20.48	23.21	25.19	29.59
11	1.834	2.603	3.053	3.816	4.575	5.578	17.28	19.68	21.92	24.73	26.76	31.26
12	2.214	3.074	3.571	4.404	5.226	6.304	18.55	21.03	23.34	26.22	28.30	32.91
13	2.617	3.565	4.107	5.009	5.892	7.041	19.81	22.36	24.74	27.69	29.82	34.53
14	3.041	4.075	4.660	5.629	6.571	7.790	21.06	23.68	26.12	29.14	31.32	36.12
15	3.483	4.601	5.229	6.262	7.261	8.547	22.31	25.00	27.49	30.58	32.80	37.70
16	3.942	5.142	5.812	6.908	7.962	9.312	23.54	26.30	28.85	32.00	34.27	39.25
17	4.416	5.697	6.408	7.564	8.672	10.09	24.77	27.59	30.19	33.41	35.72	40.79
18	4.905	6.265	7.015	8.231	9.390	10.86	25.99	28.87	31.53	34.81	37.16	42.31
19	5.407	6.844	7.633	8.907	10.12	11.65	27.20	30.14	32.85	36.19	38.58	43.82
20	5.921	7.434	8.260	9.591	10.85	12.44	28.41	31.41	34.17	37.57	40.00	45.31

APPENDIX D

Normal and Lognormal Distribution Types

Normal or Gaussian Distribution

If a variable is normally distributed then two quantities have to be specified: the mean, μ_X, which coincides with the peak of the PDF curve and the standard distribution, σ_X, which indicates the spread of the bell curve. The PDF for a normal random variable X is given by equation (72).

$$f_X(X) = \frac{1}{\sigma_X \sqrt{2\pi}} \exp\left[-\frac{1}{2}\left(\frac{X - \mu_X}{\sigma_X} \right)^2 \right] \tag{72}$$

There is no closed-form solution for the CDF of a normal random variable but tables have been developed to provide values of the CDF for the special case in which $\mu_X = 0$ and $\sigma_X = 1$ (Nowak and Collins 2000). These tables can be used to obtain values for any general normal distribution.

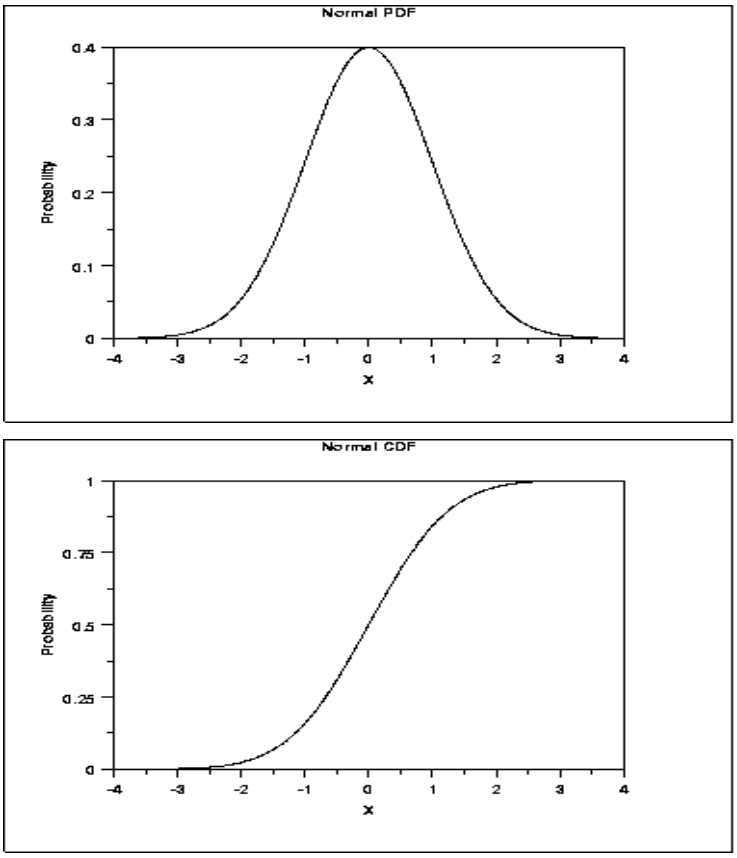

Figure 57
Graphical representation of normal distribution

Lognormal Distribution

The random variable *X* is a lognormal random variable, Figure 58, if *Y = ln(X)* is normally distributed, $F_X(x) = F_Y(y)$.

The mean and standard deviation for *Y* are given by equations (73) and (74).

$$\sigma_Y = \sigma_{\ln(X)} = \sqrt{\ln\left[\left(\frac{\sigma_X}{\mu_X}\right)^2 + 1\right]} \tag{73}$$

$$\mu_Y = \mu_{\ln(X)} = \ln(\mu_X) - \frac{1}{2}\sigma^2_{\ln(X)} \tag{74}$$

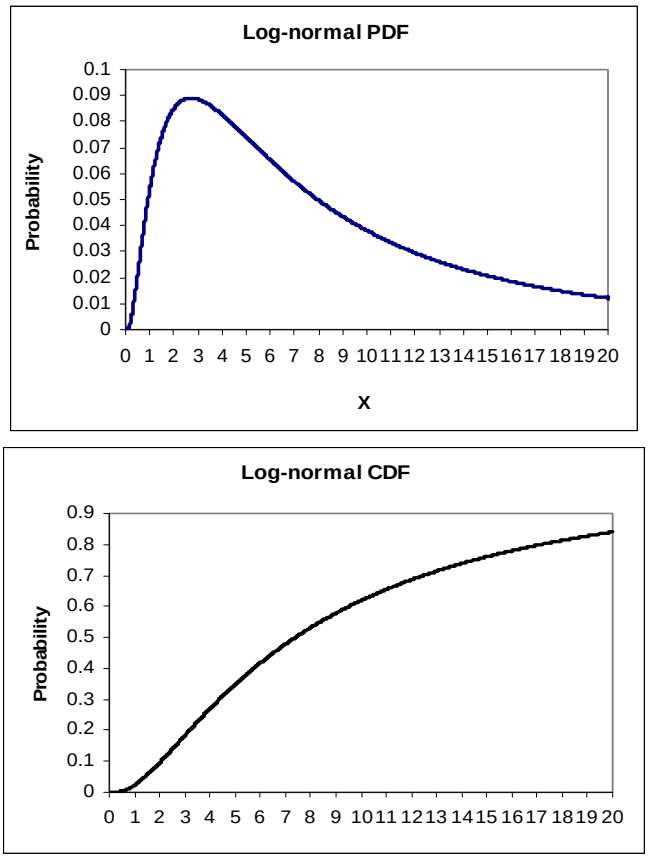

Figure 58
Graphical representation of lognormal distribution

APPENDIX E

Example Excel Template to Analyze CPT Data

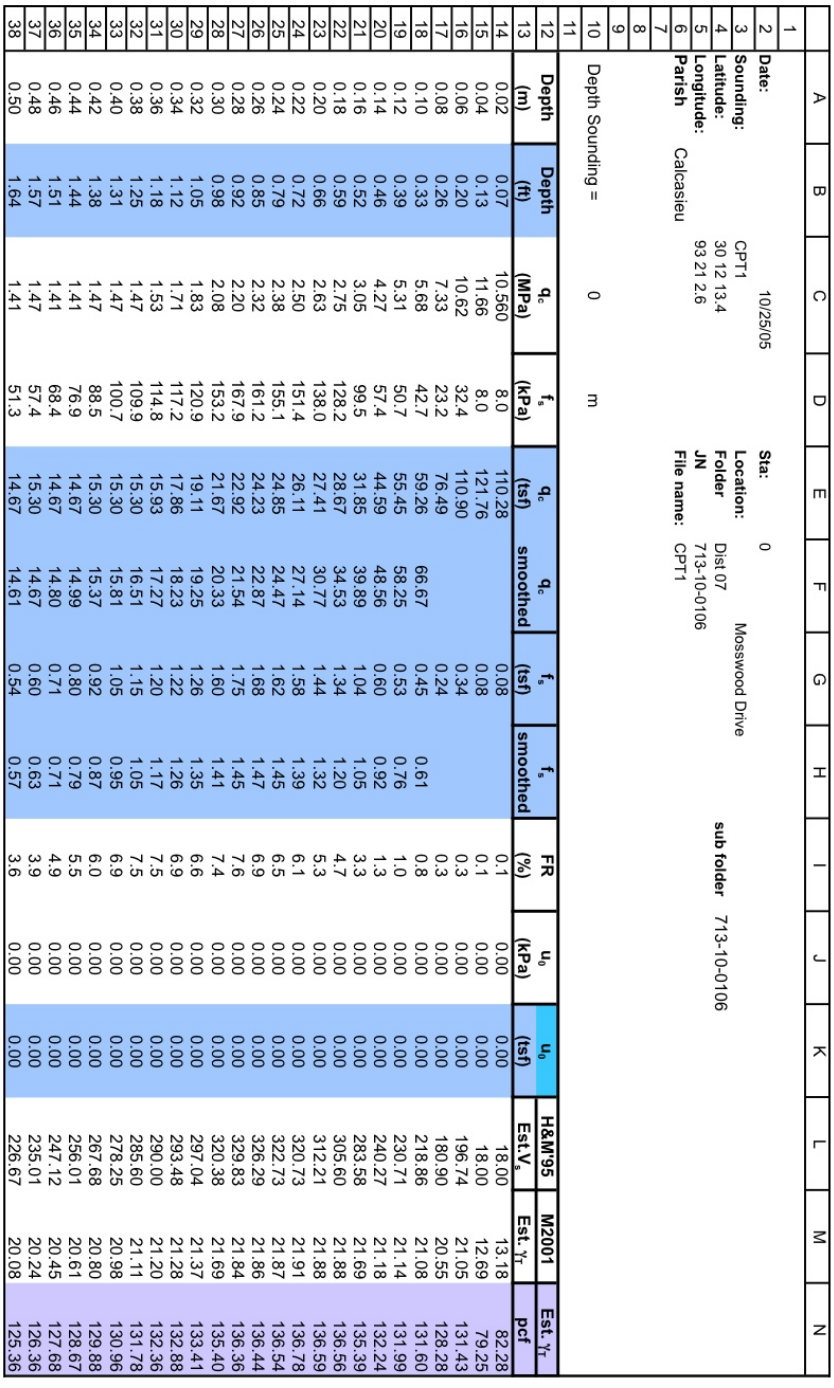

	A	B	C	D	E	F	G	H	I	J	K	L	M	N
1														
2	**Date:**		10/25/05		**Sta:**	0								
3	**Sounding:**		CPT1		**Location:**		Mosswood Drive							
4	**Latitude:**		30 12 13.4		**Folder**	Dist 07			**sub folder**	713-10-0106				
5	**Longitude:**		93 21 2.6		**JN**	713-10-0106								
6	**Parish**	Calcasieu			**File name:**	CPT1								
7														
8														
9														
10	Depth Sounding =		0	m										
11														
12		**Depth**	q_c	f_s	q_c	q_c	f_s	f_s	**FR**	u_0	u_0	**H&M'95**	**M2001**	**Est. γ_T**
13		**(m)**	**(ft)**	**(MPa)**	**(kPa)**	**(tsf)**	**smoothed**	**(tsf)**	**smoothed**	**(%)**	**(kPa)**	**(tsf)**	**Est.V_s**	**Est. γ_T**	**pcf**
14		0.02	0.07	10.560	8.0	110.28		0.08		0.1	0.00	0.00	18.00	13.18	82.28
15		0.04	0.13	11.66	8.0	121.76		0.08		0.1	0.00	0.00	18.00	12.69	79.25
16		0.06	0.20	10.62	32.4	110.90		0.34		0.3	0.00	0.00	196.74	21.05	131.43
17		0.08	0.26	7.33	23.2	76.49		0.24		0.3	0.00	0.00	180.90	20.55	128.28
18		0.10	0.33	5.68	42.7	59.26	66.67	0.45	0.61	0.8	0.00	0.00	218.86	21.08	131.60
19		0.12	0.39	5.31	50.7	55.45	58.25	0.53	0.76	1.0	0.00	0.00	230.71	21.14	131.99
20		0.14	0.46	4.27	57.4	44.59	48.56	0.60	0.92	1.3	0.00	0.00	240.27	21.18	132.24
21		0.16	0.52	3.05	99.5	31.85	39.89	1.04	1.05	3.3	0.00	0.00	283.58	21.69	135.39
22		0.18	0.59	2.75	128.2	28.67	34.53	1.34	1.20	4.7	0.00	0.00	305.60	21.88	136.56
23		0.20	0.66	2.63	138.0	27.41	30.77	1.44	1.32	5.3	0.00	0.00	312.21	21.88	136.59
24		0.22	0.72	2.50	151.4	26.11	27.14	1.58	1.39	6.1	0.00	0.00	320.73	21.91	136.78
25		0.24	0.79	2.38	155.1	24.85	24.47	1.62	1.45	6.5	0.00	0.00	322.73	21.87	136.54
26		0.26	0.85	2.32	161.2	24.23	22.87	1.68	1.47	6.9	0.00	0.00	326.29	21.86	136.44
27		0.28	0.92	2.20	167.9	22.92	21.54	1.75	1.45	7.6	0.00	0.00	329.83	21.84	136.36
28		0.30	0.98	2.08	153.2	21.67	20.33	1.60	1.41	7.4	0.00	0.00	320.38	21.69	135.40
29		0.32	1.05	1.83	120.9	19.11	19.25	1.26	1.35	6.6	0.00	0.00	297.04	21.37	133.41
30		0.34	1.12	1.71	117.2	17.86	18.23	1.22	1.26	6.9	0.00	0.00	293.48	21.28	132.88
31		0.36	1.18	1.53	114.8	15.93	17.27	1.20	1.17	7.5	0.00	0.00	290.00	21.20	132.36
32		0.38	1.25	1.47	109.9	15.30	16.51	1.15	1.05	7.5	0.00	0.00	285.60	21.11	131.78
33		0.40	1.31	1.47	100.7	15.30	15.81	1.05	0.95	6.9	0.00	0.00	278.25	20.98	130.96
34		0.42	1.38	1.47	88.5	15.30	15.37	0.92	0.87	6.0	0.00	0.00	267.68	20.80	129.88
35		0.44	1.44	1.41	76.9	14.67	14.99	0.80	0.79	5.5	0.00	0.00	256.01	20.61	128.67
36		0.46	1.51	1.41	68.4	14.67	14.80	0.71	0.71	4.9	0.00	0.00	247.12	20.45	127.68
37		0.48	1.57	1.47	57.4	15.30	14.67	0.60	0.63	3.9	0.00	0.00	235.01	20.24	126.36
38		0.50	1.64	1.41	51.3	14.67	14.61	0.54	0.57	3.6	0.00	0.00	226.67	20.08	125.36

	O	P	Q	R	S	T	U	V	W	X	Y	Z	AA	AB
1														
2														
3														
4														
5														
6														
7														
8														
9			GWT (m)			Groundwater Information								
10			1.00			Head =	0.00	(kPa)						
11								*Normalized Parameters*			Robertson (1990)		Jefferies & Davies '93	
12	σ_{vo}	σ_{vo}	u_o	σ_{vo}'	σ_{vo}'	q_{tnet}	Δu	Q	F	B_q	SBT	SBT	SBT	SBT
13	(kPa)	(tsf)	(kPa)	(kPa)	(tsf)	(kPa)	(kPa)				Ic	Soil Type	Ic**	Soil Type
14	0.26	0.00	0.00	0.26	0.00	10559.74	0.00							
15	0.52	0.01	0.00	0.52	0.01	11659.48	0.00	22531.48	0.07	0.00	0.88	7.00	1.35	6.00
16	0.94	0.01	0.00	0.94	0.01	10619.06	0.00	11314.65	0.30	0.00	0.91	7.00	1.34	6.00
17	1.35	0.01	0.00	1.35	0.01	7323.65	0.00	5427.02	0.32	0.00	0.77	7.00	1.12	7.00
18	1.77	0.02	0.00	1.77	0.02	5673.23	0.00	3203.25	0.75	0.00	1.10	7.00	1.43	6.00
19	2.19	0.02	0.00	2.19	0.02	5307.81	0.00	2419.29	0.95	0.00	1.20	7.00	1.52	6.00
20	2.62	0.03	0.00	2.62	0.03	4267.38	0.00	1630.27	1.34	0.00	1.37	6.00	1.68	6.00
21	3.05	0.03	0.00	3.05	0.03	3046.95	0.00	998.56	3.27	0.00	1.80	6.00	2.17	5.00
22	3.49	0.04	0.00	3.49	0.04	2741.51	0.00	785.79	4.67	0.00	1.98	6.00	2.37	5.00
23	3.93	0.04	0.00	3.93	0.04	2621.07	0.00	667.54	5.26	0.00	2.05	6.00	2.44	5.00
24	4.36	0.05	0.00	4.36	0.05	2495.64	0.00	571.79	6.06	0.00	2.13	5.00	2.53	5.00
25	4.80	0.05	0.00	4.80	0.05	2375.20	0.00	494.62	6.53	0.00	2.18	5.00	2.58	4.00
26	5.24	0.05	0.00	5.24	0.05	2314.76	0.00	441.82	6.96	0.00	2.22	5.00	2.62	4.00
27	5.68	0.06	0.00	5.68	0.06	2189.32	0.00	385.72	7.67	0.00	2.28	5.00	2.68	4.00
28	6.11	0.06	0.00	6.11	0.06	2068.89	0.00	338.62	7.40	0.00	2.29	5.00	2.67	4.00
29	6.54	0.07	0.00	6.54	0.07	1823.46	0.00	278.94	6.63	0.00	2.28	5.00	2.63	4.00
30	6.96	0.07	0.00	6.96	0.07	1703.04	0.00	244.59	6.88	0.00	2.32	5.00	2.66	4.00
31	7.39	0.08	0.00	7.39	0.08	1517.61	0.00	205.45	7.56	0.00	2.40	5.00	2.73	4.00
32	7.81	0.08	0.00	7.81	0.08	1457.19	0.00	186.60	7.54	0.00	2.42	5.00	2.74	4.00
33	8.23	0.09	0.00	8.23	0.09	1456.77	0.00	177.04	6.91	0.00	2.39	5.00	2.70	4.00
34	8.64	0.09	0.00	8.64	0.09	1456.36	0.00	168.47	6.08	0.00	2.36	5.00	2.63	4.00
35	9.06	0.09	0.00	9.06	0.09	1395.94	0.00	154.13	5.51	0.00	2.34	5.00	2.59	4.00
36	9.47	0.10	0.00	9.47	0.10	1395.53	0.00	147.43	4.90	0.00	2.31	5.00	2.54	5.00
37	9.87	0.10	0.00	9.87	0.10	1455.13	0.00	147.42	3.94	0.00	2.23	5.00	2.42	5.00
38	10.27	0.11	0.00	10.27	0.11	1394.73	0.00	135.77	3.67	0.00	2.23	5.00	2.40	5.00